Interconnection of cellular autophagy and endosomal vesicle trafficking and its role in hepatitis B virus replication and release

Dissertation
for
the doctoral degree of
Dr. rer. Nat.

from the Faculty of Biology
University of Duisburg-Essen
Germany

Submitted by
Jia Li
Born in Chengdu, P. R. China
February, 2024

The experiments underlying the present work were conducted at the Institute for Virology at the University of Duisburg-Essen.

1. Examiner: Prof. Dr. Mengji Lu

2. Examiner: Prof. Dr. Matthias Gunzer

Chair of the Board of Examiners: Prof. Dr. Bernd Giebel

Date of the oral examination: 16.08.2024

DOI: 10.17185/duepublico/82430
URN: urn:nbn:de:hbz:465-20240912-110312-9

Table of Contents

1. Introduction

1.1 Discovery and epidemiology of the hepatitis B virus (HBV)

In the 1960s, Blumberg and Alter observed an atypical reaction between a serum from a transfused hemophilic patient and an Australian aborigine. This discovery led to the identification of the “Australian antigen” [1]. Later, accumulating evidence showed a strong correlation between the presence of the Australian antigen and serum hepatitis [2]. In 1970, David Dane utilized an electron microscope to inspect the isolated virus particles from the sera of patients with Australian antigen-associated hepatitis, revealing the famous “Dane particles” as the complete virion, a hallmark of the hepatitis B virus (HBV) [3].

HBV infection remains the most prevalent chronic viral infection in the world. According to the World Health Organization (WHO) estimates in 2019, the global seroprevalence of HBsAg was 3.8%, and there were approximately 296 million people living with chronic HBV infection (CHB). HBV infects 1.5 million people annually. The burden of HBV is unevenly distributed, with two-thirds of infections concentrated in the WHO Western Pacific Region (116 million people) and the WHO African Region (81 million people). Figure 1.1 illustrates the global distribution of HBV. Chronic HBV infection greatly elevates the risk of developing hepatitis, liver cirrhosis, and hepatocellular carcinoma (HCC). Moreover, HBV infection is the most prominent risk factor for HCC development, contributing to approximately 50% of cases [4]. According to data from the Global Burden of Disease (GBD) 2019 study, there were an estimated 331,000 deaths attributed to HBV-related cirrhosis and chronic liver disease [5].

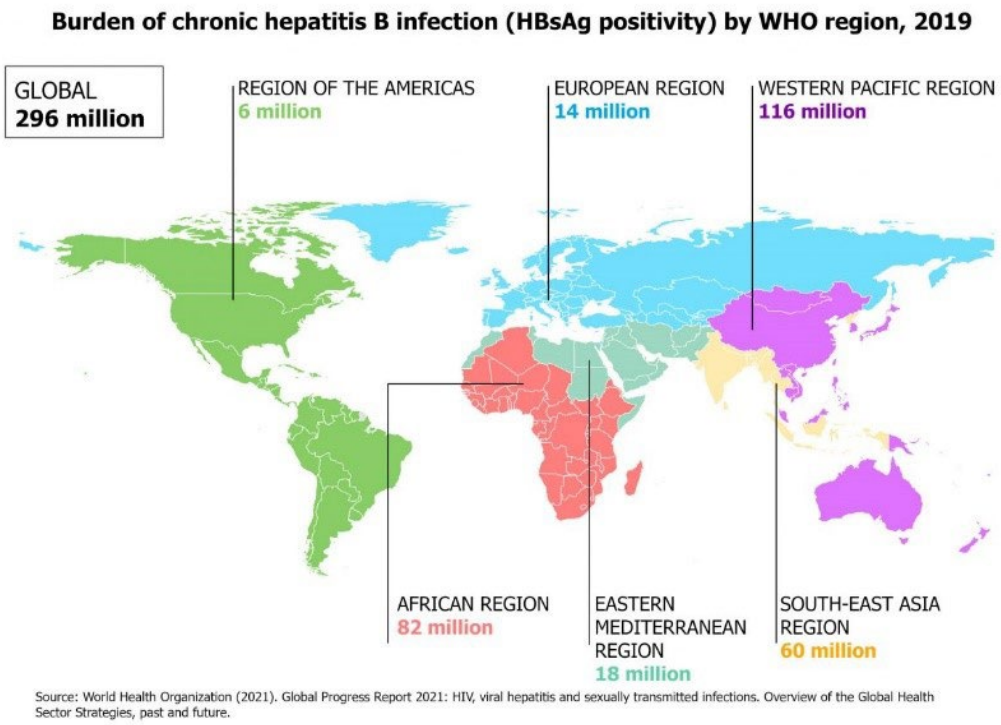

Figure1. 1 Number of reported cases of hepatitis B virus infection and estimated infections

Hepatitis B is a major global health problem. The burden of infection is highest in the WHO Western Pacific Region and the WHO African Region, where 116 million and 81 million people, respectively, are chronically infected. Sixty million people are infected in the WHO South-East Asia Region, 18 million in the WHO Eastern Mediterranean Region, 14 million in the WHO European Region, and 6 million in the WHO Region of the Americas. (Figure source: Centers for Disease Control and Prevention)

1.2 Interferon and HBV

Interferons (IFNs) are a group of cytokines that were first described in 1957 and grouped into three types: I (α, β, ϵ, κ, ω), II (γ), and III (λ) [6]. Each type of IFN has a distinct heterodimeric cell surface receptor and induces gene expression through the Janus kinase–signal transducer and activator of transcription (JAK-STAT) signaling pathway, and triggers phosphorylation of STAT1 and STAT2. Afterwards, the STATs complexes translocate into the nucleus and bind IFN-stimulated responses (IRESs) or gamma-activated sequences (GASs) to produce an antiviral response [7]. Pegylated interferon (IFN) α (PEG-IFN-α) is used to treat HBV-infected patients [8]. However, it has a limited treatment course and the responders to IFN therapy may maintain a virologic response after drug withdrawal, and the rates of achieving prolonged viral suppression or viral

clearance are low [9]. IFN-α treatment can induce an antiviral state in hepatocytes by regulating gene expression and protein translation, which exert non-cytolytic antiviral effects in several stages of the HBV life cycle. IFN-α blocks HBV transcription [10], replication [11], and RNA synthesis [12]. IFN-α treatment also reduces covalently closed circular DNA (cccDNA) [13]. Interferon-stimulated genes (ISGs) are expressed in response to stimulation by interferons. Although HBV replication can be inhibited by certain ISGs [14], HBV infection does not induce a significant ISG-mediated response in the liver [15], showing that exogenous IFN-α application may play unique roles in activating endogenous antiviral immune responses against HBV. IFNs exert indirect anti-HBV effects by modulating immune cell activities. IFNs activate macrophages, natural killer cells, dendritic cells, and T cells to produce a variety of cytokines, including IL-1β, IL-6, TNF-α, and IFN-γ [16].

1.2 HBV structure

HBV belongs to the hepadnavirus family, which is characterized as an enveloped, partially double-stranded DNA virus [17]. The mature and infectious HBV virion, also known as the Dane particle, has a diameter of 42 nm. It consists of nucleocapsids (NCs) and envelope/surface proteins (HBsAg), and virally encoded polymerases, with the viral DNA genome packaged inside. Additionally, HBV produces empty particles consisting of HBsAg without capsids or genomes, termed subviral particles (SVPs). SVPs are typically present in a 1,000- to 100,000-fold excess relative to infectious particles [18]. These SVPs manifest as filaments and spheres with diameters of 17–22 nm (Figure 1.2).

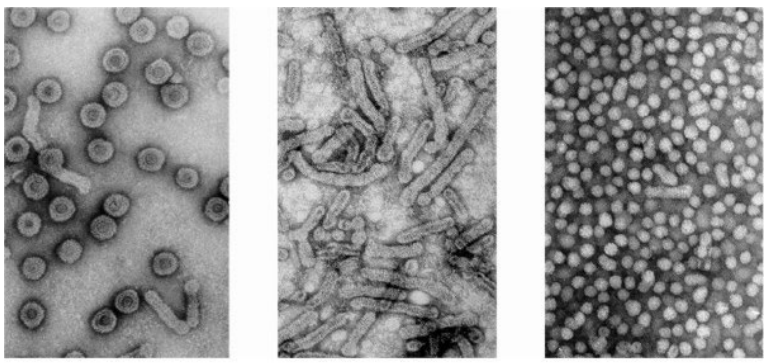

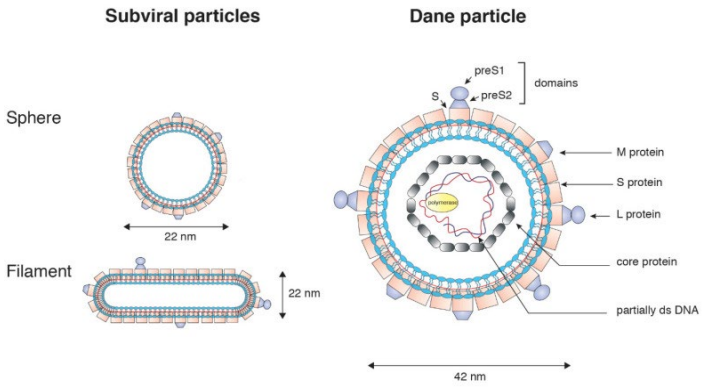

Figure1. 2 HBV morphology

Electron microscopy images (negative staining) and approximate numbers of HBV-associated particles in 1 ml of the serum from a highly viremic chronically infected HBV carrier [19], and a schematic diagram of HBV particles [20].

1.2.1 HBV genome

The HBV genome is partially double-stranded circular DNA, about 3.2 kilobase (kb) pairs in size. It encompasses four overlapping open reading frames (ORFs) denoted as S, C, P, and X (Figure 1.3).

The S ORF encodes the surface antigen (HBsAg), which can be divided into the pre-S1, pre-S2, and S regions. The core protein (HBcAg) is coded by the C ORF, while HBeAg is produced through proteolytic processing of the pre-core protein. The DNA polymerase is encoded by the P ORF. The HBV X ORF encodes HbxAg, which serves multiple functions, including signal transduction, transcriptional activation, DNA repair, and inhibition of protein degradation.

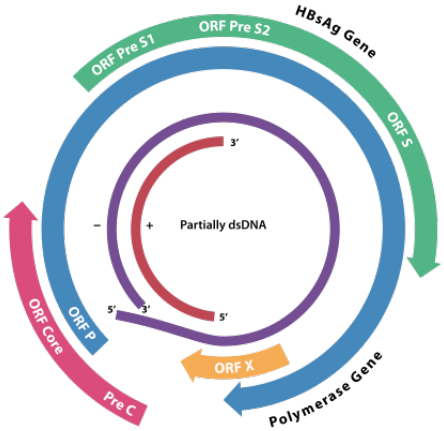

Figure1. 3 HBV genome

P ORF (polymerase open reading frame, blue) overlaps completely with the preS1/preS2/S ORF (green), and partially with preC/C ORF (pink) and X ORF (orange). The partially double-stranded DNA genome is packaged inside, with the (-) strand DNA (magenta) and the (+) strand DNA (red). (Figure source: Wikipedia)

1.2.2 HBV envelope and capsid

The envelope proteins of HBV also referred to as surface proteins or HBsAg, undergo biosynthesis as integral transmembrane polypeptides. Early electron microscopic examinations suggested that this process occurs in the endoplasmic reticulum (ER) lumen, with subsequent assembly and transport to the pre-Golgi compartment [21, 22]. HBsAg exists in three sizes: small (S-HBsAg, S), medium (M-HBsAg, M), and large (L-HBsAg, L), all sharing the C-terminal S domain. The M-HBsAg extends with the PreS2 domain (55 aa), and the L-HBsAg includes the PreS1 domain (108 aa) (Figure 1.2). Notably, PreS1 contributes essential functions during viral entry and particle morphogenesis [23]. A considerable proportion of L- and S-HBsAg contributes to the formation of subviral filamentous particles, while spherical particles are predominantly composed of S-HBsAg [24].

On the other hand, HBV capsids consist of core proteins (HBcAg) with an icosahedral symmetry structure and diameters of approximately 34 and 30 nm. The virus core protein comprises 183 residues, is divided into the N-terminal domain (NTD), is responsible for capsid assembly, and has a domain responsible for viral genome packaging and replication (arginine-rich RNA-binding C Terminal Domain, CTD) [25, 26]. The regulation of capsid formation is not fully understood.

1.3 HBV life cycle

1.3.1 The entry of the HBV

The HBV gains entry to host cells through clathrin-mediated endocytosis, interacting with the Na+-taurocholate co-transporting polypeptide (NTCP) with the help of heparan sulfate proteoglycans (HSG) [27-29]. Importantly, the preS1 region of L-HBsAg has been identified as an essential structure for binding to NTCP and HBV attachment and entry [30]. The conserved motif NPLGFFP (aa9–15) mediates the high-affinity interaction with NTCP [31]. Additional host factors, such as the epidermal growth factor receptor (EGFR) [32] and E-cadherin [33], a calcium-dependent cell-cell adhesion

protein, were also reported to interact with NTCP and mediate HBV entry. Heparan sulfate proteoglycans (HSPGs) are glycoproteins containing one or more heparan sulfate chains, which are implicated as the low-affinity binding receptor of HBV infection [34]. Binding to HSPGs is mediated by the antigenic loop in the S domain present in all HBV envelope proteins [35].

1.3.2 HBV DNA replication

The replication of the HBV genome can be divided into three phases [36]. First, the partially double-stranded, relaxed circular viral DNA (RC-DNA) contained in icosahedral core proteins is released to the nucleoplasm. Second, the RC-DNA is converted into covalently closed circular DNA (cccDNA), which contributes to virus persistence in hepatocytes. Third, cccDNA serves as a template for translating various viral RNAs by cellular RNA polymerase II. Of these, the pregenomic RNA (pgRNA) is selectively packaged into progeny capsids and serves as the template for the generation of new DNA genomes through reverse transcription [37]. The first synthesized minus-strand DNA then serves as a template for the synthesis of plus-strand DNA, resulting in the formation of RC DNA.

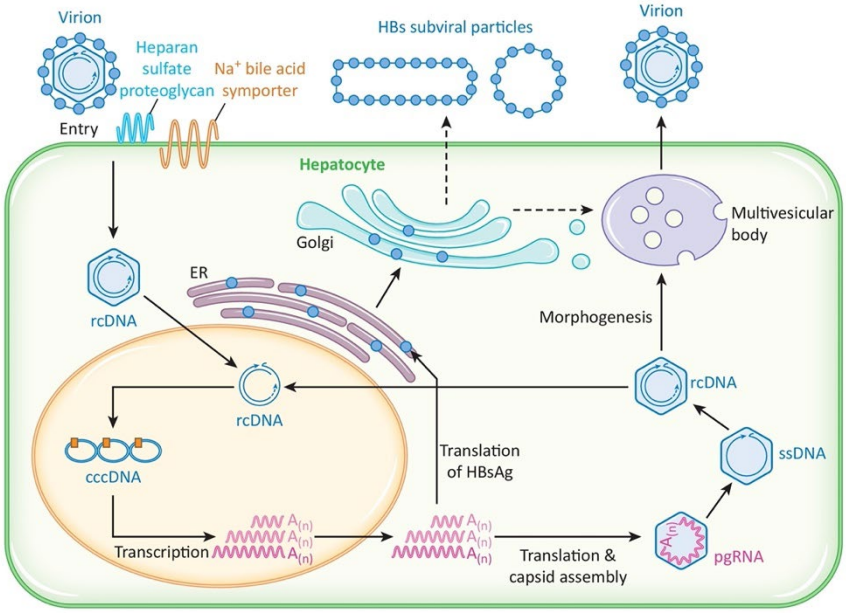

Figure1. 4 Replication cycle of HBV

HBV virions bind to HSPG on the cell surface and facilitate clathrin-mediated endocytosis through NTCP. Relaxed circular (rc)DNA genomes are converted into covalently closed circular (ccc)DNA, serving as the

transcriptional template for viral mRNAs and pregenomic (pg)RNA. The HBV pgRNA is packaged by viral capsid proteins and is reversely transcribed by the viral polymerase to produce rcDNA. The viral DNA-contained nucleocapsids are subsequently enveloped by HBsAg and released as virions, or transported to the nucleus to amplify the cccDNA pool [38].

1.3.3 Release of progeny HBV

Interactions between the capsid, surface proteins, and/or host proteins trigger the envelopment of progeny HBV. This envelopment process is intricately dependent on the presence of HBsAg, with S- and L- (but not M-) HBsAg crucial for efficient virion production [23]. The pre-S domain of L-HBsAg, especially Arg 103 and Ser 124, is mainly responsible for the interaction with viral nucleocapsids [39, 40]. The secretion of infectious virions depends on the multivesicular body (MVB)-associated endosomal sorting complex required for transport (ESCRT) machinery. The incomplete viral particles, including SVPs/HBsAg, naked nucleocapsids, and empty virions, utilize diverse pathways for their secretion. Spheres, mainly consisting of S-HBsAg, are predominantly released via the constitutive ER-Golgi secretory pathway [41, 42]. Conversely, the release of L-HBsAg, which is responsible for the formation of filaments and virions, is mediated through MVBs [41, 43, 44].

1.4 Endosomal vesicle trafficking

The endosomal vesicle trafficking has been shown to participate in the different stages of HBV maturation and release [45]. Endosomes are dynamic and heterogeneous organelles, which play pivotal roles in endocytic trafficking, recycling, and degradation [46]. They are categorized into three different types (Figure 1.4): early endosomes, late endosomes/MVBs, and recycling endosomes [47]. Their distinctive characteristics include the time taken for endocytosed material to reach them, along with specific markers such as Rabs. Early endosomes are marked by RAB5, while RAB7 distinguishes late endosomes/MVBs [48], and RAB11 characterizes recycling endosomes [49]. Early endosomes initiate the maturation process of late endosomes. This maturation involves a decrease in pH and an increase in size. Recycling endosomes contribute to the return of internalized molecules to the cell surface. Endocytic cargo is received by early endosomes primarily through the clathrin-, caveolar-, GEEC-, and ARF6-dependent pathways [50, 51]. Subsequently, internalized cargos from early endosomes follow

distinct destines: recycling back to the cell surface, maturing and assembling into late endosomes, or being further packaged into intraluminal vesicles (ILVs) within late endosomes/MVBs [52]. Ultimately, late endosomes/MVBs undergo fusion with the cell plasma membrane, releasing their cargos into the extracellular space as exosomes or delivering their contents to lysosomes for degradation [47].

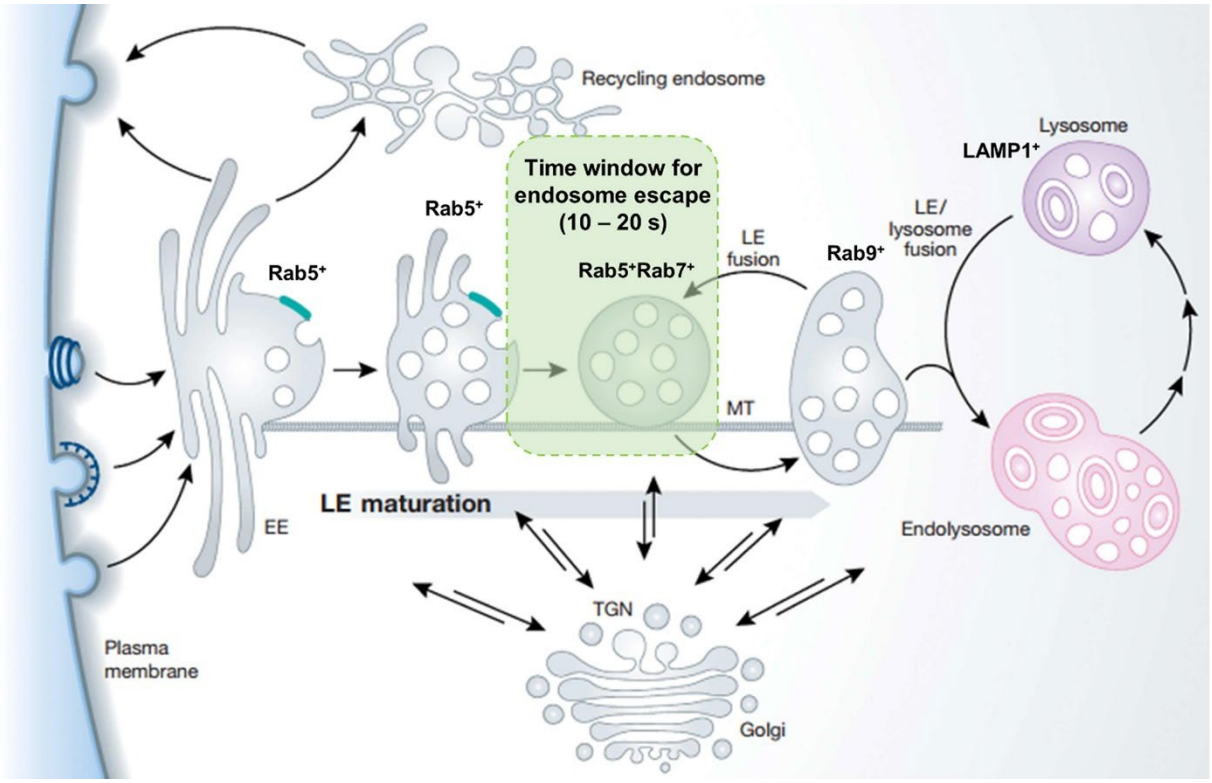

Figure1. 5 Endosome maturation process

After the endocytic vesicle formation, the cargo containing vesicles form into Rab5+ early endosomes. Early endosomes move along microtubes (MT) and the Ra5a converses into Rab7, representing the maturation to late endosome. The cargo could be released within 10-20 seconds. The unreleased cargo will accumulate in the late endosome and transfer to the lysosome (LAMP1$^+$) for degradation [53].

1.4.1 Early endosomes and HBV

Efficient transport of HBV from early to mature endosomes is crucial for the viral life cycle. Analysis of liver tissue samples from chronically HBV-infected individuals has revealed a significant increase in RAB5A mRNA and protein levels [54], underscoring the positive modulation of HBV replication by early endosomes. The threefold higher colocalization of HBsAg with RAB5A compared to autophagosomes [55], indicating that early endosomes act as the primary trafficking pathway for HBsAg. Depletion of RAB5B, another isoform

of RAB5, leads to the accumulation of L-HBsAg in the endoplasmic reticulum (ER) [56]. In an *in vitro* infection system, the silencing of RAB5 and RAB7 strongly reduces the production of encapsidated viral DNA [45], emphasizing the necessity of HBV transport from early to mature endosomes for successful viral infection. The uptake and transport of HBV core particles to early endosomes also rely on RAB5 [57].

1.4.2 Late endosomes and HBV

As early endosomes progress towards maturation into late endosomes/MVBs, the initiation of intraluminal vesicle (ILV) formation occurs, facilitated by cargo-sorting receptors such as ESCRT and accessory proteins like Alix (apoptosis-linked gene 2 (ALG-2)-interacting protein X, also called AIP1) [58]. The ESCRT machinery, consisting of ESCRT-0, -I, -II, -III, and the vacuolar protein sorting (VPS)4 ATPase complex, acts sequentially to achieve vesicle abscission and release in cells. ESCRT-0, -I, and -II play pivotal roles in cargo recognition and membrane budding, leading to the recruitment of ESCRT-III for the scission of membrane necks. VPS4, with its ATPase activity, disassembles the ESCRT complexes, facilitating their recycling back to the cytoplasm [59].

HBV exploits the ESCRT machinery for assembly and secretion. Aberrant expression of the ESCRT-0 subunit HGS inhibits HBV replication, while overexpression of HGS promotes the release of naked capsids [60]. Knockdown ESCRT-I components TSG101 and VPS28 may in turn induce more functional ESCRT-II and III to assist virus release [61]. TSG101 could also facilitate HBV assembly and egress by recognizing ubiquitylated HBc and delivering it to MVB [62]. Depletion of ESCRT-II components EAP20, EAP30, or EAP45 inhibits HBV production [61]. Overexpression of dominant negative mutant ESCRT-III subunits like CHMP3 and CHMP4 blocks HBV assembly and egress [63]. Additionally, VPS4 mutants impede HBV replication and secretion without affecting S-HBsAg release [63, 64]. The secretion of filaments requires ESCRT-III and VPS4 [43]. However, the loss of VPS4 function does not impair the level of secreted naked capsids [65], suggesting diverse export pathways for HBV naked capsids and virions. A later study proposed an ESCRT-independent mechanism for HBV capsid export, indicating a role for Alix that promotes capsid secretion by binding directly to the core via its Bro 1 domain [66]. These studies have demonstrated the requirement of ESCRT machinery for

HBV: on one hand, HBV colocalizes with ESCRTs compartments and enters MVBs for their assembly; on the other hand, ESCRTs regulate MVB biogenesis and then manipulate HBV release. The different observations in the roles of ESCRTs in HBV components release indicate more complicated mechanisms that need to be investigated. The detailed mechanisms through which HBV components access ESCRT and the assembly processes within late endosomes/MVBs remain incompletely understood. A study identified a potential association between L-HBsAg and γ2-adaptin, facilitating their entry into late endosomes/MVBs [63, 67]. Another reported adaptor, α-taxilin, interacts with the PreS1/PreS2 domain of LHBs and TSG101, aiding in the recruitment of late endosomes/MVBs by envelop proteins [68]. HBV capsid may enter the ESCRT network by hijacking γ2-adaptin, Nedd4 ubiquitin ligase, and TSG101, all of which were shown to interact with the viral core protein [61, 62, 67].

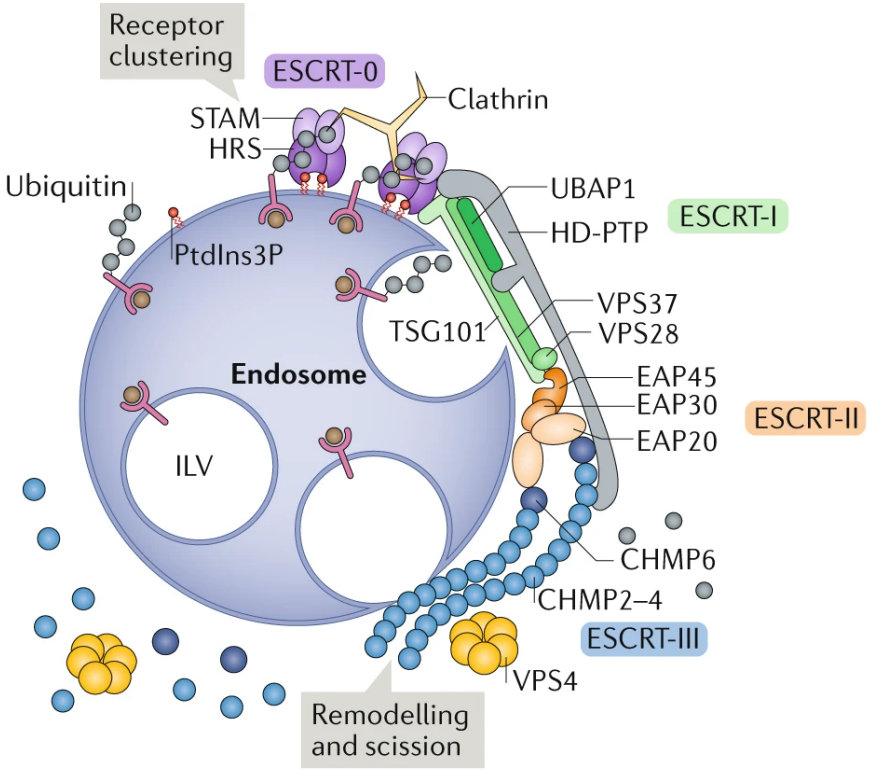

Figure1. 6 ESCRT recruitment and function at MVB

ESCRT-0 (comprising HRS and STAM) recognizes the polyubiquitylated receptor in the endosome membrane. ESCRT-0 recruits ESCRT-I and hands over ubiquitylated cargo. ESCRT-II is sequentially recruited to ESCRT-I. The two EAP20 subunits of ESCRT-II recruit CHMP6 in ESCRT-III. The filaments

are remodeled by VPS4 to achieve scission of the ILV neck. Finally, ESCRT-III disassembly after ILV scission is mediated by VPS4 [69].

1.4.3 Exosomes and HBV

Exosomes, extracellular vesicles (EVs) with diameters ranging from 30 to 200 nm, feature a single membrane and carry specific nucleic acids, proteins, and lipids [70]. Given the substantial role of late endosomes/MVBs in HBV maturation, it is plausible that progeny virions are released from cells akin to exosome secretion or exploit exosomes as vehicles for release. Previous investigations have identified HBV DNA, RNA, and proteins associated with exosomes derived from HBV-infected hepatocytes [71, 72]. Further evidence from Eberhard's group supports the presence of HBV markers on isolated exosomes, suggesting that intact HBV virions can be released via exosomes [73]. Consequently, HBV might exploit exosomes as a means of cellular escape. Considering the presence of lipid rafts within endosomal membranes, inhibitors targeting lipid metabolism, which can impede MVBs biogenesis, exosome formation, and secretion [74], may also impact HBV replication and budding.

1.5 Autophagy

Autophagy is a highly conserved eukaryotic cellular recycling process. Through the degradation of long-lived proteins and damaged organelles, and recycling building blocks, it plays important roles in maintaining cellular homeostasis. It can be induced by various stimuli, including starvation, DNA damage, hypoxia, ER stress, and infection [75].

1.5.1 The autophagy machinery

The complete autophagy involves the formation of a double-membrane structure known as autophagosome and degradation. Initiated by the isolation membrane, or phagophore, believed to primarily originate from the ER [76], and possibly other cytosolic membrane structures such as the ER-Golgi intermediate compartment (ERGIC) [77] and recycling endosomes [78]. Phagophores expand and form double-membraned autophagosomes with sequestering cargo in. Subsequently, autophagosomes fuse with lysosomes, leading to the degradation of enclosed cargoes by lysosomal hydrolases [79].

At the molecular level, the formation of the phagophore is characterized by the activation of AMP-activated protein kinase (AMPK) signaling and /or the inhibition of mammalian

target of rapamycin (MTOR) signaling, which causes the subsequent activity of the ULK1/2 (ATG1 in yeast) kinase complex. ULK1 activates the class III phosphoinositide 3-kinase complex I (PtdIns3K-C1, consisting of PIK3C3/VPS34, VPS15, BECN1/Beclin 1, and ATG14L) and recruits it to the ER membrane. The phagophores then expand and elongate with the assistance of ATG5–ATG12 conjugation, interaction with ATG16L, and multimerization at the phagophore. LC3 is inserted into the extending phagophore membrane, forming the double-membrane autophagosome [80, 81]. Autophagy serves multiple functions in mammalian cells and is regarded as a potent defense mechanism against various viral infections.

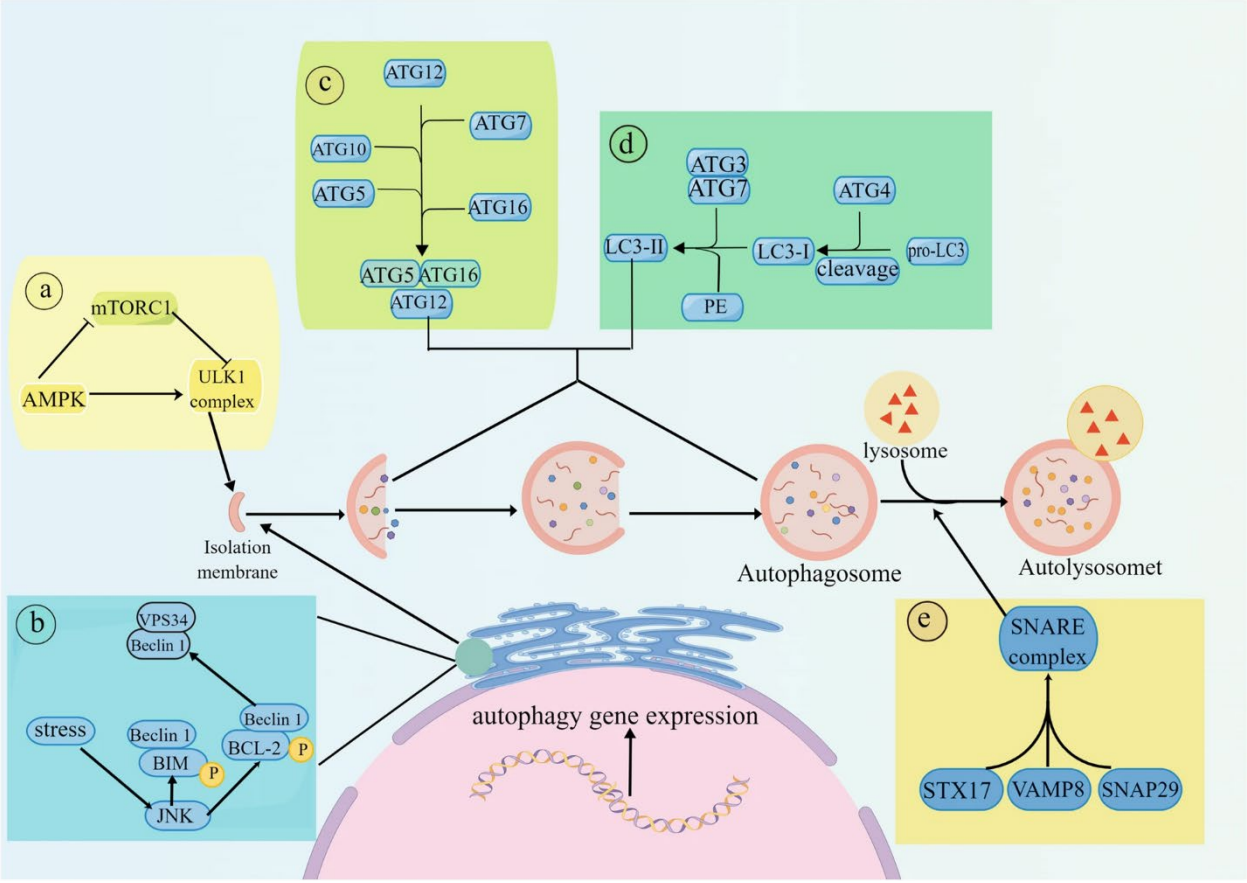

Figure1. 7 Mechanism of autophagy

The key steps of autophagy: ① Initiation: AMPK inhibits the formation of the MTORC1 complex, which weakens the inhibitory effect of MTORC1 on the formation of the ULK1 complex, thereby promoting the production of autophagic vesicles. ② Extension: The Beclin-1/VPS34 complex promotes the extension of autophagic vesicles. The activated kinase JNK releases Beclin1 from Beclin1/BCL-2 and Beclin1/BIM complexes, which then activates VPS34 and binds to it to form a complex. PI3P is produced to promote the extension of autophagic vesicles. ③ Polymerization: The ATG12-ATG5 complex binds to ATG16 and

completes polymerization. and then, the ATG5-ATG12-ATG16L polymer complex is fused with autophagic vesicles. ④ Autophagosome formation: ATG4 cleaves LC3 into LC3-I, which is then processed by phosphatidylethanolamine to form LC3-II. Subsequently, LC3-II is inserted into the autophagosomes. ⑤ Autolysosome formation: STX17 binds to SNAP29 and VAMP8 to form a soluble N-ethylmaleimide-sensitive factor attachment protein receptor (SNARE) complex, allowing lysosomes to fuse with autophagosomes and form autolysosomes to degrade cargos [82].

1.5.2 Autophagy and HBV

Autophagy has recently been found to efficiently support HBV replication during viral assembly and production [81, 83, 84].

HBV induces autophagy mainly through mechanisms involving hepatitis B x protein (HBx) and HBsAg. Specifically, HBx activates PI3KC3, MTOR, and AMPK signaling pathways, enhancing autophagosome formation [85, 86]. On the other hand, HBsAg is sufficient to induce autophagy through the PERK, ATF6, and IRE1-regulated unfolded protein response (UPR) and ER stress [87].

Autophagy supports HBV replication. Drugs such as rapamycin [88], dexamethasone [89], and cisplatin [90] induce autophagy and enhance HBV replication. Conversely, autophagy suppression prevents HBV replication both in vivo and in vitro. Blocking autophagy by 3-MA, a PtdIns3K inhibitor, or with a specific siRNA targeting the PIK3C3 or ATG7 genes causes a reduction in HBV DNA replication [86]. Autophagosomes also act as a physical scaffold for viral replication. Prange's group demonstrated that HBV replication relies on the ATG5-12-16L1 elongation complex [91]. HBcAg co-localizes with LC3 mediated through ATG12 tethered to the phagophore. The silencing of ATG5, ATG12, and ATG16L1 suppress core protein translation and hampers proper core protein trafficking to NC assembly/envelope generation sites, resulting in impaired core proteins/NCs association with envelope membranes. More recent evidence indicates that autophagic membrane-associated core particles are almost DNA replication-competent [83]. In vivo studies also support the essential role of autophagy in HBV replication. Liver-specific ATG5 knockout HBV transgenic mice show a significant reduction in HBV DNA levels in the mouse liver and sera [84]. Glucosamine application induces autophagosome formation, greatly enhancing HBV replication in the liver tissue of an HBV hydrodynamic injection mouse model [92]. HBV exploits autophagy also for its envelopment. Li *et al.* reported that S-HBsAg co-localizes with autophagosomes, and a blockage of autophagy

significantly decreases extracellular virion secretion, providing evidence for autophagosomes' contribution to viral envelop formation [87].

The modulation autophagy signaling pathway also regulates HBV replication. Glucose starvation activates AMPK and reduces AKT/MTOR signaling activity thereby enhancing autophagy and promoting HBV replication [93]. Decreased *O*-GlcNAcylation induces ER stress and inhibits AKT/MTOR signaling, leading to increased autophagy and enhanced HBV replication [94]. IFN-α also inhibits the AKT/MTOR signaling pathway and triggers autophagy and promotes HBV replication in hepatoma cells [95]. miRNAs are small, highly conserved noncoding RNAs known to play a role in regulating host-virus interactions. Evidently, miRNAs are able to modulate AKT/MTOR signaling pathway-induced autophagy and thereby modulate HBV replication. In hepatoma cells, the miR-99 family promotes HBV replication post-transcriptionally through IGF-1R/PI3K/AKT/MTOR/ULK1 signaling-induced autophagy [96], and miR-192-3p increases HBV replication through inhibiting ZNF143/AKT/MTOR signaling [97]. In contrast, the expression and export of HBeAg appear to be less or not dependent on autophagy. Consistent with our previous findings, the autophagic process and associated proteins do not seem to regulate HBV transcription or promoter activity, implying their involvement in the post-transcriptional steps of the HBV life cycle [84, 86, 93, 96].

1.5.3 Autophagic degradation of HBV

The lysosome is one of the final destinations of autophagosomes, and it's also an important determinant of viral loads. Although autophagy initiation is vital for efficient HBV replication, substantial evidence suggests that a significant portion of HBsAg, capsid- and virion-associated HBV DNA undergoes degradation through autophagy. Decreased fusion of autophagosomes with lysosomes increases HBV production. Liu *et al.* [98] published data indicats that HBx helps HBV evade autophagic degradation by impairing lysosomal maturation. Inhibiting RAB7, a crucial protein for autophagosome-lysosome fusion, or knockdown of its effector PLEKHM1 prevents fusion, thereby preserving the lysosomal degradation of HBV and causing strongly increased HBV yields [99]. Chloroquine (CQ), an agent preventing lysosomal acidification and autophagic degradation, has a similar effect [99]. Glucosamine, a glucose derivative, exhibits a comparable impact [92]. The soluble N-ethylmaleimide-sensitive factor attachment

protein receptor (SNARE) complex, consisting of synaptosomal-associated protein 29 (SNAP29), vesicle-associated membrane protein 8 (VAMP8), and syntaxin 17 (STX17), controls autophagosome-lysosome fusion thereby modulating autophagic degradation of HBV virions and SVPs [100].

Moreover, interference with lipid metabolisms to modulate autophagosome-lysosome fusion also affects HBV replication. Silencing SAC1-like phosphatidylinositol phosphatase (SAC1) upregulates phosphatidylinositol-4-phosphate (PI4P) on the autophagosome membrane and blocks autophagy-lysosome fusion thereby promoting HBV replication [101]. Thus, efficient viral replication appears to rely on early autophagy while concurrently avoiding complete degradation. In contrast, autophagic membranes that successfully fuse with the lysosomes and complete lysosome enzymatic function are advantageous for controlling HBV replication. Treatment with epigallocatechin-3-gallate (EGCG) enhances lysosomal acidification and exhibits anti-HBV activity [102]. Promoting autolysosome-dependent degradation by overexpression SAC1 and activating AMPK inhibits HBV replication and production [101, 103]. Eva-1 homolog A（EVA1A), a host protein, enhances HBV degradation in patients with low viral loads [104]. Therefore, gaining a better understanding of modulating autophagosome-lysosome fusion may be helpful in developing more efficient strategies to control HBV production.

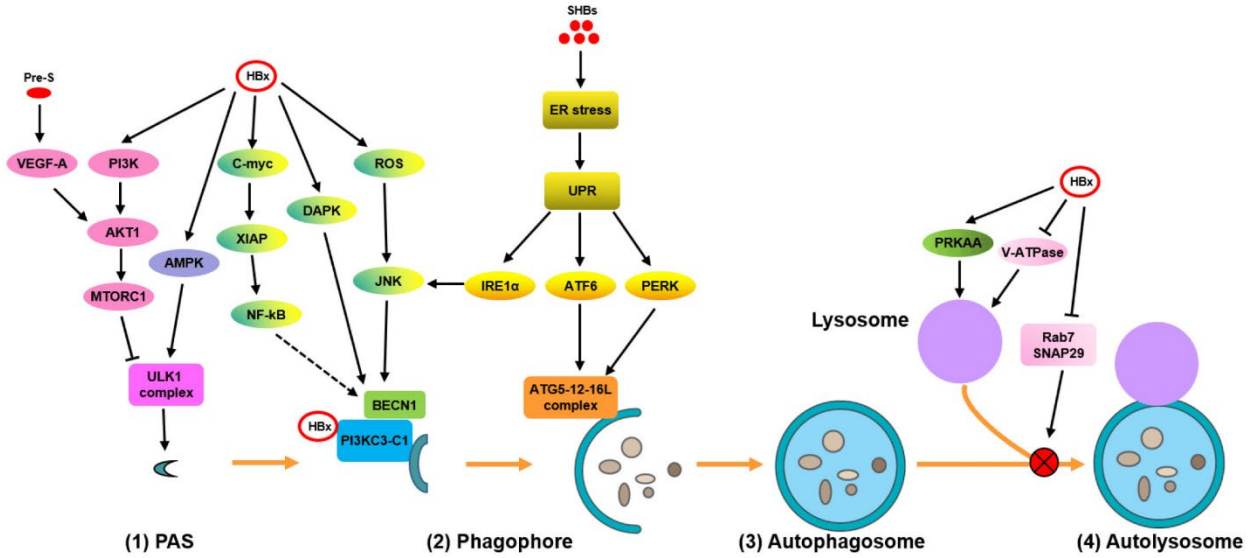

Figure1. 8 HBV infection modulates the different phases of autophagy

(1) HBx targets the PtdIns3K, death-associated protein kinase (DAPK), reactive oxygen species/c-Jun N-terminal kinases (ROS/JNK), and c-myc-XIAP-NF-κB pathways either directly or indirectly and induces

autophagy. (2) HBV subverts the autophagy elongation complex ATG5-12-16L1 for NC assembly/envelope maturation. SHBs trigger endoplasmic reticulum stress-induced unfolded protein response and activate IRE1α and ATF6 signaling to induce UPR-related autophagy. (3) HBV blocks the fusion of autophagosomes with lysosomes by interfering with RAB7 or SNAP29 expression or by impairing lysosomal acidification through the inhibition of V-ATPase activity [81].

1.5.4 Crosslink of the endosomal and autophagic pathway with HBV

ESCRTs also have been shown related to autophagosome formation [105]. Rusten *et al.* summarized that ESCRT proteins control autophagy across four stages: inducing ER stress to initiate autophagy, facilitating phagophore closure, mediating fusion of autophagosomes with late endosomes/MVBs to form amphisome, and enabling fusion with lysosomes for degradation [106]. During the early steps, ATG12-ATG3 interacts with Alix to promote basal autophagic flux [107]. Takahashi *et al.* showed that the ESCRT-III components, CHMP2A, CHMP3, CHMP7, and VPS4A, are potential regulators of phagophore closure [108]. Among these, CHMP2A translocates to the phagophore to regulate the separation of inner and outer membranes, ultimately forming double-membrane autophagosomes. The coordination between autophagic and endosomal pathways also regulates HBV assembly and secretion. While autophagy is traditionally viewed as an autodigestive pathway, it has been shown to also facilitate cellular secretion. Nevertheless, the mechanisms underlying the “autophagic secretion” process remain unclear. In our latest study, we investigated the function of a protein named Gα-interacting vesicle-associated protein (GIV/Girdin). GIV was found to enhance HBV replication by increasing endosomal trafficking and reducing autophagic degradation of HBV proteins. Disrupting endocytosis by knockdown of GIV and its effectors led to the retention of HBsAg in ER and promotes autophagy and lysosomal degradation of HBV proteins. The results suggest that autophagy could promote HBV replication and production only when endosomal trafficking is at least partly functional [55]. Another study in our group found tunicamycin-induced ER stress and autophagic flux promoted HBV replication and the release of virions, SVPs, and naked capsids via the autophagosome-MVB axis [109]. Thus, the autophagic process is not merely a bypass of the endosomal pathway but rather a major pathway closely connected to late endosomes/MVBs for SVP and virion production. Amphisome, an intermediate organelle formed by the fusion of late endosomes with autophagosomes, is conventionally destined for degradation upon fusion

with lysosomes [110]. The regulation of amphisome formation and trafficking also affects HBV egress. Silencing RAB11, a small GTPase required for amphisome formation, leads to the reduction of extracellular HBV DNA levels [83]. These observations underscore the importance of the intricate interplay between autophagy, endosomal trafficking, and HBV egress.

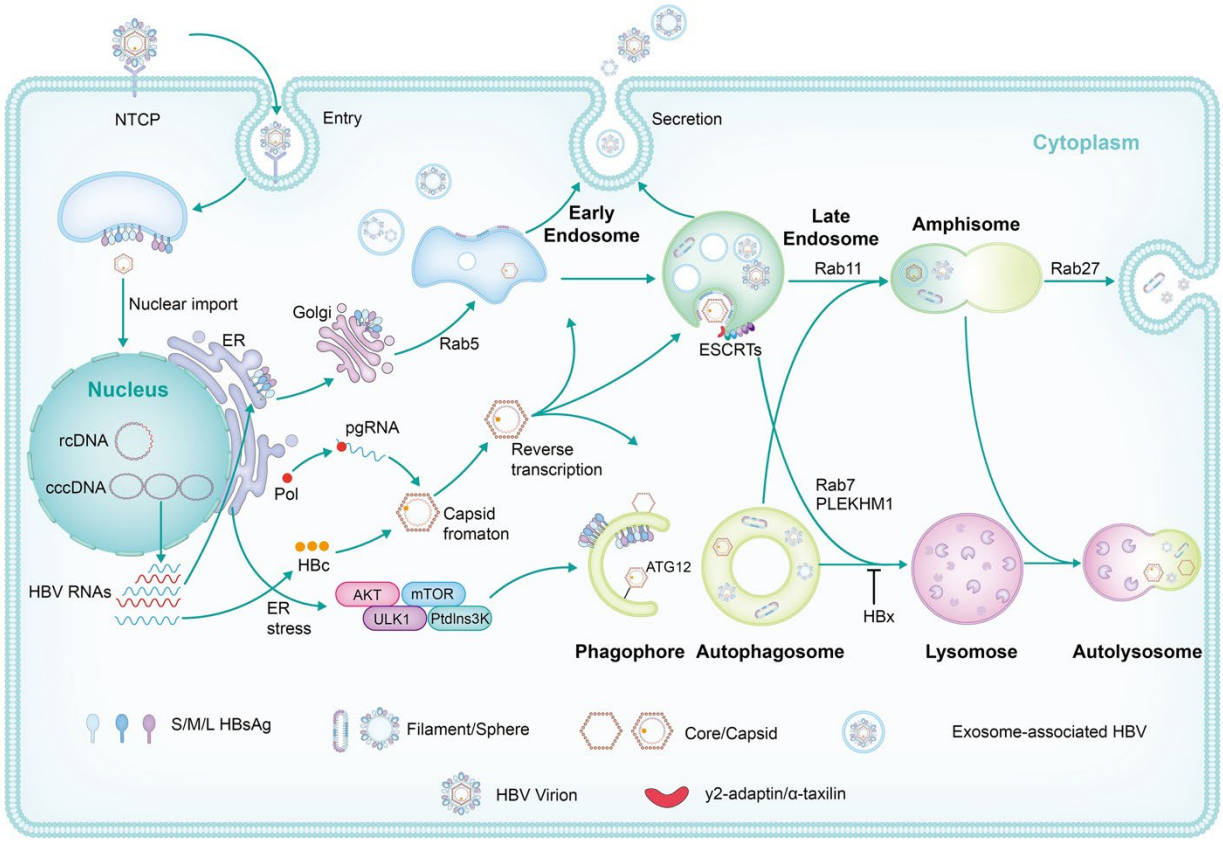

Figure1. 9 HBV life cycle and trafficking along endosomal and autophagic pathways

The HBV infection cycle in hepatocytes includes receptor binding, entry, transport of capsids to the nuclear pore complex, covalently closed circular DNA (cccDNA) formation, transcription and translation, and assembly of capsids, viral particles, and subviral particles (SVPs). HBV enters host cells through clathrin-mediated endocytosis by interacting with the Na+-taurocholate co-transporting polypeptide (NTCP). HBsAg biosynthesis occurs at the endoplasmic reticulum (ER). HBsAg is subsequently transported to the pre-Golgi compartment, or to the early endosome and then released from host cells. The secretion process for HBV virions and filamentous SVPs depends on the multivesicular body (MVB)-associated endosomal sorting complex required for transport (ESCRT) machinery, which involves γ2-adaptin, α-taxilin, CHMP3, Nedd4, Alix, and Vps4. The abnormal buildup of HBsAg within the ER lumen induces ER stress and suppresses AKT/mTOR signaling, which, in turn, stimulates autophagy. The majority of autophagosomes normally undergo fusion with lysosomes for cargo degradation, assisted by RAB7. However, HBx intervenes by

inhibiting the fusion of autophagosomes with lysosomes, thereby promoting HBV accumulation and release. Moreover, autophagosomes are also capable of fusing with late endosomes, forming amphisomes. HBV compartments accumulated in amphisomes can be released depending on RAB11 and RAB27, indicating the autophagy-late endosome/MVB axis regulates HBV assembly and release [111].

2. Aims of the project

The disruption of the endosome vesicle pathway, including blocking late endosome/MVB formation and the production and secretion of exosomes, may critically affect HBV production and release. GW4869 is a neutral sphingomyelinase inhibitor and the most widely used pharmacological agent for blocking exosome generation. Given the pivotal role of numerous Rab proteins in regulating intracellular pathways of late endosomes/MVBs, we focused on RAB27A and -B, two proteins required for exosome release through MVBs. Thus, in this project, we addressed two fundamental points: First, whether interventions affecting late endosomes/MVBs function and exosome secretion also impair HBV replication and secretion; and second, to unravel the molecular mechanisms underlying these processes.

To execute this study, we performed and investigated the following:

1. Identification of GW4869's impact on HBV replication: Evaluate whether GW4869 modulates HBV replication in both hepatoma cells and primary human hepatocytes.
2. Assessment of endoplasmic reticulum stress: Examine whether GW4869 induces endoplasmic reticulum stress through HBV protein accumulation in cells.
3. Changes of AKT/MTOR in GW4869 regulation: Investigate the function of AKT/MTOR in the regulation of HBV replication in response to impaired exosome secretion.
4. Effects on autophagosome formation: Determine whether GW4869 increases the formation of autophagosomes.
5. Impact on HBV trafficking: Examine how GW4869 alters HBV trafficking along endosomal and autophagic pathways.
6. Promotion of amphisome formation: Identify whether GW4869 promotes the formation of amphisomes, serving as platforms for HBV secretion.
7. Roles of neutral sphingomyelinase: Investigate whether GW4869's modulation of HBV replication and trafficking is mediated through neutral sphingomyelinase.

8. Roles of RAB27A and -B in exosome-dependent HBV secretion: Determine whether RAB27A and -B control exosome-dependent HBV secretion.
9. Roles of RAB27A and -B in HBV distribution: Investigate whether silencing RAB27A and -B alters HBV trafficking along endosomal and autophagic pathways.
Through these comprehensive steps, we aimed to unravel the intricate connections between disruptions in the endosomal vesicle pathway, exosome secretion, and the life cycle of HBV, providing valuable insights into potential therapeutic targets for HBV-related interventions.

3. Materials and methods

3.1 Materials

3.1.1 Plasmids

The HBV plasmid pSM2 was kindly provided by Prof. Hans Will as previously reported [112].

3.1.2 Reagents

The list of the reagents used in the present study is shown as follows:

Name	Company
RPMI 1640 Medium	Gibco
DMEM High Glucose medium	Gibco
Opti-MEM® I (1×) Reduced Serum Medium	Gibco
Penicillin-streptomycin	Gibco
HEPES Buffer Solution	Gibco
MEM Non-Essential Amino Acids Solution	Gibco
Trypsin-EDTA	Gibco
HEPES Buffer Solution	Gibco
Fetal Bovine Serum (FBS)	Gibco
William’s Medium E	Biotech GmbH
2-propanol	Roche
DNAase I	Roche
DIG High Prime DNA Labeling	Roche

and Detection Starter Kit II	
G418	AppliChem
Tris	AppliChem
$MgCl_2$	MP BioMedicals
Glycine	AppliChem
Nonidet P-40	AppliChem
EDTA solution (pH 8.0)	AppliChem
Tris buffer (pH7.4 / 8.0 / 8.8)	AppliChem
Ethanol	AppliChem
Chloroform	Carl ROTH
Roti-phenol	Carl ROTH
NaCl	Carl ROTH
10× SDS-PAGE	Carl ROTH
10% SDS	Carl ROTH
4',6-Diamidino-2-phenylindole (DAPI)	Carl ROTH
Seal for microscopy	Carl ROTH
Stacking Gel Buffer	BIO-RAD
Resolving Gel Buffer	BIO-RAD
30% Acrylamide Solution	BIO-RAD
10x Tris/Glycine Buffer	BIO-RAD
10x Tris/Glycine Running Buffer	BIO-RAD
D-PBS	Invitrogen
Lipofectamine® 2000 Reagent	Invitrogen
TRIzol® Reagent	Invitrogen
Total Exosome Isolation	Invitrogen
Lysotracker Red	Invitrogen
Sodium Acetate (3M, pH 5.5)	Ambion
Fetal Bovine Serum	Sigma-Aldrich
TEMED	Sigma-Aldrich
Dimethyl sulfoxide (DMSO)	Sigma-Aldrich
Cell Counting Kit-8	Sigma-Aldrich

Acridine Orange	Sigma-Aldrich
Amersham ECL Western blotting Reagent	GE Healthcare
Amersham Protran 0.45 NC	GE Healthcare
QIAprep Spin Miniprep Kit	Qiagen
QIAGEN Plasmid Midi Kit	Qiagen
QIAGEN Plasmid Maxi Kit	Qiagen
DNA Blood Mini Kit	Qiagen
QuantiFast SYBR Green RT-PCR kit	Qiagen
Proteinase K	Qiagen
RNase A	Qiagen
Red lysis & Loading Buffer	Cell Signaling
Western Lightning Ultra, Chemiluminescent Substrate	PerkinElmer
Tween 20	Biochemica
peqGOLD protein marker IV (10-170kDa)	Peqlab
Yeast RNA	Ambion
Protein A/G Sepharose	Abcam
Calpeptin	Sigma-Aldrich
Y27632	Sigma-Aldrich
GW4869	Sigma-Aldrich
Imipramine	Sigma-Aldrich
Endosindin2	Sigma-Aldrich
CID1067700	Sigma-Aldrich
Chloroquine	Sigma-Aldrich
EBSS	Thermo Fisher

3.1.3 Buffers

The list of buffers used in the present study is shown as follows:

Name	**Component**
Lysis buffer for HBV EcDNA extraction	50 mM Tris pH 7.4 1 mM EDTA

	1% Nonidet P-40
Denaturation buffer	1.5 M NaCl 0.5 M NaOH
Neutralization buffer	2.0 M NaCl 1.0 M Tris-base 2.5% hydrochloric acid
Wash buffer 1 for Southern blotting	2× SSC; 0.1% SDS
Wash buffer 2 for Southern blotting	0.1× SSC; 0.1% SDS
12 % SDS Separation gel (10 ml)	3.3 ml ddH_2O 4.0 ml 30% acrylamide 2.5 ml 1.5M Tris pH 8.8 100 µl 10% SDS 100 µl 10% AP 4 µl TEMED
5% SDS Concentration gel (5 ml)	3.15 ml deionized water 720 µl 30 % acrylamide 540 µl 1.0 M Tris pH 6.8 45 µl 10% SDS 25 µl 10% AP 5 µl TEMED
10× TBS	0.5 M Tris-HCl, pH 7.6 1.5 M NaCl

3.1.4 Instruments

The list of all the instruments used in the present study is shown as follows:

Name	**Company**
-20 °C Freezer	AEG, Germany
-80 °C Freezer	Thermo Forma, Germany
Amersham Hybond^{TM}-N^{+}	GE Healthcare, USA
BIO WIARD KOJAIR	BIO-FLOW Technik, Germany
Hybridization Oven/Sharker	Amersham Pharmacia, USA

Model 785 Vacuum Blotter	BIO-RAD, USA
CAWOMAT 2000 IR	CAWO photochemisches Werk GmbH, Germany
Centrifuge	Eppendorf, Germany
CO_2 incubator	BINDER, Germany
Rotor-Gene Q	Qiagen, Germany
Sample Bag for BetaplateTM Maximum membranes Size 102*258mm	PerkinElmer
FUJI medical X-ray film (18×24)	FUJI FILM Corporation
Cover glasses	ZEISS
LSM710 Confocal Microscope	ZEISS

3.1.5 siRNAs

The sequences of all siRNAs used in the present study are purchased from Qiagen and shown as follows:

Name	Product Name	GeneGlobe ID
siR-C	Allstars Negative Control siRNA	SI03650318
siATG5	Hs_APG5L_6 FlexiTube siRNA	SI02655310
siRAB27A	Hs_RAB27A_7 FlexiTube siRNA	SI00065541
siRAB27B	Hs_RAB27B_4 FlexiTube siRNA	SI00060428
siSMPD2	Hs_SMPD2_8 FlexiTube siRNA	SI04142838

3.1.6 Primers

The sequences of commercial used in the present study are purchased from Qiagen and shown as follows:

Name	Product Name	Cat.No.
SMPD2	Hs_SMPD2_1_SG QuantiTect Primer Assay	QT01008581
β-actin	Hs_ACTB_2_SG QuantiTect primer assay	QT01680476

The synthesized primer pairs were used as follows:

HBV RNA primers: 5'- CCGTCTGTGCCTTCTCATCT -3' (sense) and 5'- TAATCTCCTCCCCCAACTCC -3' (anti-sense).

HBV DNA primers: 5'-GTTGCCCGTTTGTCCTCTAATTC-3' (sense) and 5'-GGAGGGATACATAGAGGTTCCTT-3' (anti-sense).

3.1.7 Antibodies

Antibodies against the following proteins were used:

Name	Source	Company
AKT	Rabbit pAb	Cell Signaling Technology
phospho-AKT	Rabbit pAb	Cell SignalingTechnology
MTOR	Rabbit pAb	Cell Signaling Technology
phospho-MTOR	Rabbit mAb	Cell Signaling Technology
AMPK	Rabbit pAb	Cell Signaling Technology
phospho-AMPK	Rabbit pAb	Cell Signaling Technology
ULK1	Rabbit pAb	Cell Signaling Technology
phospho- ULK1 S555	Rabbit pAb	Cell Signaling Technology
anti-p62	Rabbit pAb	Cell Signaling Technology
anti-LC3	Rabbit pAb	Cell Signaling Technology
anti-LC3	Mouse mAb	Cell Signaling Technology
p70S6 K	Rabbit pAb	Cell Signaling Technology
phospho-p70S6 K	Rabbit mAb	Cell Signaling Technology
anti-RAB5A	Rabbit pAb	Cell Signaling Technology
anti-EEA1	Mouse mAb	Cell Signaling Technology
anti-LAMP1	Rabbit mAb	Cell Signaling Technology
anti-PDI	Rabbit mAb	Cell Signaling Technology
anti-Bip	Rabbit mAb	Cell Signaling Technology
anti-eIF2α	Rabbit mAb	Cell Signaling Technology
phospho- eIF2α	Rabbit mAb	Cell Signaling Technology
anti-ATF6	Rabbit mAb	Cell Signaling Technology
anti-RAB27A	Rabbit mAb	Cell Signaling Technology
anti-RAB27B	Rabbit mAb	Cell Signaling Technology
anti-HBsAg	Rabbit mAb	Cell Signaling Technology
anti-HBcAg	Rabbit mAb	Cell Signaling Technology

anti-CD63	Mouse mAb	Santa Cruze
Anti-HBsAg	Horse hAb	Abcam
anti-β-actin	Mouse mAb	Sigma
IgG	Mouse mAb	Sigma

Secondary antibodies against the following proteins were used:

Name	**Reactivity**	**Company**
Alexa Fluor 488-conjugated	Mouse	Cell Signaling Technology
Alexa Fluor 488-conjugated	Rabbit	Cell Signaling Technology
Alexa Fluor 594-conjugated	Mouse	Cell Signaling Technology
Alexa Fluor 594-conjugated	Rabbit	Cell Signaling Technology
Alexa Fluor 594-conjugated	Horse	Cell Signaling Technology
Alexa Fluor 647-conjugated	Rabbit	Cell Signaling Technology

3.2 Methods

3.2.1 Plasmid extraction

The transformation of plasmids into *E. coli* strains (DH5α, Invitrogen) were performed according to the manufacturer's instructions.

(1) Take competent cells out of -80 °C and thaw on ice (approximately 20-30 min).

(2) Remove agar plates (containing the appropriate antibiotic) from storage at 4 °C and let them warm up to room temperature.

(3) Mix 1-5 μl of DNA (usually 10 pg-100 ng) into 20-50 μl of competent cells in a 1.5 ml microcentrifuge. Gently mix by flicking the bottom of the tube with your finger a few times.

(4) Incubate the competent cells/DNA mixture on ice for 20-30 min.

(5) Heat shock each transformation tube by placing the bottom 1/2 to 2/3 of the tube into a 42 °C water bath for 90-120 s.

(6) Put the tubes back on ice for 2 min.

(7) Add 300 μl LB or SOC media (without antibiotic) to the bacteria and grow in 37 °C shaking incubator for 45-60 min.

(8) Plate some or all of the transformation onto a 10 cm LB agar plate containing the appropriate antibiotic.

(9) Incubate plates at 37 °C overnight.

(10) Pick a single colony from a freshly streaked selective plate and inoculate a starter culture of 2-5 ml LB medium containing the appropriate selective antibiotic. Incubate for approx. 8 h at 37 °C with vigorous shaking (approx. 300 rpm).

(11) Dilute the starter culture 1/500 to 1/1000 into a selective LB medium. For high-copy plasmids, inoculate 25 ml medium with 25-50 µl of starter culture. For low-copy plasmids, inoculate 100 ml medium with 250-500 µl of starter culture. Grow at 37 °C for 12-16 h with vigorous shaking (approx. 300 rpm)

(12) Harvest the bacterial cells by centrifugation at 6,000 g for 15 min at 4 °C.

(13) Resuspend the bacterial pellet in 4 ml (high-copy plasmids) or 10 ml (low-copy plasmids) Buffer P1.

(14) Add 4 ml or 10 ml Buffer P2, mix thoroughly by vigorously inverting the sealed tube 4-6 times, and incubate at room temperature (15-25 °C) for 5 min.

(15) Add 4 ml or 10 ml of chilled Buffer P3, mix immediately and thoroughly by vigorously inverting 4-6 times, and incubate on ice for 15 min or 20 min.

(16) Centrifuge at 15,000 g for 30 min at 4 °C. Collect the supernatant containing plasmid DNA promptly. Re-centrifuge the supernatant at 15,000 g for 15 min at 4 °C. Collect the supernatant containing plasmid DNA promptly.

(17) Equilibrate a QIAGEN-tip 100 or QIAGEN-tip 500 by applying 4 ml or 10 ml Buffer QBT, and allow the column to empty by gravity flow.

(18) Apply the supernatant from step 16 to the QIAGEN-tip and allow it to enter the resin by gravity flow.

(19) Wash the QIAGEN-tip with 2 x 10 ml or 2 x 30 ml Buffer QC.

(20) Elute DNA with 5 ml Buffer QF.

(21) Precipitate DNA by adding 3.5 ml (0.7 volumes) room-temperature isopropanol to the eluted DNA. Mix and centrifuge immediately at 15,000 g for 30 min at 4°C. Carefully decant the supernatant.

(22) Wash the DNA pellet with 2 ml room-temperature 70% ethanol, and centrifuge at 15,000 g for 10 min. Carefully decant the supernatant without disturbing the pellet.

(23) Air-dry the pellet for 5-10 min, and redissolve the DNA in 100 µl sterile water. DNA concentration was quantified by NanoDrop microvolume spectrophotometers.

(24) Finally, purified plasmid DNA was confirmed by restriction enzyme digestion.

3.2.2 Cell culture and transfection

The human hepatoma cell line HepG2.2.15, which harbors integrated dimers of the HBV genome (GenBank Accession Number: U95551) and shows a constantly detectable level of HBV replication, was cultured in RPMI-1640 medium (Gibco, USA) with 10% fetal bovine serum (FBS, Gibco), 100 U/ml penicillin-streptomycin (Gibco), 10% NEAA (Gibco), 10% HEPES (Gibco) and 500 μg/ml G418 (AppliChem, Germany). Another human hepatoma cell line Huh7 was cultured in Dulbecco's Modified Eagle's Medium (DMEM, Gibco) and supplemented with 10% FBS, 100 U/ml 100 U/ml penicillin-streptomycin, 10% NEAA, and 10% HEPES. Primary human hepatocytes were kindly provided by Dr. Ruth Broering, University Hospital Essen, which were cultured in William E medium with 250 μl insulin, 2% DMSO, and 125 μl hydrocortisone hemisuccinate. All cell cultures were incubated in a humidified atmosphere containing 5% CO_2 at 37 ºC.

The cultivation and viral infection of primary human hepatocytes are shown as follows:

(1) 2 days before HBV infection, separate the PHHs from patient and seed them into a 12-well plate.

(2) 1 day before HBV infection, wash the cells with PBS one time. PHHs were incubated with 20 μl HBV virion (2×10^{10} copies/ml, 1:50) and 1 ml WM1 medium (WM2 medium + PEG 8000) at 37 °C for 24 h.

(3) At the end of incubation (0-day post-HBV infection), wash the cells with PBS 3 times. Then PHHs were incubated with 1 ml WM2 medium.

(4) At 2, 4, and 6, days post HBV infection, harvest the supernatant, wash the cells with PBS 1 time, and change new medium with 1 ml WM2 medium.

(5) At 10 days post HBV infection, harvest the supernatant to detect HBsAg and HBeAg, wash the cells with PBS 1 time, and change with a no-glucose medium and culture for 48 h or 72 h.

(6) At 13 days (72 h post-treatment), collect the supernatant and cells for further detection.

Plasmids or siRNAs were transfected into cells at indicated concentrations using the Lipofectamine 2000 transfection reagent (Invitrogen) according to the manufacturer's instructions. The protocol of transfection used in this study is as follows:

(1) 1 day before transfection, seed HepG2.2.15 cells/Huh7 cells into a 6-well plate.

(2) On the day of transfection, dilute 1.5 μl of 20 μM siRNA into 250 μl Opti-MEM (Solution A).

(3) Dilute 5 μl Lipo2000 into 250 μl Opti-MEM (Solution B), and incubate them at room temperature for 5 min.

(4) Add 250 μl Opti-MEM (Solution A) into 250 μl Opti-MEM (Solution B), and incubate the complex at room temperature for 20 min.

(5) Discard the old medium from a 6-well plate, and wash with PBS once.

(6) Add 1 ml Opti-MEM® I (1×) Reduced Serum Medium (Gibco) into each well, and then add 500 μl Lipo2000-siRNA complex (from step 4) drop by drop.

(7) 4-6 hours later, change the new medium with 2 ml 1640/DMEM medium with 10%FBS, then put the cells at 37 ºC in a humidified atmosphere until the interested time points.

3.2.3 RNA extraction

Total cellular RNA was extracted by using Trizol reagent (Invitrogen, Switzerland), followed by digestion with the DNase Set (Roche, Switzerland). The protocol of RNA extraction in detail is as follows:

(1) Collect the cells from a 12-well plate with 500 μl Trizol reagent by pipetting the cells up and down several times.

(2) Incubate the homogenized sample for 5 min at room temperature to permit complete dissociation of the nucleoprotein complex.

(3) Add 100 μl chloroform, and shake the samples vigorously by hand for 15 s.

(4) Incubate at room temperature for 2-3 min. Centrifuge at 12,000 g at 4 °C for 15 min.

(5) Transfer the aqueous phase (about 250 μl) to a new 1.5 ml EP tube and add 250 μl isopropanol.

(6) Incubate at room temperature for 10 min. Centrifuge at 12,000 g at 4 °C for 10 min.

(7) Remove the supernatant from the tube, and wash the RNA pellet with 100 μl 75% ethanol.

(8) Vortex the samples briefly, and centrifuge at 12,000 g at 4 °C for 5 min.

(9) Discard the supernatant, and air dry the RNA pellet for 5-10 min.

(10) Finally, elute the RNA into 50 µl RNase-free water. Measure the concentration of RNA by NanoDrop microvolume spectrophotometers.

(11) The concentration of all samples is then diluted into 100 ng/µl by adding RNase-free water, and then stored at -80 °C or for real-time RT-PCR.

3.2.4 Real-time RT-PCR

The levels of relative mRNA expression in cells were determined by real-time RT-PCR analysis using a commercial QuantiFast SYBR Green RT-PCR kit (Qiagen, Germany). HBV RNA levels in cells were also measured using real-time RT-PCR with the primer pair: 5'-CCGTCTGTGCCTTCTCATCT-3' (forward) and 5'-TAATCTCCTCCCCCAACTCC-3' (reverse). Finally, the ratio of mRNA levels was normalized to internal control beta-actin. The protocol of real-time RT-PCR for RNA is as follows:

Reaction mixture as follows:

Component	Volume (20 µl)
2× SYBR Green RT-PCR Master Mix	10 µl
10× primers	2 µl
QuantiFast RT mix	0.2 µl
RNase-free water	6.8 µl
Template RNA	1 µl

cycler conditions:

(1) 50 °C, 10 min for reverse transcription

(2) 95 °C, 5 min for initial activation of Hotstar Taq DNA polymerase

(3) 95 °C, 10 s for denaturation

(4) 60 °C, 30 s for annealing and extension step

40 cycles for DNA (steps 3 to 4)

3.2.5 Analysis of HBV gene expression

Quantification of the levels of HBsAg and HBeAg in the supernatants:

The levels of HBsAg and HBeAg in the culture medium were determined using the Architect System and the HBsAg and HBeAg CMIA kits (Abbott Laboratories, Germany) according to the manufacturer's instructions.

Quantification of the levels of HBsAg and HBeAg in the cells:

The cells were collected in 500 µl PBS and frozen/thawed for 4 cycles. The pellets were removed by centrifugation at 6,000 g for 5 min. The supernatants were used for HBsAg and HBeAg detection by the Architect System and the HBsAg and HBeAg CMIA kits.

Quantification of HBV DNA levels:

HBV progeny DNA was extracted from the culture medium using the DNA Blood Mini Kit (Qiagen) and quantified by real-time polymerase chain reaction (PCR) (Invitrogen).
HBV DNA was extracted from intracellular core particles in hepatoma cell lines and detected by real-time PCR (mention below).
The protocol of quantitative real-time PCR for quantification of total HBV DNA levels is as follows:
Purification of HBV DNA from culture medium:

(1) Pipette 20 µl QIAGEN Protease into the bottom of a new 1.5 ml EP tube.

(2) Add 200 µl culture medium to the EP tube.

(3) Add 200 µl Buffer AL to the sample. Mix by pulse-vortexing for 15 s.

(4) Incubate at 56 °C for 10 min.

(5) Add 200 µl ethanol (96–100%) to the sample, and mix again by pulse-vortexing for 15 s.

(6) Carefully apply the mixture from step 5 to the QIAamp spin column without wetting the rim, close the cap, and centrifuge at 6,000 g for 1 min. Place the QIAamp spin column in a clean 2 ml collection tube, and discard the tube containing the filtrate.

(7) Carefully open the QIAamp spin column and add 500 µl Buffer AW1 without wetting the rim. Close the cap and centrifuge at 6,000 g for 1 min. Place the QIAamp spin column in a clean 2 ml collection tube, and discard the collection tube containing the filtrate.

(8) Carefully open the QIAamp spin column and add 500 µl Buffer AW2 without wetting the rim. Close the cap and centrifuge at full speed for 3 min.

(9) Place the QIAamp spin column in a new 2 ml collection tube and discard the collection tube with the filtrate. Centrifuge at full speed for 1 min.

(10) Place the QIAamp spin column in a clean 1.5 ml EP tube, and discard the collection tube containing the filtrate. Carefully open the QIAamp spin column and add 50 µl ddH_2O.

Incubate at RT for 1 min, and then centrifuge at 6,000 g for 1 min.

(11) Store the samples at -20 °C or using as a template for real-time PCR for detecting HBV progeny DNA directly.

Reaction mixture for real-time PCR:

Component	Volume (20 μl)
2× UDG mix	10 μl
Hope-forward prime	0.4 μl
Hope-reverse prime	0.4 μl
$MgCl_2$	0.8 μl
BSA	1 μl
Template	2 μl
Aqua	5.4 μl

cycler conditions:

(1) 95 °C, 15 s for denaturation

(2) 60 °C, 15 s for annealing

(3) 72 °C, 10 s for extension step

45 cycles (steps 1 to 3)

3.2.6 Encapsidated DNA and southern blotting analysis

HBV replicative intermediates from intracellular core particles were extracted from hepatoma cell lines and detected by Southern blotting, respectively. The encapsidated HBV DNA in nucleocapsids was also detected by Southern blotting. However, HBV nucleocapsid in cell lysates was analyzed in a native agarose gel and then detected by Western blotting analysis.

The protocol of Southern blotting for detecting HBV replication is as follows:

EcDNA extraction:

(1) 3- or 4-days post-transfection wash the cells in a 6-well plate with PBS 1 time.

(2) Add 800 μl iced lysis buffer and incubate on ice for 10 min.

(3) Collect the cell lysates into a 2 ml EP tube, vortex vigorously for 15 s, and then incubate on ice for 10 min.

(4) Centrifuge at 13,200 rpm for 2 min.

(5) Transfer the supernatant to a new 2 ml EP tube, then add 8 μl of 1 M $MgCl_2$ and 8 μl of 10 mg/ml DNase I (Roche), mix gently, and incubate for 30 min at 37 °C.

(6) Shortly centrifuge, then add 40 μl of 0.5 M EDTA (pH 8.0) to a final concentration of 25 mM, mixed by the vortex.

(7) Shortly centrifuge, and add 80 μl 10% SDS, mix by the vortex.

(8) Shortly centrifuge, and add 20 μl 20 mg/ml proteinase K.

(9) Incubate at 55 °C for 2 h.

(10) Add 900 μl Phenol/chloroform mix into the tube for extraction, vortex, and static for 2 min, then centrifuge at 13,000 rpm at RT for 10 min.

(11) Suck up the first layer of liquid and add 0.7 V of isopropanol, 0.1 V of 3 M NaAc (pH 5.2), and 2 μl of 10 mg/ml yeast RNA, incubate overnight at -20 °C.

(12) 13,200 rpm at 4 °C for 15 min, discard the supernatant carefully.

(13) Wash the pellet with 1 ml 75% ethanol, up and down 2 times gently without disrupting the whole pellet, and centrifuge at 8,000 rpm at RT for 5 min. Discard the supernatant carefully, then air dry for 5-10 min.

(14) Dissolve the pellet in 15 μl ddH_2O.

(15) Dilute 1 μl of EcDNA pellet in 9 μl ddH_2O for real-time PCR as before.

Run agarose gel:

(16) Prepare 1% agarose gel.

(17) Electrophoresis for 1.5 h at 50 V.

(18) Wash with ddH_2O one time, then denaturation for 30 min at RT with gentle agitation.

(19) Wash with ddH_2O one time, then neutralize for 30 min at RT with gentle agitation.

(20) Wash the agarose gels with ddH_2O one time, and then soak in 20× SSC.

(21) Transfer the membranes (from down to up including white fiberboard, filter paper, Nylon membrane, green plastic membrane, and agarose gels), and cover the cover. 13Hg for 2 h.

(22) Fix DNA on the membranes at 150 J/cm^2 2 times.

Hybridization probe preparation:

(1) Digest plasmid pSM2 (1 μg/μl) which contains HBV dimer by restriction enzyme EcoR I.

Component	Volume (100 µl)
EcoR I	1 µl
10× NEB 2	10 µl
pSM2	10 µl
Aqua	79 µl

(2) After digestion at 37 °C for 2 h, 25 µl 5× green loading buffer was added. Run 0.8% agarose gel at 130 V for 2 h to separate two bands (3.2 kb for HBV fragment and 2.7 kb for vector), and cut 3.2 kb band for agarose gel extraction.

(3) Agarose gel extraction to quantify the HBV fragment concentration and dilute into 25 ng/µl. The HBV fragments were put at -80 °C for long-term storage or used directly for Southern blotting hybridization.

Hybridization:

(1) Add 1 µg template DNA (linear or supercoiled) and autoclaved, double distilled water to a final volume of 16 µl to a reaction vial.

(2) Denature the DNA by heating it in a boiling water bath for 10 min and quickly chilling it in an ice/water bath. Mix and then denature at 95 °C for 5 min.

(3) Mix DIG-High Prime thoroughly and add 4 µl to the denatured DNA, mix and centrifuge briefly. Incubate for 1 h or overnight at +37°C.

(4) Stop the reaction by adding 2 µl 0.2 M EDTA (pH 8.0) and/or by heating to +65°C for 10 min.

(5) Pre-heat an appropriate volume of DIG Easy Hyb buffer (10 ml/100 cm^2 filter) to hybridization temperature (+37 to +42°C). Prehybridize the filter for 30 min with gentle agitation in an appropriate container.

(6) Denature DIG-labeled DNA probe (about 25 ng/ml DIG Easy Hyb buffer) by boiling for 5 min and rapidly cooling in ice/water.

(7) Add denatured DIG-labeled DNA probe to pre-heated DIG Easy Hyb buffer (3.5 ml/100 cm^2 membrane) and mix well but avoid foaming (bubbles may lead to background).

(8) Pour off the prehybridization solution and add the probe/hybridization mixture to the membrane. Incubate overnight with gentle agitation.

(9) Wash 2 × 5 min in ample 2 × SSC, 0.1% SDS at +15 to +25°C under constant agitation.

(10) Wash 2 × 15 min in 0.5 × SSC, 0.1% SDS (prewarmed to wash temperature) at +65 to +68°C under constant agitation.

Immunological detection:

(11) After hybridization and stringency washes, rinse the membrane briefly (1-5) min in the Washing buffer.

(12) Incubate for 30 min in 100 ml Blocking solution.

(13) Incubate for 30 min in 20 ml Antibody solution.

(14) Wash 2 × 15 min in 100 ml Washing buffer.

(15) Equilibrate for 2-5 min in 20 ml Detection buffer.

(16) Place membrane with DNA side facing up on a development folder (or hybridization bag) and apply 1 ml CSPD ready-to-use (bottle 5). Immediately cover the membrane with the second sheet of the folder to spread the substrate evenly and without air bubbles over the membrane. Incubate for 5 min at +15 to +25°C.

(17) Squeeze out excess liquid and seal the edges of the development folder.

(18) Incubate the damp membrane for 10 min at +37°C to enhance the luminescent reaction.

(19) Expose to an appropriate imager for 5-20 min or to X-ray film for 15-25 min at +15 to +25°C.

3.2.7 Western blotting analysis

Western blotting analysis was performed to detect the relative protein expression. Briefly, after transfection or treatment, cells were washed with phosphate-buffered saline and lysed with 1× lysis buffer (Cell Signaling Technology, USA). Protein samples were resolved by sodium dodecyl sulfate-polyacrylamide (SDS) gel electrophoresis and then electrotransferred to nitrocellulose membranes. The membranes were incubated with the indicated primary antibodies overnight at 4 °C after being blocked with 5% milk in 1× TBST. The membranes were washed with 1× TBST and incubated (as appropriate) with a secondary peroxidase-affiniPure Rabbit anti-mouse IgG antibody (Jackson ImmunoResearch West Grove, USA) or a peroxidase-affiniPure goat anti-rabbit IgG

antibody (Jackson ImmunoResearch). Immunoreactive bands were visualized using an enhanced chemiluminescence system (GE Healthcare, UK).

The protocol of Western blotting in detail is as follows:

(1) Aspirate culture media from a 12-well plate, and wash the cells with PBS.

(2) Lyses the cells by adding 120 μl of 1× red lysis buffer (Cell Signaling Technology, USA). Scrape off the cells from the plate immediately and transfer them to a new precool 1.5 ml centrifuge tube.

(3) Heat the samples at 95 ºC for 10 min; then cool on ice.

(4) Prepare for SDS-PAGE gel.

(5) Load protein samples into SDS-PAGE gel: 2.5 μl protein marker/well, 8 μl sample/well for purpose band.

(6) Run at 90 V for 30 min first, and then change to 120 V for 1.5 h.

(7) Transfer to Nitrocellulose (NC) membrane, 250 mA for 1 h.

(8) Incubate the membranes in 5% milk at RT for 1 h.

(9) Wash the membranes with 1× TBST.

(10) Incubate the membranes in primary antibody (1:1,000, by 0.25% milk in 1×TBST) at 4 ºC overnight with gentle agitation.

(11) Wash the membranes with 1× TBST for 10 min 3 times.

(12) Incubate the membranes in 5 ml HRP-conjugated secondary antibody (1:15,000, by 0.25% milk in 1× TBST) at RT with gentle agitation for 1 h.

(13) Wash the membranes with 1× TBST for 10 min 3 times.

(14) Put the membrane in plastic wrap and add 600 μl ECL buffer/membrane, then put it into black-box for exposure.

3.2.8 HBV virion and naked capsid analysis

HBV virion and naked capsid were precipitated by Protein A/G Sepharose （Abcam, UK） after anti-HBsAg and anti-HBcAg incubation, respectively. HBV DNA in the precipitated particles was detected by real-time polymerase chain reaction (PCR) (Invitrogen) followed by extraction using the DNA Blood Mini Kit (Qiagen).

The protocol of HBV virion and naked capsid precipitation and detection in detail is as follows:

(1) Collect cell culture supernatant and centrifuge at 6,000 g for 5 min.

(2) Mix 200 μl of supernatant with indicative first antibody (usually 1:200 dilution) in a tube. Place the mixture on a slow-rotating mixer overnight at 4 ºC.

(3) Wash Protein A/G Sepharose (30 μl per sample) with PBS: Pipette the appropriate amount of Protein A/G Sepharose beads, briefly centrifuge, and aspirate the supernatant. Repeat this process three times, each time adding twice the volume of PBS.

(4) Resuspend the beads by adding an equal volume of PBS. Mix thoroughly using a pipette.

(5) Mix each sample with 30 μl Protein A/G Sepharose. Place the mixture on a slow-rotating mixer for 4 h, at 4 ºC.

(6) Subject beads and conjugated antibodies to sedimentation by short centrifugation and discarded the supernatant.

(7) Disrupt the bound particles by incubating each sample with 200 ul Buffer AL at room temperature for 10 min. Subsequently, perform DNA extraction using the QIAGEN DNA Kit and conduct real-time PCR to detect HBV DNA.

3.2.9 Exosome precipitation

The exosome in the supernatant was precipitated using the Total Exosome Isolation Reagent (Invitrogen, USA). Cells were cultured and treated in the presence of 10% FBS for 48 h and (after two PBS washes) without FBS for the last 24 h. The cell culture supernatant samples were collected and then performed according to the manufacturer's instructions.

The protocol of total exosome precipitation in detail is as follows:

(1) Collected supernatants were centrifuged at 2,000 x g for 30 min to remove cell debris.

(2) Each sample was combined with 1/2 volume of total exosome isolation reagent and mixed well by vortexing until a homogenous solution was formed.

(3) The samples were incubated at 4 °C overnight, then centrifuged at 4 °C at 10,000 x g for 1 h.

(4) The supernatant was aspirated and discarded, and the exosome pellet was resuspended with PBS buffer for DNA extraction and HBsAg/HBeAg detection. For protein detection in the exosome, directly lysis the exosome with red loading buffer and load on SDS-PAGE gel after boiling.

3.2.10 Immunofluorescence staining and quantification

Immunofluorescence (IF) staining was performed as described previously [113].

The protocol of immunofluorescence staining in detail is as follows:

(1) Remove the cell culture medium and wash with PBS.

(2) Fix the cells with 200 µl 4% formaldehyde, and incubate at RT for 10 min.

(3) Wash the cells with 200 µl PBS for 5 min 3 times.

(4) Incubate with 200 µl 0.1% Triton X-100 at RT for 10 min.

(5) Wash the cells with 200 µl PBS for 5 min 3 times.

(6) Block with 150 µl 5% FBS in PBS, at RT for 30 min.

(7) Wash the cells with 200 µl PBS for 5 min 3 times.

(8) Incubate with 150 µl primary-antibody (1:200) at RT for 1 h.

(9) Wash the cells with 200 µl PBS for 5 min 3 times.

(10) Incubate with 150 µl second-antibody (1:200) at RT for 1 h.

(11) Wash the cells with 200 µl PBS for 5 min 3 times.

(12) Incubate with 150 µl DAPI (1:1000) at RT for 10-15 min.

(13) Wash the cells with 200 µl PBS for 5 min 3 times.

(14) Mount coverslip with a drop of fluorescent mounting medium (Dako). Seal the coverslip and prevent drying and movement under a microscope.

(15) The samples were visualized with an LSM 710 microscope (Carl Zeiss, Germany) with a Plan-Apochromat 63×/1.40 oil Iris M27 objective. Images were acquired by ZEN acquisition software (Carl Zeiss, Germany) and analyzed by ImageJ software. The number of LC3B puncta in cells was quantified as described previously [96].

3.2.11 Cell proliferation assay

Cell proliferation was determined by a Cell Counting Kit-8 Assay kit (Sigma-Aldrich, USA) according to the manufacturer's protocol. The protocol of CCK8 in detail is as follows:

(1) Inoculate cells (about 1×10^4/well in 100 µl medium) in a 96-well plate. Pre-incubate the plate in a humidified incubator at 37 °C and with 5% CO_2.

(2) 24 h later, treated the cell with indicated small chemical reagents for the indicated time point.

(3) At the interested timepoint, add 10 µl of the CCK8 solution to each well of the plate. Note: Be careful not to introduce bubbles to the wells, as they interfere with the O.D. reading.

(4) Incubate the plate for 1 h in the incubator at 37 °C and with 5% CO_2.

(5) Measure the O.D. absorbance at 450 nm using a microplate reader.

3.2.12 Detection of lysosomal activity

The lysosomal activity was detected by acridine orange (AO) (Sigma) staining or Lysotracker Red (Invitrogen) staining. AO staining and Lysotracker Red staining were carried out as described previously [100]. The protocol of dye staining in detail is as follows:

(1) Prepare the working solution. Dilute the 1 mM Lysotracker Red stock solution in the growth medium to the final working concentration of 50 nM. Dilute acridine orange stock solution in the growth medium to the final working concentration of 5 µM.

(2) Remove the culture medium at the desired time point and add the prewarmed (37°C) probe-containing medium. Incubate the cells for 15 minutes for acridine orange staining and 30 minutes for incubation for Lysotracker Red staining.

(3) Next cells were washed with PBS and fixed with 200 µl 4% formaldehyde, incubated at RT for 10 min.

(4) Wash the cells with 200 µl PBS for 5 min 3 times.

(5) Incubate with 150 µl DAPI (1:1000) at RT for 10-15 min.

(6) Wash the cells with 200 µl PBS for 5 min 3 times.

(7) Mount coverslip with a drop of fluorescent mounting medium (Dako). Seal the coverslip and prevent drying and movement under a microscope.

(8) The fluorescent signals at 488 nm (green) or 594 nm (red) for AO or 594 nm (red) for Lysotracker Red were imaged with an LSM 710 confocal microscope (Carl Zeiss, Germany).

3.2.13 Statistical analysis

Data are presented as mean ± SEM. Statistical analyses were performed using Graph Pad Prism software version 7 (La Jolla, CA, USA). Analysis of variance with two-tailed Student’s t-test or by one-way ANOVA with a Tukey posttest was used to determine

significant differences. Differences were considered statistically significant when $p<0.05$. All experiments were repeated independently at least three times.

4. Results

4.1 Chemical inhibitors of exosome biogenesis modulate the production and release of HBV virions and SVPs.

4.1.1 Chemical inhibitors of exosome biogenesis modulate endosome and autophagosome formation in hepatoma cells.

Calpeptin, Y27632, GW4869, imipramine, and endosidin2, which are distinct small molecules targeting endosomal membrane trafficking or lipid metabolism [74], disrupt late endosome/MVB function and exosome biogenesis and secretion. Initially, we assessed the impact of these inhibitors on endosome and autophagosome formation in HepG2.2.15 cells. HepG2.2.15 cells were cultured with the indicated concentrations of these drugs. Cells were collected after 48 h and the samples were subjected to western blotting to detect proteins related to endosomes (RAB5A, EEA1, and CD63) and lysosomes (LAMP1, Lysosomal-associated membrane protein 1). The results showed that calpeptin, GW4869, and endosidin2 reduced the levels of RAB5A and its effector protein, EEA1, while others increased RAB5A and EEA1 levels (Figure 4.1, A). Minimal changes were observed in the levels of late endosome markers CD63. All the drugs elevated LAMP1 levels. Furthermore, all five drugs increased LC3-II levels, though to varying extents. Notably, calpeptin, GW4869, and imipramine significantly increased SQSTM1/p62 (sequestosome 1) and LC3-II levels, both in the absence and presence of chloroquine (CQ) (Figure 4.1, B), indicating enhanced autophagosome formation and decreased autophagic degradation. Y27632 increased LC3-II levels but decreased SQSTM1/p62 levels, while endosidin2 had a minor effect on LC3-II and p62. Thus, these drugs exhibited diverse impacts on endosome and autophagosome formation, as well as cargo degradation.

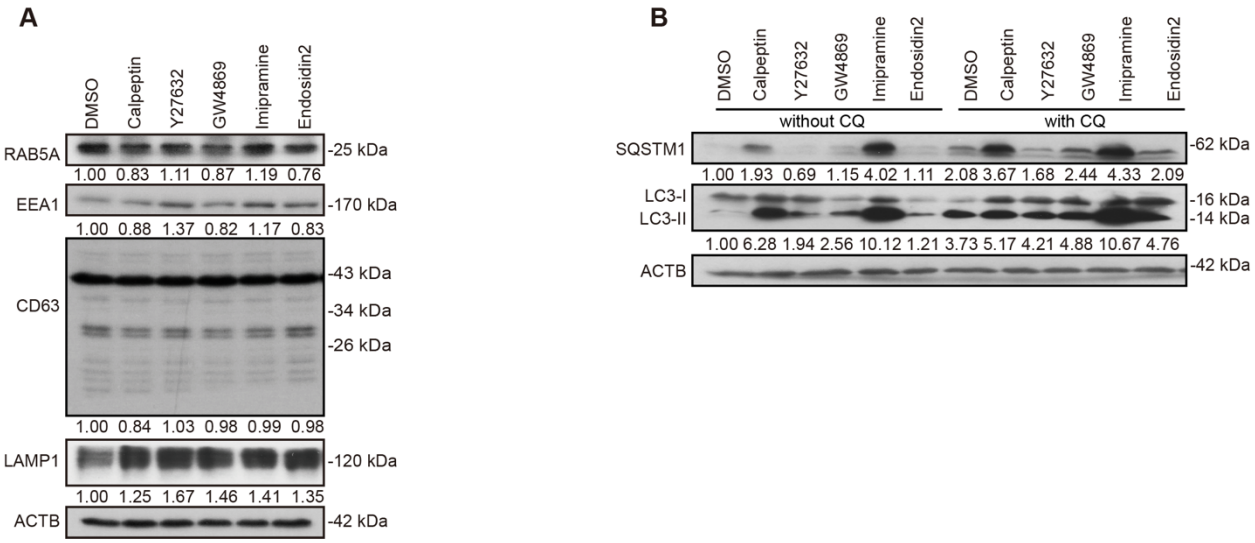

Figure 4. 1 Chemical inhibitors of exosome biogenesis modulate endosome and autophagosome formation in hepatoma cells

HepG2.2.15 cells were treated with Calpeptin (40 μM), Y27632 (5 μM), GW4869 (5 μM), imipramine (50 μM), and endosidin2 (30 μM) in the absence and presence of 10 μM CQ, and harvested after 48 h. (A) The expression levels of RAB5A, EEA1, CD63, and LAMP1 and (B) SQSTM1/p62 and LC3 were detected by western blotting. The relative levels of indicated proteins were determined by quantifying the grey scales of bands using ImageJ software and ACTB as a loading control.

4.1.2 Chemical inhibitors of exosome biogenesis have diverse effects on HBV progeny secretion and replication

To address the effects of these inhibitors on HBV replication, we detected the levels of intracellular (encapsidated) HBV DNA and HBsAg in HepG2.2.15 cells, and secreted HBV DNA, HBsAg, and HBeAg in culture supernatants after 72 h of treatment with the indicated drugs. Calpeptin and imipramine increased intra- and extracellular HBV DNA (Figure 4.2, A), along with elevated intra- and extracellular HBsAg levels (Figure 4.2, B). Notably, Y27632 only slightly increased intracellular HBV DNA levels but significantly reduced HBV DNA secretion, while leaving HBsAg and HBeAg levels unchanged. GW4869 treatment dramatically elevated intracellular HBV DNA and HBsAg levels but decreased extracellular HBV DNA levels with increased HBsAg and HBeAg production. Finally, endosidine2 had no notable effect on HBV replication.

Apparently, calpeptin and imipramine treatment strongly triggered cellular autophagy and concomitantly reduced autophagic degradation, corresponding to an increased release of HBV virions and subviral particles (SVPs). Y27632 increased autophagic degradation,

as evidenced by the increased LC3 expression level and decreased SQSTM1/p62 level, resulting in reduced HBV DNA secretion. Endosidine2 marginally affected endosomal and autophagic components, having no impact on HBV production and release. The most interesting was the significantly altered ratio between intra- and extracellular HBV DNA levels after GW4869 treatment, suggesting reduced release of HBV virions, leading to an accumulation of HBV virions or nucleocapsids. Therefore, we examined the effect of GW4869 on HBV production and release in detail.

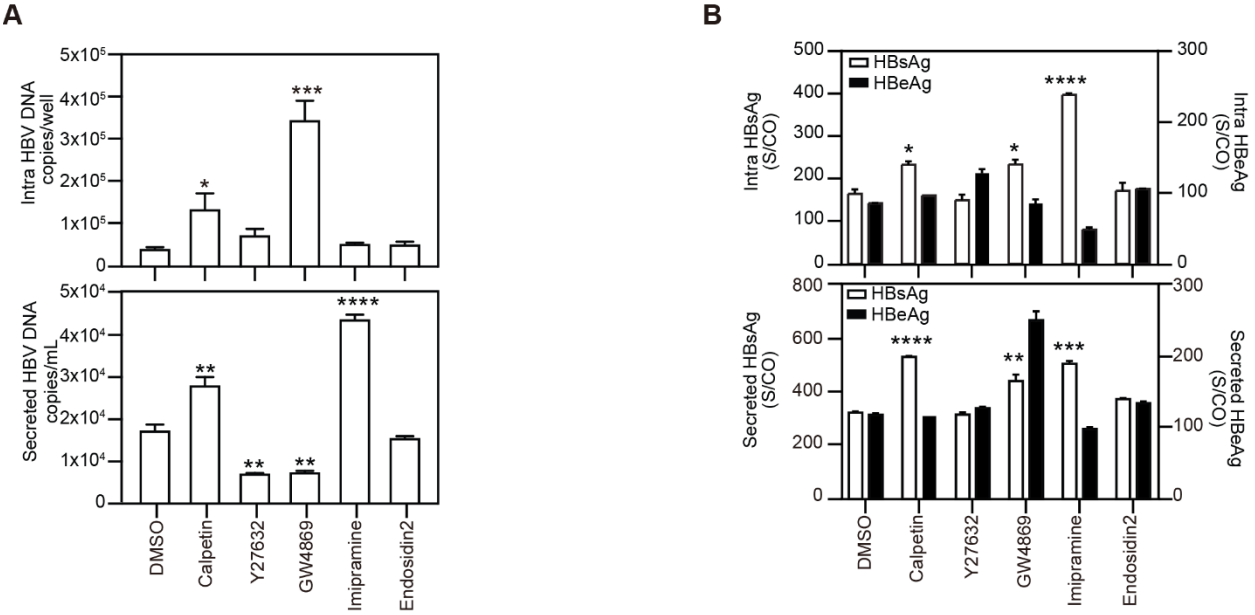

Figure 4. 2 Chemical inhibitors of exosome biogenesis have diverse effects on HBV secretion and replication

HepG2.2.15 cells were treated with Calpeptin (40 μM), Y27632 (5 μM), GW4869 (5 μM), imipramine (50 μM), and endosidin2 (30 μM), and harvested after 72 h. (A) The levels of encapsidated HBV replicative intermediates (Intracellular HBV DNA) and the levels of total HBV DNA in the culture supernatants were measured by real-time PCR. (B) HBsAg and HBeAg levels in the cell lysates (Intra, intracellular) and in the culture supernatants (secreted) were measured by CMIA. *P < 0.05; **P < 0.01; ***P < 0.001; ****P < 0.0001.

4.2 GW4869 treatment blocks HBV virion secretion and sequesters SVPs and virions within cells.

4.2.1 Selected concentrations of GW4869 did not affect cell proliferation

HepG2.2.15 and Huh7 cells were cultured with different concentrations of GW4869 ranging from 1 to 10 μM at indicated time points from 48 to 72 h, and cell viability was

monitored using the cell counting kit-8 (CCK-8) assay (Figure 4.3, A and B). According to the CCK-8 assay results, concentrations ranging from 1 to 5 μM did not affect cell proliferation of HepG2.2.15. The concentrations below 5 μM during the 48 h did not affect cell proliferation in Huh7 cells. Finally, concentrations below 5 μM for HepG2.2.15 and 2 μM for Huh7 cells were selected for further experiments. The experiments with Huh7 cells were analyzed at 48 h to reduce undesired effects on cell growth.

Figure 4. 3 Detection of cell viability by Cell Counting Kit 8 (CCK-8)

(A) HepG2.2.15 cells and (B) pSM2-transfected Huh7 cells were treated with different concentrations of GW4869 for 48 h and 72 h. Cell viability was determined by CCK-8 assay. *P < 0.05; **P < 0.01; ***P < 0.001; ****p < 0.0001; and ns, not significant.

4.2.2 GW4869 blocks HBV virion secretion at an early time point in HepG2.2.15 cells

The effects of GW4869 on HBV gene expression and replication were investigated in HepG2.2.15. First, the cells were treated with 2 and 5 μM of GW4869 for 4 h (Figure 4.4, A). GW4869 treatment slightly increased intracellular HBV DNA levels but effectively decreased HBV DNA levels in the culture supernatants at a concentration of 5 μM. GW4869 also slightly increased the levels of intracellular HBsAg but not that of secreted HBsAg. The levels of total HBV RNA were not changed by GW4869. A prolonged treatment with GW4869 for 72 h led to a great increase in the amount of intracellular HBV DNA in a dose-dependent manner, while the total secreted HBV DNA and HBV virion-associated DNA levels were significantly decreased (Figure 4.4, B). Moreover, the levels of intra- and extracellular HBsAg were also increased. Though the levels of total HBV RNA remained unchanged, the encapsidated HBV RNA was significantly inhibited by 5 μM GW4869. Additionally, the confocal microscopic analysis demonstrated that GW4869 treatment led to a significant increase in HBsAg and HBcAg expression levels (Figure 4.4, C).

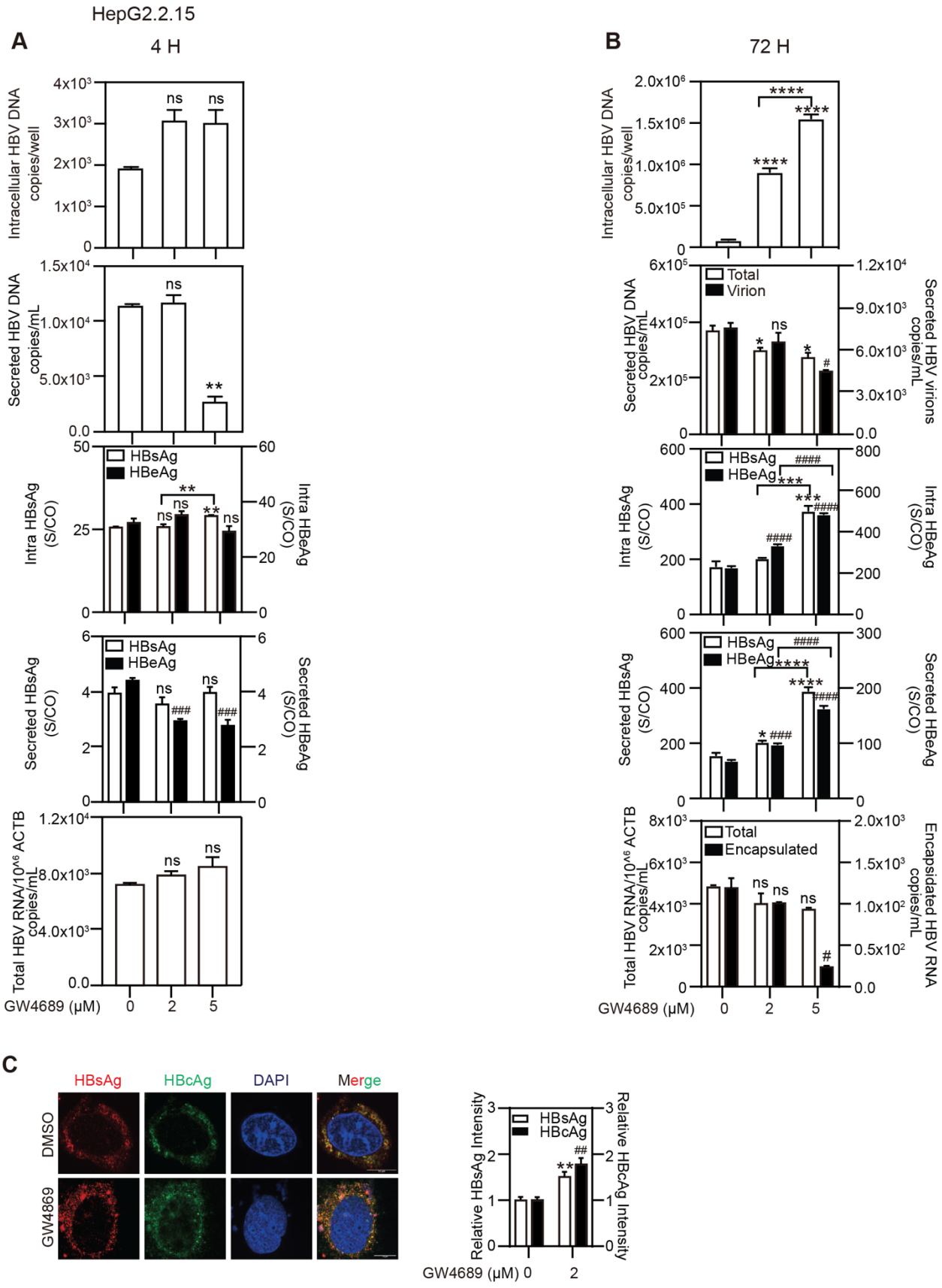
HepG2.2.15
A
4 H
Intracellular HBV DNA copies/well
Secreted HBV DNA copies/mL
Intra HBsAg (S/CO)
Intra HBeAg (S/CO)
Secreted HBsAg (S/CO)
Secreted HBeAg (S/CO)
Total HBV RNA/10^6 ACTB copies/mL
HBsAg
HBeAg
ns
GW4689 (μM) 0 2 5
B
72 H
Total
Virion
Secreted HBV virions copies/mL
Total
Encapsulated
Encapsidated HBV RNA copies/mL
C
HBsAg
HBcAg
DAPI
Merge
DMSO
GW4869
Relative HBsAg Intensity
Relative HBcAg Intensity
GW4689 (μM) 0 2

Figure 4. 4 GW4869 blocks HBV virion secretion at an early time point in HepG2.2.15 cells

HepG2.2.15 cells were treated with 2 and 5 μM GW4869 for (A) 4 h and (B) 72 h. The levels of intracellular HBV DNA, and the HBV virion-associated DNA levels in the culture supernatants were determined by real-time PCR. The levels of intracellular and secreted HBsAg and HBeAg were measured by CMIA. Total HBV RNAs and encapsidated HBV RNAs were extracted and quantified by real-time reverse transcription (RT)-PCR. (C) HepG2.2.15 cells were treated with 2 μM GW4869 for 48 h. The expression levels of HBsAg and HBcAg were detected by IF staining and confocal microscopy. Scale bar: 10 μm. *, $^{\#}P < 0.05$; **, $^{\#\#}P < 0.01$; $^{\#\#\#}P < 0.001$; ****, $^{\#\#\#\#}P < 0.0001$; and ns, not significant.

4.2.3 GW4869 blocks HBV virion secretion in Huh7 cells and primary human hepatocytes

Huh7 cells were transiently transfected with pSM2, a plasmid containing a dimeric wild-type HBV genome, and subsequently treated with 1 and 2 μM concentrations of GW4869 for 48 h (Figure 4.5, A). Following GW4869 treatment, the levels of intracellular HBV DNA markedly increased. However, GW4869 exhibited minimal to no effects on the secreted HBV virion-associated DNA levels, as well as intra- and extracellular HBsAg, and total HBV RNA levels at the given concentrations. Differing from HepG2.2.15 cells, GW4869 increased encapsidated HBV RNA in Huh7 cells at the concentration of 1 μM. Microscopic analysis revealed a significant increase in HBsAg expression levels in individual Huh7 cells (Figure 4.5, B). However, the total amount of intracellular HBsAg only slightly increased due to reduced cell growth post-GW4869 treatment.

To validate the principle in a more natural cell-culture model, primary human hepatocytes (PHHs) were infected with HBV, cultured for 8 days, and subsequently treated with 5 μM GW4869 for 48 h. After GW4869 treatment, the levels of secreted HBV DNA, HBsAg, and HBeAg decreased, while the total intracellular HBV RNA level slightly increased (Figure 4.5, C). Altogether, GW4869 treatment led to the intracellular accumulation of encapsidated HBV DNA and a reduction in HBV virion release.

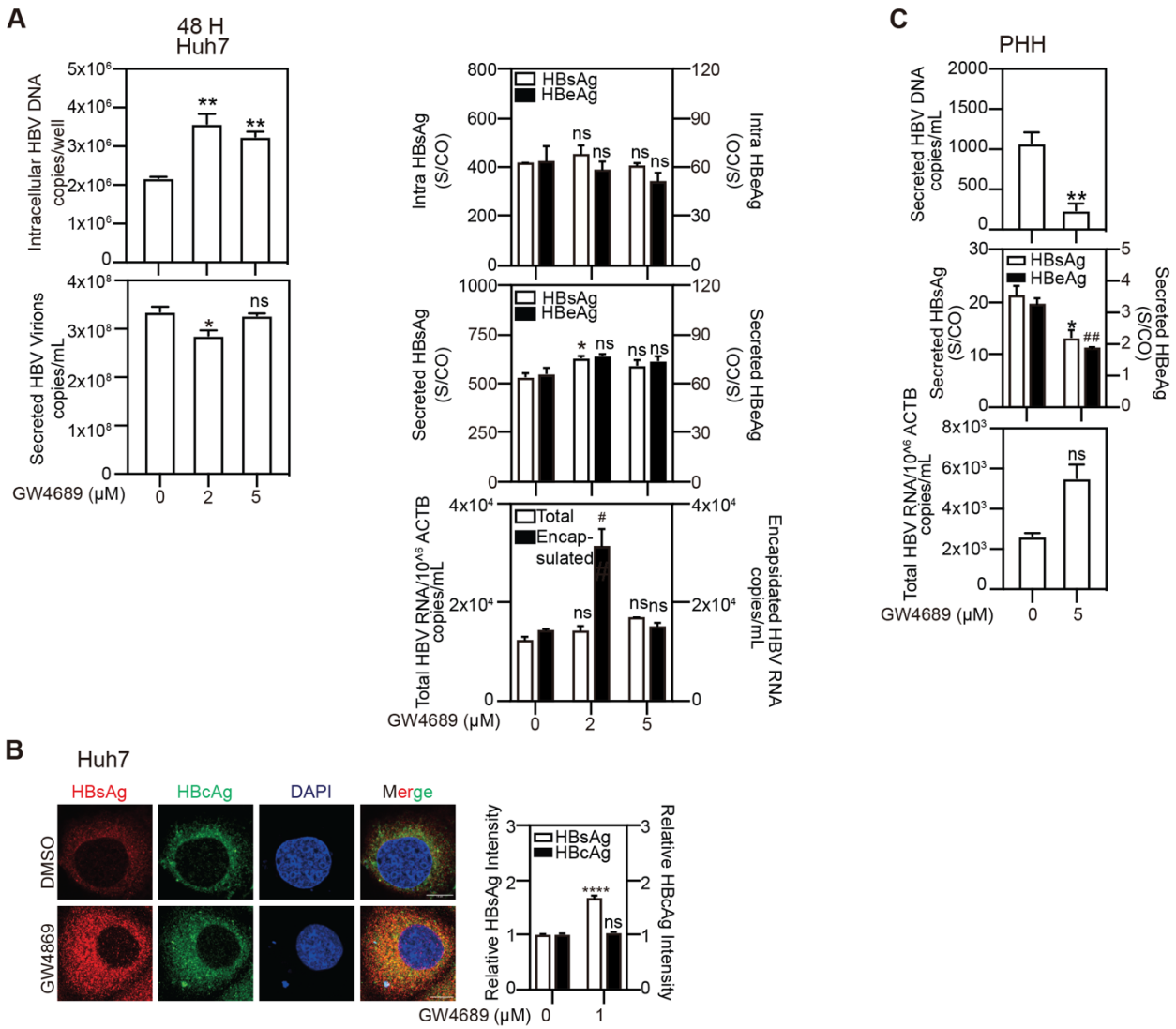

Figure 4. 5 GW4869 blocks HBV virion secretion in HBV-infected Huh7 cells and primary human hepatocytes

(A-B) Huh7 cells were transfected with a plasmid pSM2 with a replication-competent HBV genome dimer. 6 h post-transfection, the cells were treated with 1 and 2 μM GW4869 for 48 h. (A) The total HBV DNA level in the culture supernatants was measured by real-time PCR. The secreted HBsAg and HBeAg levels were measured by CMIA. HBV RNAs were extracted and quantified by real-time RT-PCR. (B) The expression levels of HBsAg and HBcAg were detected by IF staining and confocal microscopy. Scale bar: 10 μm. (C) Primary human hepatocytes (PHHs) were infected with purified HBV particles (MOI=30). Eight days post-infection, PHHs were treated with GW4869 at the concentration of 5 μM and harvested after 48 h. The total HBV DNA level in the culture supernatants was measured by real-time PCR. The secreted HBsAg and HBeAg levels were measured by CMIA. HBV RNAs were extracted and quantified by real-time RT-PCR. *P < 0.05; **P < 0.01; ****P < 0.0001; and ns, not significant.

4.3 GW4869 induces endoplasmic reticulum stress and inactivation of the AKT-MTOR signaling pathway.

4.3.1 GW4869 induces accumulation of HBsAg in the endoplasmic reticulum

Accumulation of HBV proteins on endoplasmic reticulum (ER) induce ER stress, triggering cellular autophagy to facilitate HBV replication and production [87, 109]. To invesgate whether GW4869-induced HBsAg accumulation was localized in the ER compartment, we utilized immunofluorescence (IF) staining and confocal microscopy. The fluorescence intensity of protein disulfide isomerase Family A Member 2 (PDIA2), an identified ER marker, and the percentage of PDIA2^{+}HBsAg increased from 5.3% to 12.1% after GW4869 treatment, compared to the DMSO control (Figure 4.6). These findings indicated that GW4869 treatment results in ER expansion and the accumulation of HBsAg within the ER.

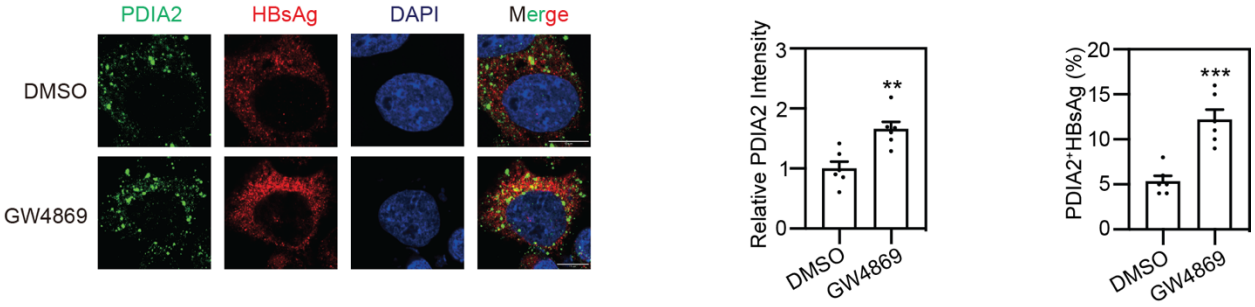

Figure 4. 6 GW4869 increases HBsAg accumulating in the endoplasmic reticulum

HepG2.2.15 cells were treated with 2 μM GW4869 for 48 h. The fluorescence intensity of PDIA2 and its colocalization with HBsAg was evaluated by IF staining and confocal microscopy. Scale bar: 10 μm. **P < 0.01; ***P < 0.001.

4.3.2 Accumulated HBV proteins induce endoplasmic reticulum stress

We then addressed the question of whether ER stress increases due to the accumulation of HBV proteins. HepG2.2.15 cells, pSM2-transfected Huh7 cells, and HBV-infected PHH were treated with the indicated concentrations of GW4869 for 48 h, and cell lysates were harvested. ER stress-related markers, including Immunoglobulin binding protein (Bip)/78-kDa glucose-regulated protein (GRP78), total and phosphorylated eukaryotic initiation factor 2alpha (eIF2α), and activating transcription factor 6 (ATF6), were detected by western blotting. The expression levels of PDI and the ER stress markers tested

increased after GW4869 treatment (Figure 4.7, A-C). Thus, GW4869 treatment induced HBsAg accumulation and then triggered ER stress in hepatic cells.

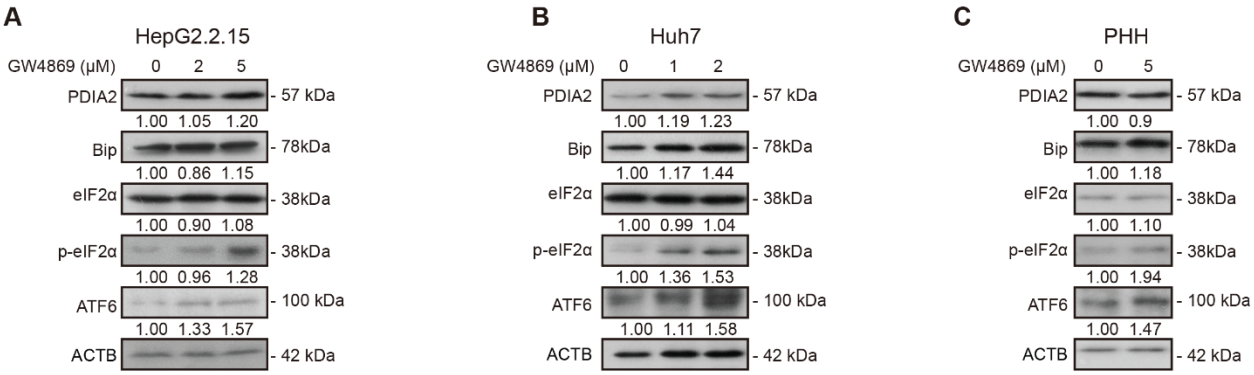

Figure 4. 7 Accumulated HBV proteins induce endoplasmic reticulum stress

(A) HepG2.2.15 cells, (B) pSM2-transfected Huh7 cells and (C) HBV-infected PHHs were treated with GW4869 for 48 h. The levels of PDIA2, Bip/GRP78, eIF2α, p-eIF2α, and ATF6 were detected by western blotting. The relative levels of indicated proteins were determined by quantifying the grey scales of bands using ImageJ software and ACTB as a loading control.

4.3.3 Increased ER stress inactivates the AKT-MTOR signaling pathway

Increased ER stress can modify the activation of the AKT-MTOR signal pathway HBV infection [109]. Therefore, we examined the levels of total and phosphorylated AKT and MTOR, along with their downstream molecules, in HepG2.2.15 cells, pSM2-transfected Huh7 cells, and HBV-infected PHH. GW4869 treatment reduced the levels of total and phosphorylated AKT and MTOR in HepG2.2.15 cells. Additionally, downstream molecules, including total and phosphorylated RPS6KB, were significantly decreased, especially at a GW4869 concentration of 5 μM (Figure 4.8, A). The levels of total ULK1 decreased but the levels of phosphorylated ULK1 were upregulated upon GW4869 treatment. However, in HBV *de novo* synthesized Huh7 cells and PHHs (Figure 4.8, B-C), GW4869 treatment increased the total AKT and MTOR expression levels but decreased the phosphorylated AKT and MTOR levels. Collectively, GW4869 inactivates the AKT-MTOR signaling pathway.

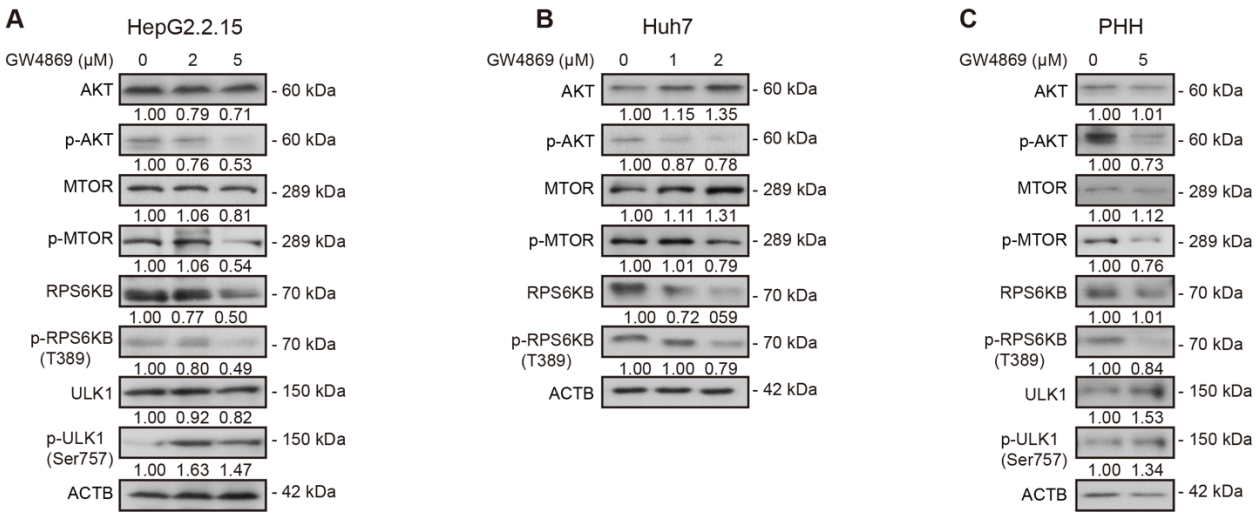

Figure 4. 8 Increased endoplasmic reticulum stress inactivates the AKT-MTOR signaling pathway

(A) HepG2.2.15 cells, (B) pSM2-transfected Huh7 cells and (C) HBV-infected PHHs were treated with GW4869 for 48 h. The levels of AKT, MTOR, RPS6KB, ULK1, and their corresponding phosphorylated forms were detected by western blotting. The relative levels of indicated proteins were determined by quantifying the grey scales of bands using ImageJ software and ACTB as a loading control.

4.3.4 GW4869 does not increase endoplasmic reticulum stress without HBV infection

PHHs were treated with GW4869 and cell lysates were collected for western blotting after 48 h treatment. In the absence of HBV infection, GW4869 showed minor effects on ER stress (Figure 4.9). This demonstrated that GW4869 induces the accumulation of HBV within cells, leading to ER stress in a feedback loop.

Taken together, GW4869 treatment effectively induces ER stress by causing the accumulation of HBV proteins in cells and inhibits the AKT-MTOR signaling pathway.

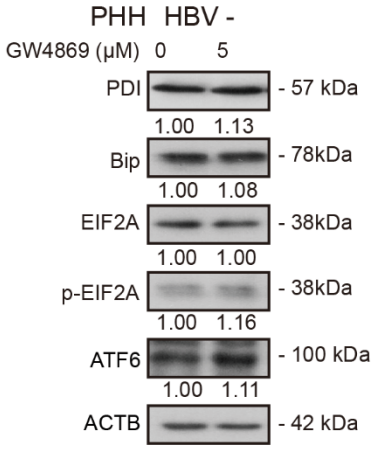

Figure 4. 9 GW4869 does not increase endoplasmic reticulum stress without HBV infection

PHHs were treated with GW4869 for 48 h. The levels of PDI, Bip/GRP78, eIF2α, p- eIF2α, and ATF6 were detected by western blotting. The relative levels of indicated proteins were determined by quantifying the grey scales of bands using ImageJ software and ACTB as a loading control.

4.4 GW4869 increases the formation of autophagosomes but prevents autophagic degradation by inhibiting autophagosome-lysosome fusion.

4.4.1 GW4869 increases the formation of autophagosomes and decreases degradation

Increased ER stress and the inhibition of the AKT-MTOR signaling pathway have been shown to induce cellular autophagy [96, 109]. Considering this, it was hypothesized that GW4869 treatment might augment cellular autophagy through the potentiation of ER stress and suppression of the AKT-MTOR signaling pathway. HepG2.2.15 cells and HBV-transfected Huh7 cells were treated with different concentrations of GW4869 for 48 h. Western blotting analysis demonstrated an accumulation of SQSTM1/p62 and LC3-II proteins after GW4869 treatment in a dose-dependent manner (Figure 4.10, A). Consistency with western blotting findings was confirmed by IF staining. IF staining also showed that GW4869 increased the immunofluorescence intensity of SQSTM1/p62 (Figure 4.10, B). GW4869 treatment resulted in an increased number of LC3 positive puncta and the immunofluorescence intensity of LC3, similar to CQ treatment (Figure 4.10, C). The increased p62 expression level suggested that GW4869 decreased autophagic degradation. To verify this, we conducted a DQ-Red BSA trafficking assay. Under normal conditions, DQ-Red BSA undergoes uptake, transportation to lysosomes, and subsequent cleavage by lysosomal hydrolases, resulting in robust red fluorescence. In this study, GW4869 treatment resulted in the remarkable reduction of DQ-Red BSA-derived fluorescence in HepG2.2.15 cells, suggesting reduced cargo degradation by lysosomes (Figure 4.10, D).

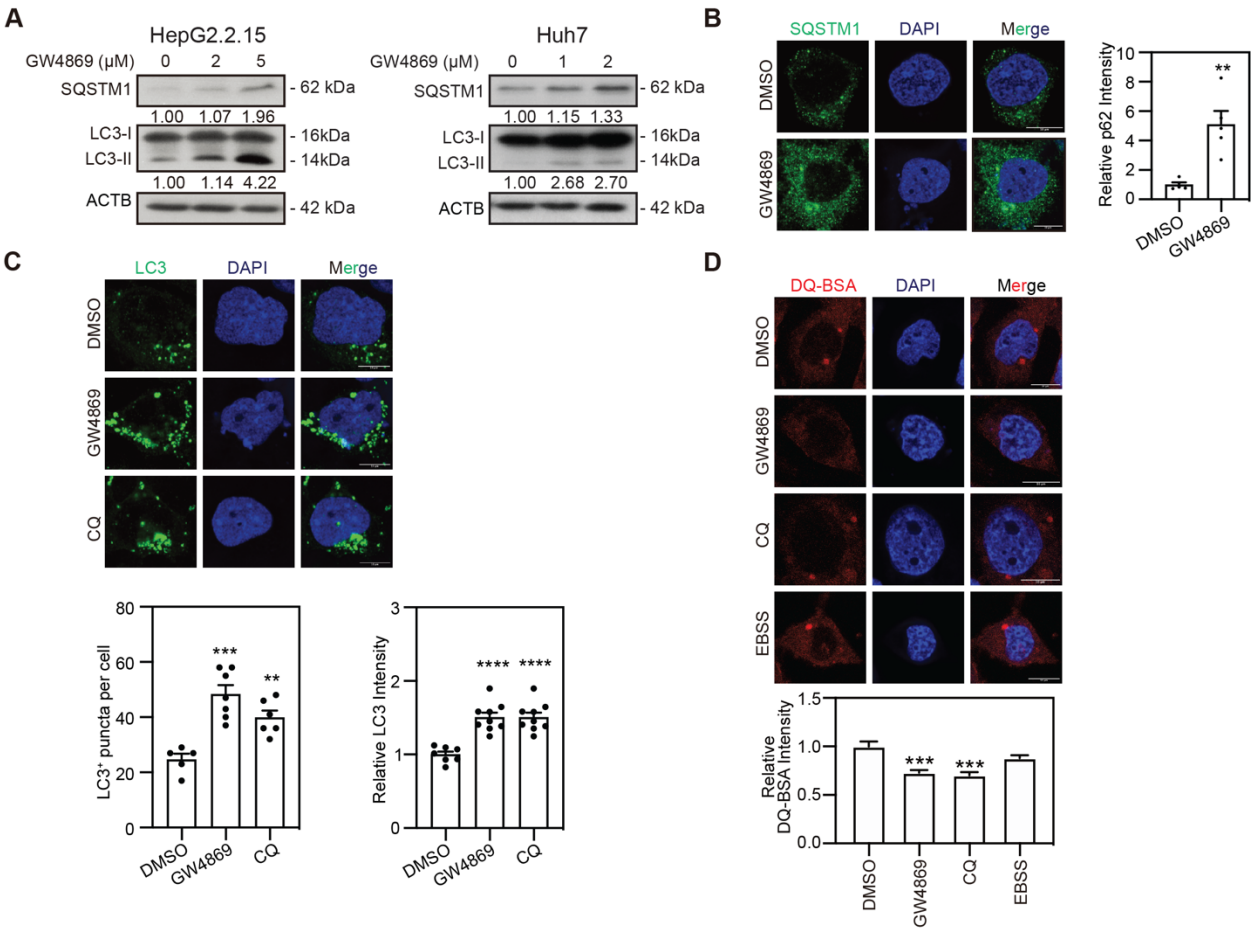

Figure 4. 10 GW4869 increases autophagosome formation and decreases its degradation

(A) HepG2.2.15 cells were treated with 2 and 5 μM GW4869, and pSM2-transfected Huh7 cells were treated with 1 and 2 μM GW4869 for 48 h. The levels of intracellular SQSTM1/p62 and LC3 were detected by western blotting. The relative levels of indicated proteins were determined by quantifying the grey scales of bands using ImageJ software and ACTB as a loading control. (B) HepG2.2.15 cells were treated with 2 μM GW4869 for 48 h. The relative fluorescence intensity of SQSTM1/p62 was detected by confocal microscopy. (C) HepG2.2.15 cells were treated with 2 μM GW4869 for 48 h and cells were treated with 10 μM CQ for 24 h as a positive control. The numbers of LC3 positive puncta per cell and the relative fluorescence intensity of LC3 were analyzed by ImageJ software. (D) HepG2.2.15 cells were treated with 2 μM of GW4869 for 48 h, followed by incubation with 10 mg/mL of DQ Red BSA for 30 min. The fluorescence signal of DQ Red BSA was analyzed by confocal microscopy. Scale bar: 10 μm. **p < 0.01; ***p < 0.001; ****p < 0.0001; and ns, not significant.

4.4.2 GW4869 does not change lysosome activity

We next investigated the reasons behind the observed reduction in lysosomal degradation. Drawing on prior studies, we considered two plausible explanations. First,

we examined the possibility of decreased lysosomal enzymatic activity. To assess this, we used the fluorescence dyes LysoTracker Red and acridine orange (AO) to detect lysosomal enzymatic activity. HepG2.2.15 cells were treated with GW4869 for 48 h and then stained with 100 nM LysoTracker Red for 1 h or 5 μM AO for 15 min. The fluorescence intensities of LysoTracker Red (Figure 4.11, A) or AO (Figure 4.11, B) in cells showed no significant changes with the GW4869 treatment, indicating preserved lysosomal enzymatic activity. Consequently, it was hypothesized that GW4869 might impede lysosomal degradation by preventing autophagosome-lysosome fusion. To assess this hypothesis, we employed IF staining and confocal microscopy to analyze the colocalization of autophagosome and lysosome markers, LC3 and LAMP1. GW4869-treated cells exhibited a reduced colocalization of LC3 and LAMP1 (Figure 4.11, D), providing evidence that GW4869 treatment impaired autophagosome-lysosome fusion, resulting in decreased autophagic degradation. In agreement with these results, a decreased colocalization of HBsAg and LAMP1 was evident upon GW4869 treatment (Figure 4.11, E), suggesting that the hindered degradation of HBsAg likely accounted for its intracellular accumulation. Collectively, these findings demonstrated that GW4869 prevents autophagic degradation by decreasing the fusion of autophagosomes with lysosomes without alterations in lysosome enzymatic activity.

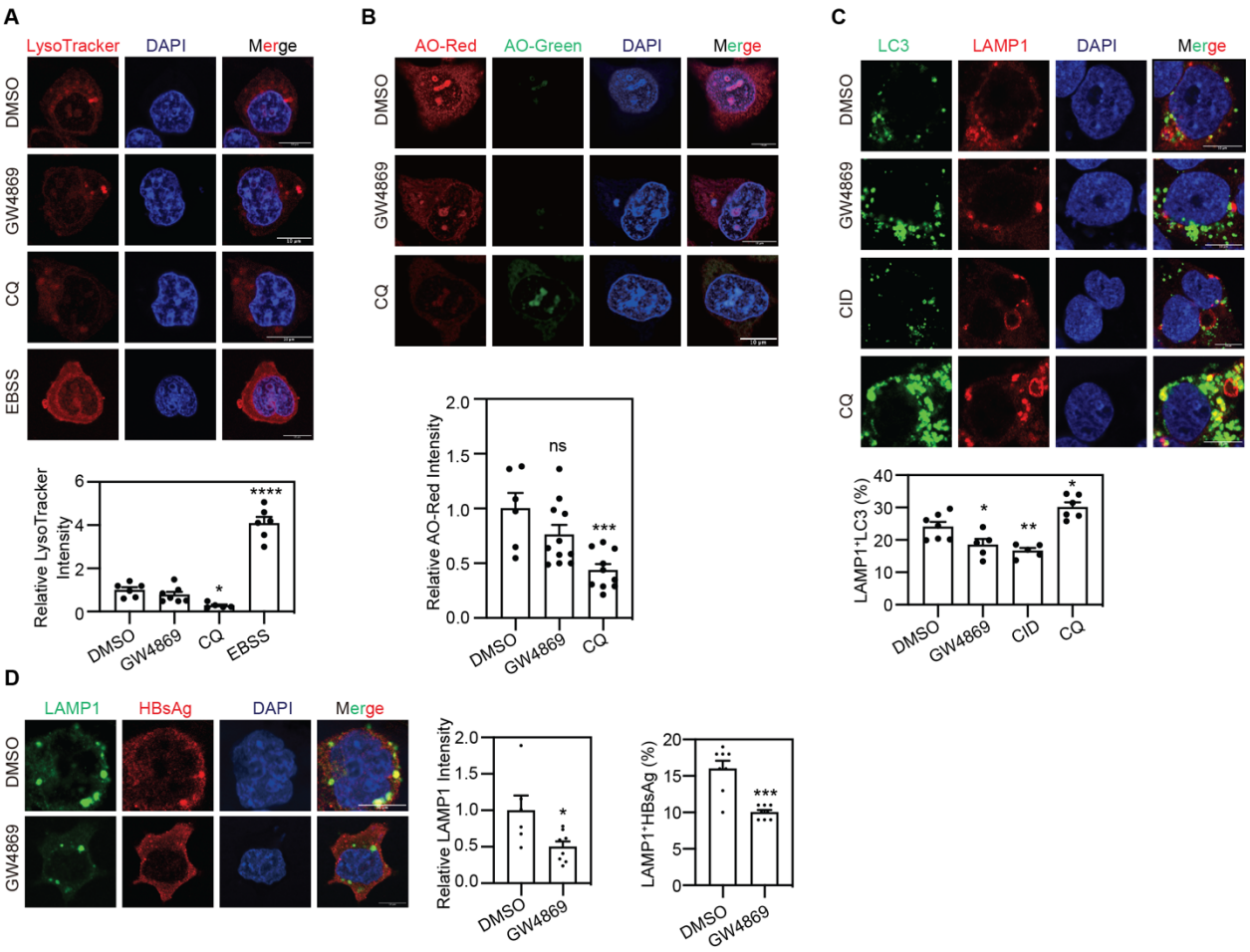

Figure 4. 11 GW4869 does not change lysosome activities

HepG2.2.15 cells were treated with 2 μM of GW4869 for 48 h, followed by incubation with (A) 10 mg/mL of DQ Red BSA for 30 min, (B) 100 nM of LysoTracker Red for 1 h or 5 μM of acridine orange (AO) for 15 min. Cells treated with 10 μM of CQ for 24 h or incubated with Earle's balanced salt solution (EBSS) for 2 h were used as control. The fluorescence signals of LysoTracker Red and AO fluorescence signal were analyzed by confocal microscopy. The fluorescence intensity of the markers of autophagosome (LC3), lysosome (LAMP1), and the colocalization of LC3 with LAMP1, and HBsAg with LAMP1 were analyzed using ImageJ software. Scale bar: 10 μm. *p < 0.05; **p < 0.01; ***p < 0.001; ****p < 0.0001; and ns, not significant.

4.5 GW4869 treatment promotes the association of HBV virions and SVPs with late endosomes/MVBs and autophagosomes.

4.5.1 GW4869 treatment blocks early endosome formation and impairs its association with HBV

Mechanistically, GW4869 inhibits the ceramide-mediated inward budding of the cell membrane, thereby impairing the formation of late endosomes/MVBs and the release of mature exosomes from MVBs [74]. To begin, we aimed to address how GW4869 treatment influences the formation of endosomes. HepG2.2.15 cells were treated with the indicated concentrations of GW4869. The expression levels of early endosome markers, RAB5A and EEA1, as well as late endosome/MVB markers, CD63 and CD81, and the lysosome marker LAMP1 were examined by western blotting analysis. Their association with HBV was detected by confocal microscopy. The western blotting results showed that the expression levels of RAB5A and its effector, EEA1, decreased after GW4869 treatment (Figure 4.12, A). Consistently, IF staining showed a lower immunofluorescence intensity of RAB5A and reduced colocalization of RAB5A and HBsAg following GW4869 treatment (Figure 4.12, B). These findings suggested that GW4869 impairs early endosome formation and functionality.

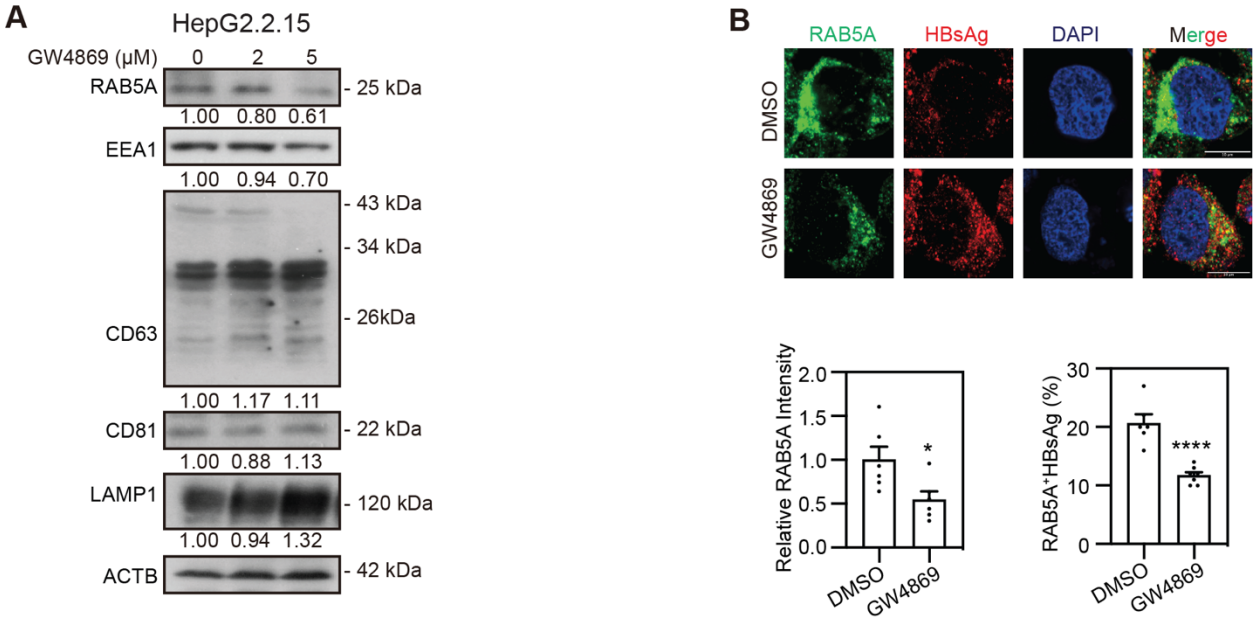

Figure 4. 12 GW4869 treatment blocks early endosome formation and impairs its association with HBV

HepG2.2.15 cells were treated with 2 μM GW4869 for 48 h. (A) The levels of intracellular RAB5A, EEA1, CD63, CD81, and LAMP1 were detected by western blotting. The relative levels of indicated proteins were determined by quantifying the grey scales of bands using ImageJ software and ACTB as a loading control. (B) The expressions of RAB5A and HBsAg were detected by IF staining and confocal microscopy. The colocalization was analyzed using ImageJ software. Scale bar: 10 μm. *p < 0.05; ****p < 0.0001.

4.5.2 GW4869 treatment enhances HBcAg transported to late endosomes

The expression levels of CD63 and CD81 were relatively unaffected by GW4869 treatment. However, GW4869 treatment prominently enhanced the colocalization of CD63 and HBcAg, while the colocalization of CD63 and HBsAg exhibited no substantial alteration (Figure 4.13). These results indicated that GW4869-mediated interference with late endosomes/MVBs promotes the association of HBcAg with $CD63^+$ late endosomes/MVBs.

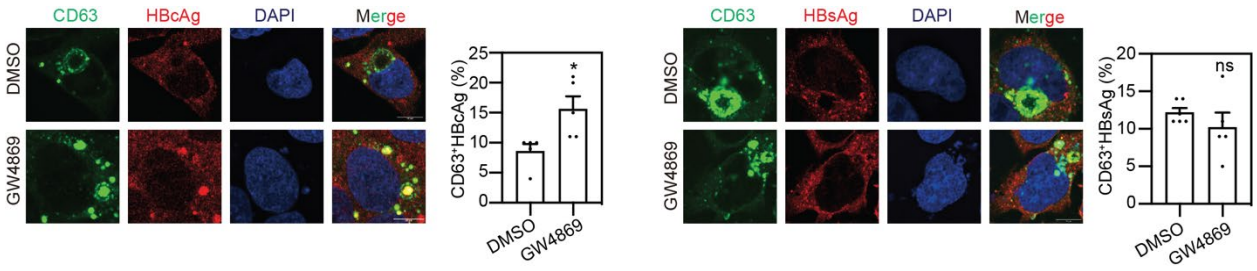

Figure 4. 13 GW4869 treatment enhances HBcAg transported to late endosomes

HepG2.2.15 cells were treated with 2 μM GW4869 for 48 h. The expressions of CD63, HBcAg, and HBsAg were detected by IF staining and confocal microscopy. The colocalization was analyzed using ImageJ software. Scale bar: 10 μm. *p < 0.05; and ns, not significant.

4.5.3 GW4869 treatment enhances HBV virions and subviral particles transported to autophagosomes

Investigations conducted in our laboratory have underscored the collaborative contribution of the autophagic and endosomal pathways to HBV virion and SVP production [55, 109]. Autophagy is an alternative pathway for HBV production and secretion, particularly in response to triggering ER stress [109]. To examine the interplay between autophagosomes and HBsAg/HBcAg, we utilized confocal microscopy. Notably, 48 h after GW4869 treatment, a significant increase in the colocalization of both LC3 with HBsAg and HBcAg was observed (Figure 4.14), implying that GW4869 treatment directs HBV proteins towards autophagosomes. This observation may be attributed to the

accumulation of late endosomes, engendering negative feedback on early endosomal trafficking while stimulating autophagy.

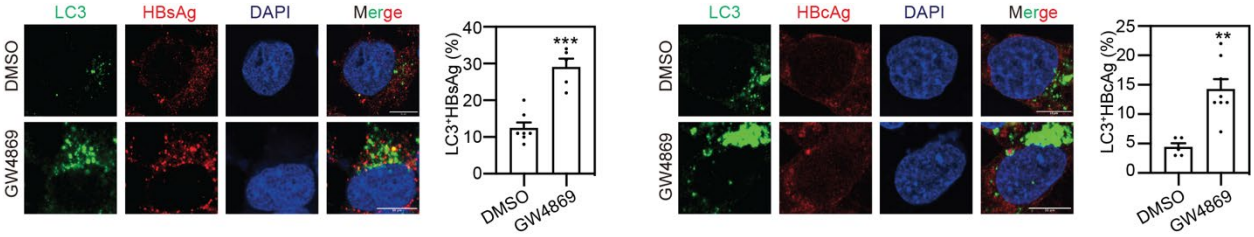

Figure 4. 14 GW4869 treatment enhances HBV virions and subviral particles transported to autophagosomes

HepG2.2.15 cells were treated with 2 μM GW4869 for 48 h. The expressions of LC3, HBsAg, and HBcAg were detected by IF staining and confocal microscopy. The colocalization was analyzed using ImageJ software. Scale bar: 10 μm. **p < 0.01; ***p < 0.001.

4.5.4 GW4869 changes the morphology of late endosomes

GW4869 treatment not only influenced the functions but also altered the morphology of late endosomes. In HepG2.2.15 cells treated with GW4869, CD63-positive structures presented a distinctive bracelet-like pattern decorated with small diamonds, in contrast to a solid dough-like appearance observed in the absence of GW4869 (Figure 4.15). These findings suggested that GW4869 disrupts the formation of late endosomes/MVBs and imparts alterations in their structural morphology.

Overall, a blockage of exosome secretion not only disrupted the trafficking of HBsAg to early endosomes but also reserved HBV proteins within late endosomes/MVBs and autophagosomes.

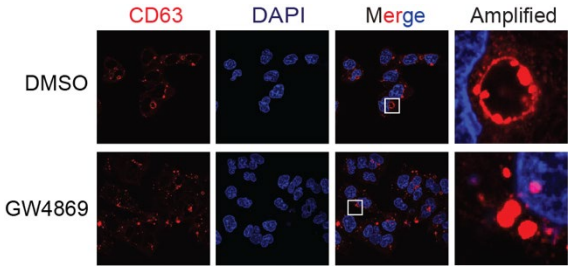

Figure 4. 15 GW4869 changes the morphology of late endosomes

HepG2.2.15 cells were cultured in 10% FBS media and treated with 2 μM GW4869 for 48 h. The late endosomes/MVBs were stained with anti-CD63 and imaged by confocal microscopy.

4.6 The $LC3^+CD63^+$ amphisome-like structure acts as a platform for HBV secretion

4.6.1 GW4869 increases autophagosome formation and improves its association with HBV

Amphisomes, intermediate organelles resulting from the fusion of autophagosomes with late endosomes/MVBs, function in cargo degradation and secretion [114-116]. Thus, we used $LC3^+CD63^+$ as the marker for autophagosomes. We then analyzed the possible association between amphisomes and HBV components. To this end, HepG2.2.15 cells were treated with 2 μM GW4869 for 48 h and were then subjected to three-color IF staining with the antibodies against LC3, CD63, and HBsAg, followed by imaging with a confocal microscopy (Figure 4.16, A). The results indicated a 7% increase in the colocalization of CD63 and LC3, indicating that GW4869 promoted the fusion of late endosomes/MVBs with autophagosomes, leading to amphisome formation. Three-color IF staining further revealed structures positive for HBsAg, LC3, and CD63 ($HBsAg^+LC3^+CD63^+$) in HepG2.2.15 cells, providing direct evidence of the structural association between HBsAg and amphisomes. Interestingly, the number of $HBsAg^+LC3^+CD63^+$ structures significantly increased after GW4869 treatment, indicating an accumulation of HBV in amphisomes due to impaired exosome release. To validate these findings from HepG2.2.15 cells, pSM2 transfected-Huh7 cells were treated with 1 μM GW4869 for 48 h. Confocal microscopic examination showed an increased number of amphisomes, reaching 11%, and HBsAg colocalization with amphisomes, reaching 58% (Figure 4.16, B). These data suggested that GW4869 increases amphisome formation and the accumulation of HBsAg with amphisomes when the endosomal pathway is impaired.

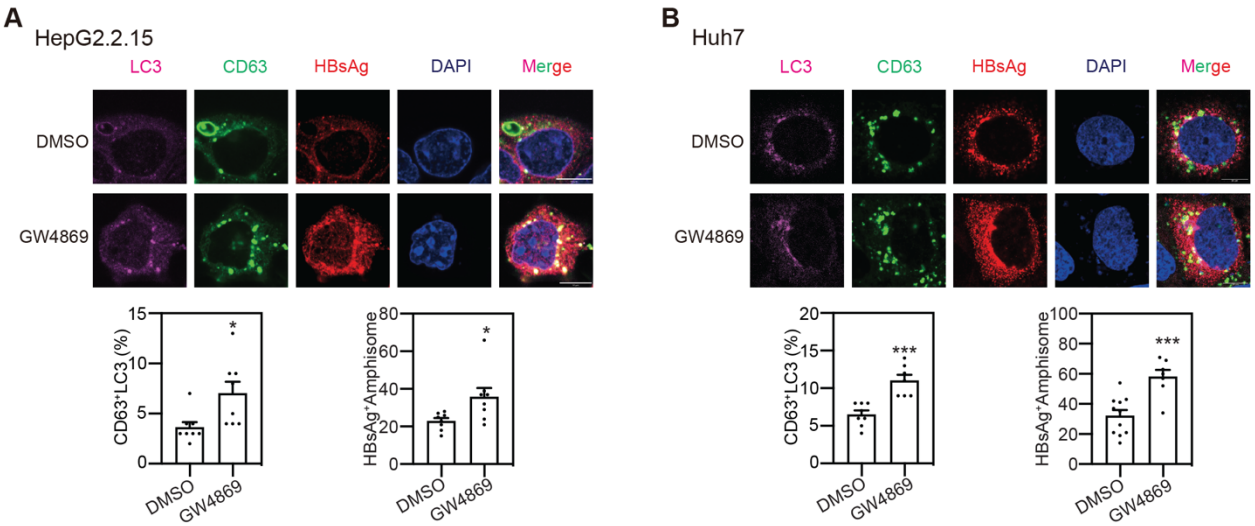

Figure 4. 16 GW4869 increases autophagosome formation and improves its association with HBV

(A) HepG2.2.15 cells were treated with 2 μM GW4869 and (B) pSM2-transfected Huh7 cells were treated with 1 μM GW4869 for 48 h. Cells were stained with anti-LC3, anti-CD63, and anti-HBsAg. The $HBsAg^{+}LC3^{+}CD63^{+}$ complexes were analyzed by IF staining and confocal microscopy. Scale bar: 10 μm. *P < 0.05; ***P < 0.01.

4.6.2 HBV is enriched in exosomes

In our previous study, HBV DNA, HBsAg, and HBcAg were found to be co-fractioned with exosomes by western blotting [109]. In the present study, we aimed to enrich intact exosomes from cell culture media using PEG precipitation [117] and a commercially available total exosome isolation kit. Sustainable detection of HBV DNA was achieved in fractions precipitated by different concentrations of PEG incubation (Figure 4.17, A) and those precipitated by an exosome kit (Figure 4.17, B). Notably, GW4869 treatment also increased the HBV DNA level in the enriched exosome, suggesting a structural association between HBV components and exosomes, and implying a shared egress pathway for HBV secretion and exosomes.

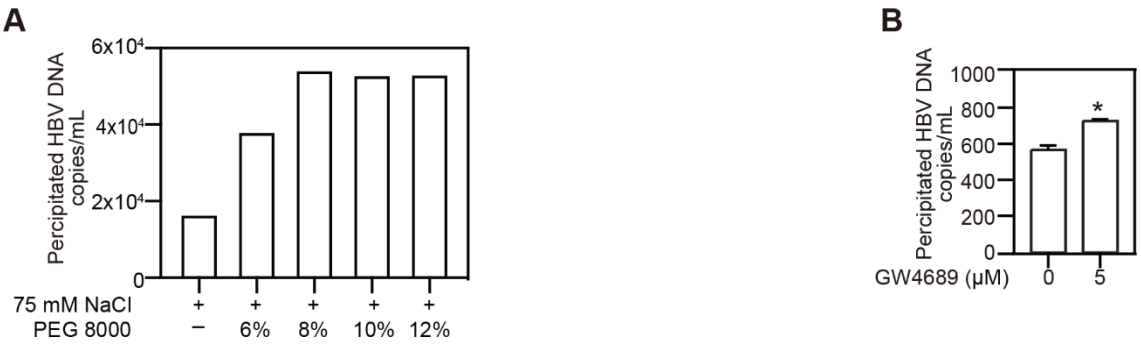

Figure 4. 17 HBV is enriched in exosomes

HepG2.2.15 cells were cultured in 10% FBS media and treated with 2 μM and 5 μM GW4869 for 48 h and without FBS for the last 24 h. Total exosomes were precipitated using (A) the PEG precipitation method and (B) total exosome isolation reagents. DNA was extracted from precipitated fractions using a DNA extraction kit. HBV DNA levels were quantified by real-time PCR. *P < 0.05.

4.6.3 Amphisomes play a crucial role in HBV trafficking and release

To comprehensively examine the involvement of amphisomes in HBV secretion, we employed a specific siRNA to target the *ATG5* gene in HepG2.2.15 cells (Figure 4.18, A). The knockdown of *ATG5* led to a significant reduction in the number of amphisomes and impaired HBV trafficking to amphisomes, underscoring the indispensable role of autophagy in amphisome formation and function. Despite a combined treatment with GW4869, a full restoration of amphisome numbers or their association with HBV was not achieved. Furthermore, *ATG5* silencing led to reduced LC3 immunofluorescence intensity and its association with HBsAg compared with siNC control. Nevertheless, the combined treatment with GW4869 recovered LC3 levels and partially increased the association of HBsAg with LC3. Notably, *ATG5* silencing did not affect the immunofluorescence intensity of CD63 or the association of HBsAg with CD63. These findings suggested that autophagosome formation is required for HBsAg trafficking to amphisomes.

The knockdown of *ATG5* intensified GW4869’s suppressive impact on HBV DNA release while attenuating GW4869's facilitation of HBsAg release without exacerbating the intracellular accumulation of HBsAg (Figure 4.18, B). Collectively, targeting *ATG5* by siRNA interferes with amphisome formation and significantly reduces HBV DNA and HBsAg secretion, which is consistent with the proposed role of amphisomes in HBV secretion.

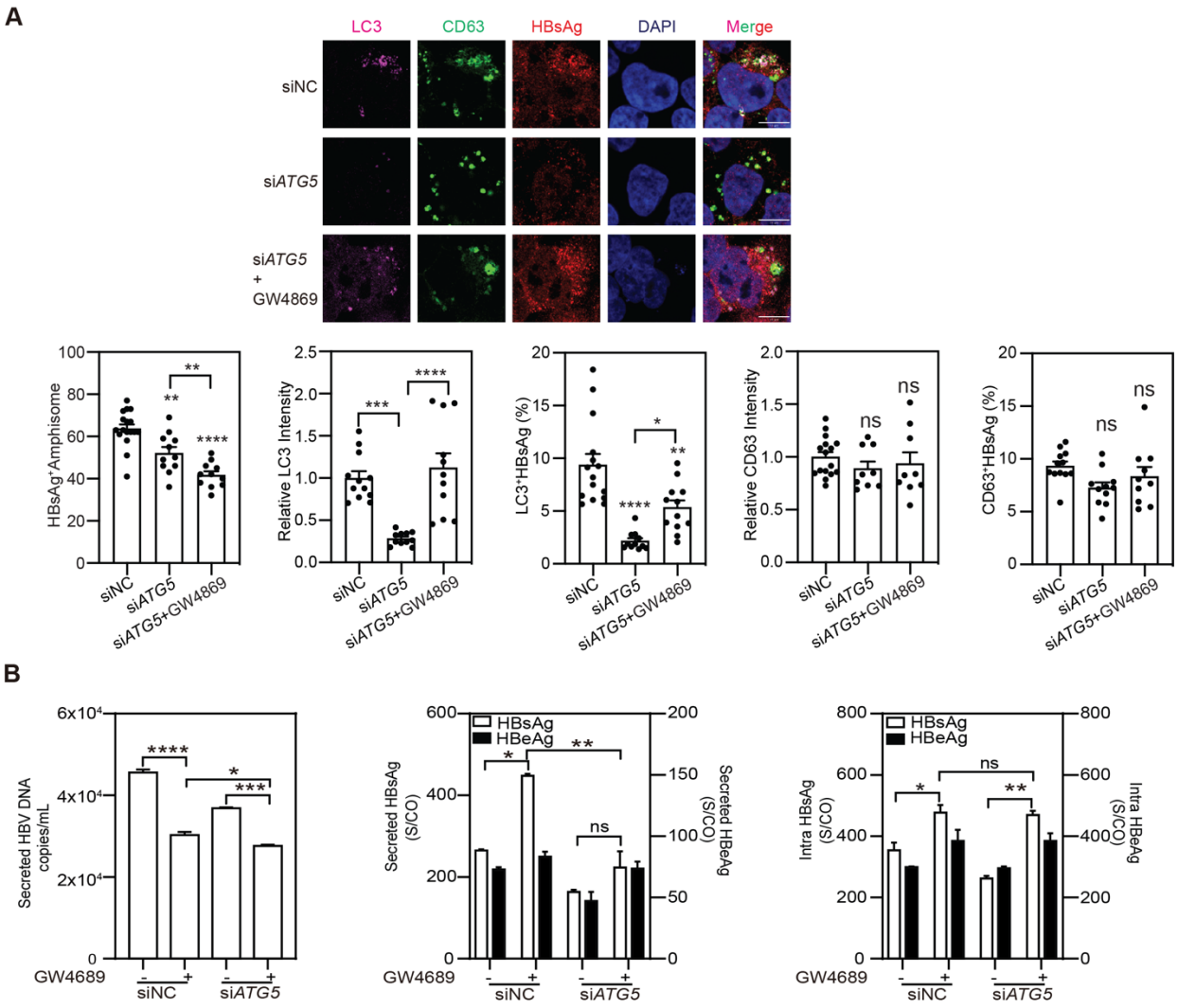

Figure 4. 18 Amphisomes play a crucial role in HBV trafficking and release

HepG2.2.15 cells were transfected with 40 nM of si*ATG5*, the transfection mixture was removed after 6 h and treated with 2 μM GW4869 for 72 h. (A) Cells were stained with anti-LC3, anti-CD63, and anti-HBsAg. The $HBsAg^+LC3^+CD63^+$ complexes were analyzed by IF staining and confocal microscopy. Scale bar: 10 μm. (B) The secreted HBV DNA, HBsAg, and HBeAg, intracellular HBsAg and HBeAg were detected. *P < 0.05; **, ##P < 0.01; ***, ###P < 0.01; ****P < 0.001; and ns, not significant.

4.7 GW4869 modulates HBV replication and trafficking through neutral sphingomyelinase

4.7.1 Knockdown of neutral sphingomyelinases blocks HBV secretion and retains HBV in cell

To validate the involvement of neutral sphingomyelinase (nSMase), the target of GW4869, in HBV replication and trafficking, hepatic cells were transfected with a specific

siRNA targeting nSMase, si*SMPD2*. The efficiency of si*SMPD2* in reducing SMPD2 mRNA levels was confirmed through real-time RT-PCR, demonstrating a significant decrease in *SMPD2* mRNA levels (Figure 4.19, A). Similar to the impact of GW4869 treatment, *SMPD2* silencing resulted in increased levels of intracellular HBV DNA and HBsAg in pSM2-transfected Huh7 cells (Figure 4.19, B) and HepG2.2.15 cells (Figure 4.19, C). Notably, *SMPD2* silencing significantly decreased HBV DNA secretion while promoting HBsAg secretion. It should be mentioned that *SMPD2* silencing had no measurable effect on HBV RNA expression.

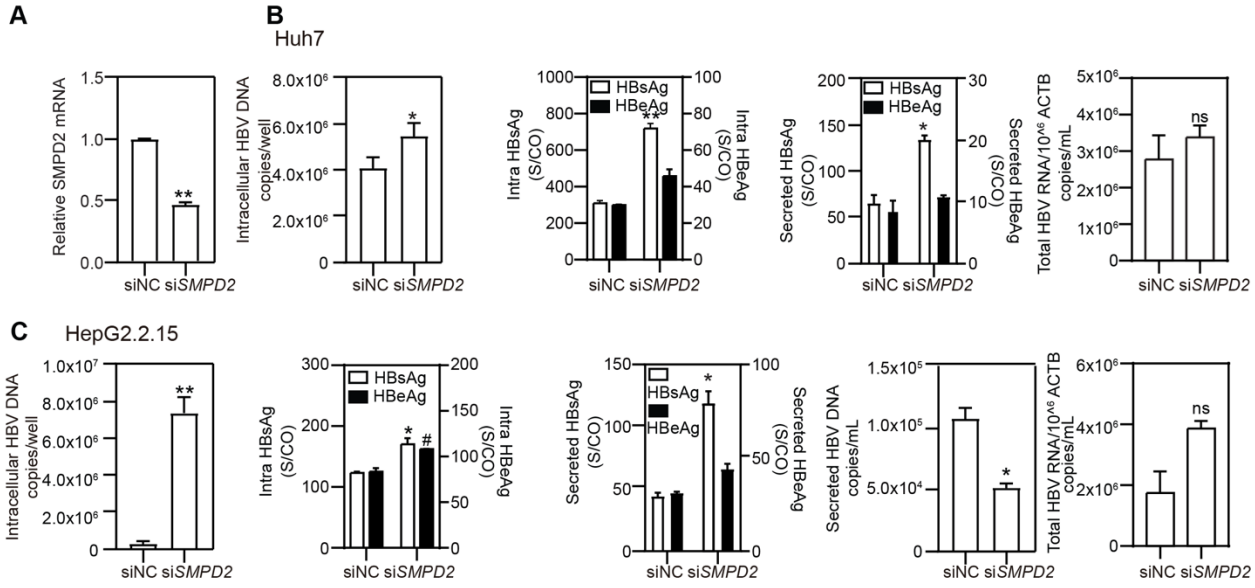

Figure 4. 19 Knockdown of neutral sphingomyelinases blocks HBV secretion and retains HBV in cells

(A) Huh7 cells were transfected with si*SMPD2* for 72 h and total RNA was collected. Real-time quantitative PCR analysis of *SMPD2* mRNA expression in Huh7 cells. (B) Huh7 cells were co-transfected with pSM2 and si*SMPD2* and (C) hepG2.2.15 cells were transfected with siNC or si*SMPD2* at a concentration of 40 nM and harvested after 72 h. The levels of intracellular and secreted HBV DNA, secreted and intracellular HBsAg and HBeAg, and total HBV RNAs were detected. *, #$p < 0.05$; **$p < 0.01$; and ns, not significant.

4.7.2 Knockdown of neutral sphingomyelinases retains HBV in the endoplasmic reticulum and reduces HBV transport to the early endosomes

We explored whether the knockdown of nSMases has the same effect on HBsAg trafficking as observed with GW4869. HepG2.2.15 cells were transfected with 40 nM si*SMPD2* for 72 h, and cells were fixed for IF staining. Similar to GW4869 treatment, si*SMPD2* transfection increased the expression level of PDIA2 and its colocalization with

HBsAg (Figure 4.20, A), indicating that more HBsAg was retained within the ER. Further investigations revealed that *SMPD2* silencing primarily decreased the expression level of RAB5A and its association with HBsAg (Figure 4.20, B).

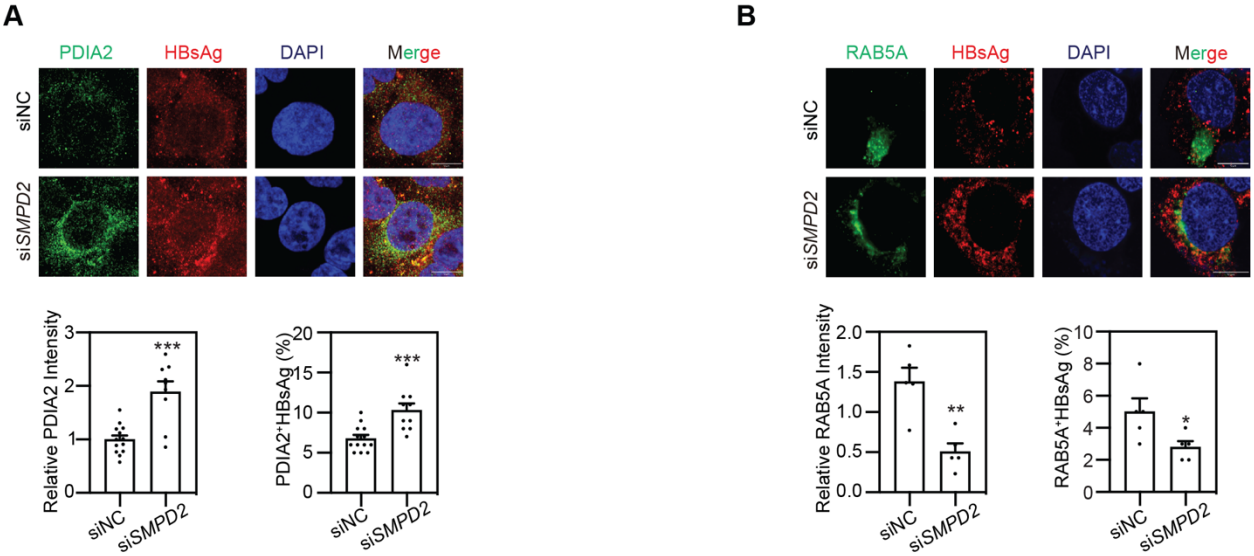

Figure 4. 20 Knockdown of neutral sphingomyelinases retains HBV in the endoplasmic reticulum and reduces HBV transport to the early endosomes

HepG2.2.15 cells were transfected with 40 nM siNC or siSMPD2 for 72 h. The expression levels of (A) PDIA2, (B) RAB5A were detected by IF staining and confocal microscopy. The colocalization of HBsAg with these markers was analyzed using ImageJ software. Scale bar: 10 μm. *p < 0.05; **p < 0.01; ***p < 0.001.

4.7.3 Knockdown of neutral sphingomyelinases increases autophagosomes and decreases autophagic degradation

Moreover, *SMPD2* silencing also decreased the association of autophagosomes with LAMP1 and increased the expression level of LC3. The colocalization ratio of HBsAg and LAMP1 decreased, while that with LC3 increased, indicating that less HBsAg was transported to lysosomes for degradation and, instead, an accumulation of HBsAg in autophagosomes (Figure 4.21).

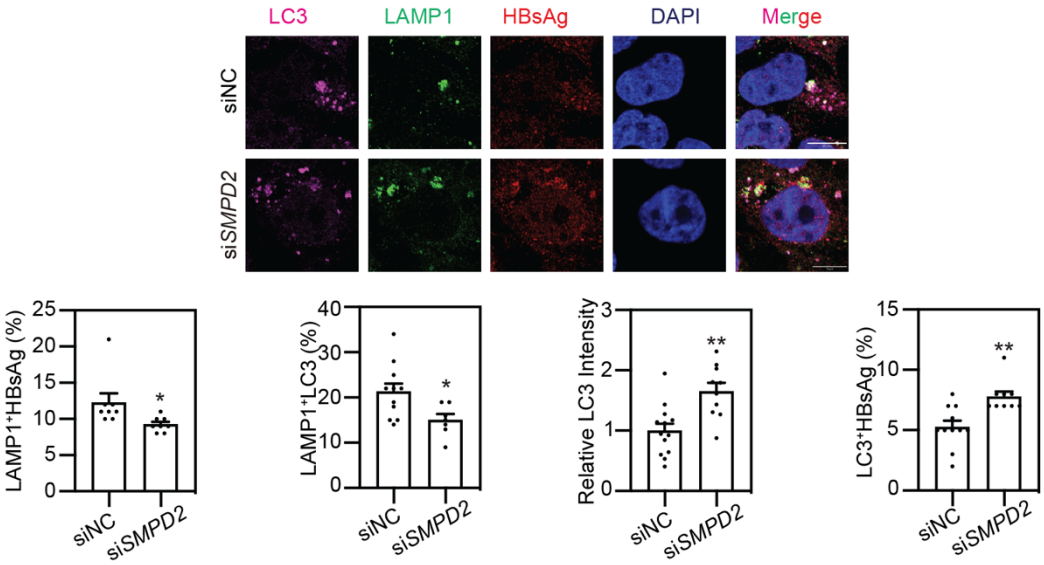

Figure 4. 21 Knockdown of neutral sphingomyelinases decreases HBsAg and autophagosome degradation

HepG2.2.15 cells were transfected with 40 nM siNC or si*SMPD2* for 72 h. The expression levels of LC3, LAMP1, and HBsAg were detected by IF staining and confocal microscopy. The colocalization of these markers was analyzed using ImageJ software. Scale bar: 10 μm. *p < 0.05; **p < 0.01.

4.7.4 Knockdown of neutral sphingomyelinases increases HBV transport to late endosomes and amphisomes

Additionally, *SMPD2* silencing led to an increased immunofluorescent intensity of CD63 and enhanced colocalization of HBsAg with CD63. The percentage of amphisomes increased from 13.3% to 26% after si*SMPD2* transfection, accompanied by an increase in the number of $HBsAg^{+}LC3^{+}CD63^{+}$ structures (from 41.4% to 51.6%) (Figure 4.22). Thus, *SMPD2* silencing and GW4869 treatment had the same effect on HBV replication and trafficking. GW4869 modulates HBV replication and trafficking through neutral sphingomyelinase.

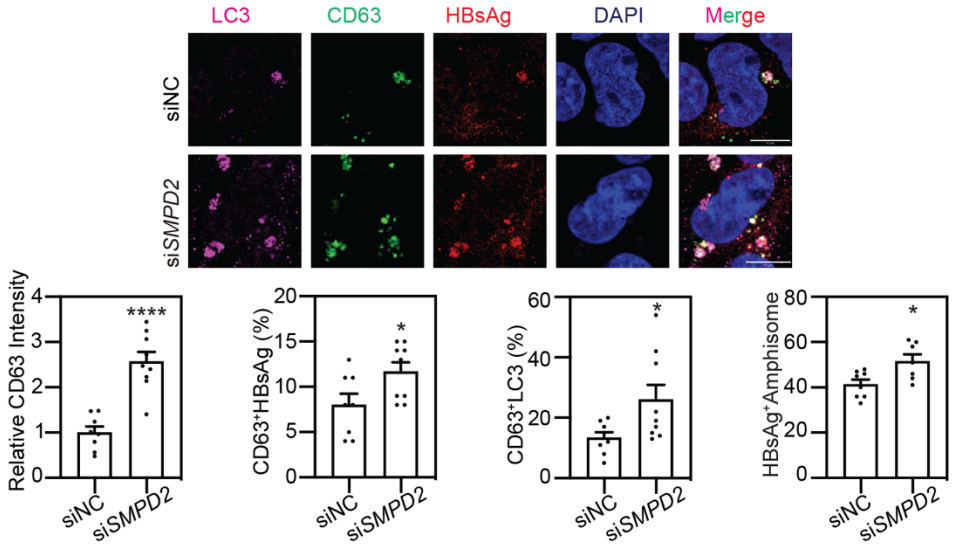

Figure 4. 22 Knockdown of neutral sphingomyelinases increases HBV transported to late endosomes and amphisomes

HepG2.2.15 cells were transfected with 40 nM siNC or si*SMPD2* for 72 h. The expression levels of LC3, CD63, and HBsAg were detected by IF staining and confocal microscopy. The colocalization of these markers was analyzed using ImageJ software. Scale bar: 10 μm. *p < 0.05; ****p < 0.0001.

4.8 RAB27A controls the intracellular trafficking and secretion of HBV virions and SVPs while RAB27B mainly plays a role in HBV intracellular distribution.

4.8.1 Knockdown of RAB27A and -B leads to accumulations of autophagosomes and late endosomes/MVBs in cells

To gain further insight into the role of endosomal membrane trafficking in HBV release, *RAB27A* and *-B*, two small GTPases controlling different steps of vesicular trafficking and exosome release were targeted. First, IF staining verified that both *RAB27A* and *-B* were fairly colocalized with CD63 (Figure 4.24, A). Next, gene silencing of *RAB27A* and *-B* was performed and five different siRNA sequences were tested for their silencing efficiency by western blotting (Figure 4.23, B). Among the candidate siRNAs, si*RAB27A*_7 and si*RAB27B*_4 were selected for the following experiments as they achieved a reduction of protein expression by more than 50%.

It is proposed that the secretion of certain cellular proteins by the autophagic pathway via exosome release is dependent on *RAB27A* [118, 119]. In HepG2.2.15 cells, *RAB27A* and *-B* were individually silenced using 40 nM siRNA. Cells were harvested 72 h later and subjected to western blotting analysis. The expression levels of CD63 and LC3 increased

in both *RAB27A* and *-B* -silenced cells compared to control cells (Figure 4.23, C), which was consistent with the known functions of *RAB27A* and *-B* in cargo export mediated by late endosomes/MVBs and autophagosomes. To examine the impact of *RAB27A* and *-B* silencing on autophagy flux, we combined their silencing with the CQ treatment. Interestingly, si*RAB27A* and *-B* transfection combined with 10 μM of CQ did not significantly increase LC3-II levels (Figure 4.23, D). This finding suggested that the increased accumulation of autophagosomes by *RAB27A* and *-B* silencing is primarily a consequence of inhibiting autophagic degradation and secretion than the generation of new autophagosomes.

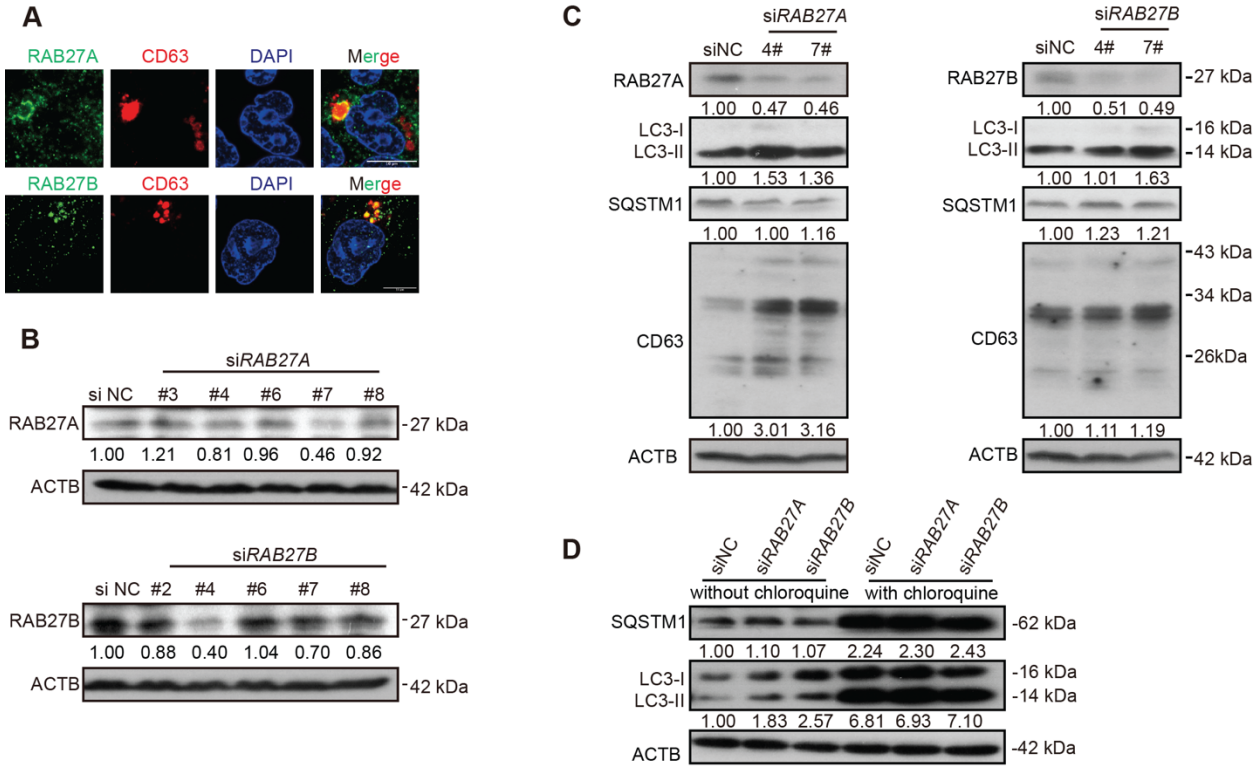

Figure 4. 23 Knockdown of *RAB27A* and *-B* accumulate autophagosomes and late endosomes/MVBs in cells

(A) HepG2.2.15 cells cultured at 10% FBS medium for 48 h were subjected to IF co-staining with anti-CD63, anti-RAB27A or anti-RAB27B, and analyzed by confocal microscopy. Scale bar:10 μm. (B) HepG2.2.15 cells were transfected with different sequences of si*RAB27A* and si*RAB27B*, respectively, and harvested after 72 h. (C) HepG2.2.15 cells were transfected with si*RAB27A*, si*RAB27B,* and siNC for 48 h, and then treated with 10 μM chloroquine for another 24 h, only medium culture acted as a control. The expression levels of RAB27A, RAB27B, SQSTM1/p62, CD63, and LC3 were analyzed by western blotting. The relative levels of indicated proteins were determined by quantifying the gray scales of bands using ImageJ software and ACTB as a loading control.

4.8.2 Knockdown of RAB27A blocks HBV secretion

To assess the impact of silencing these two proteins on HBV secretion, we measured intra- and extracellular levels of HBV DNA and HBsAg. Silencing *RAB27A* led to an increase in intracellular HBV DNA, while the levels of released HBV DNA and HBsAg in the supernatants were reduced (Figure 4.24). However, silencing *RAB27B* had only a minor effect on intracellular HBV DNA levels and did not influence the secreted HBV DNA and HBsAg levels.

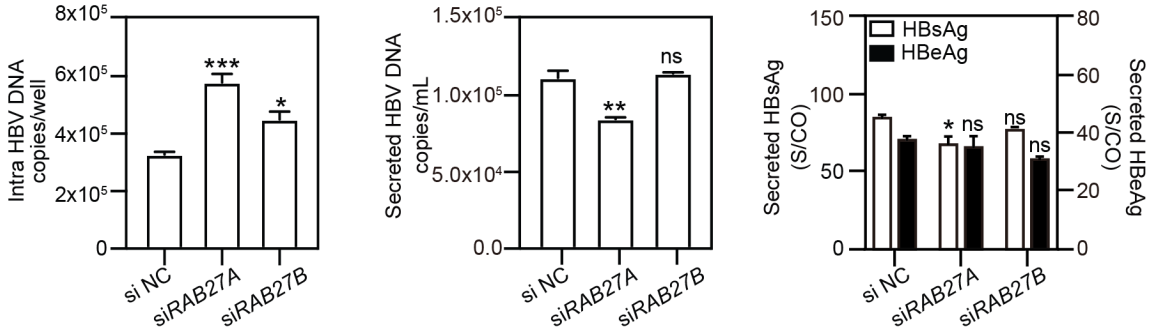

Figure 4. 24 Knockdown of *RAB27A* blocks HBV secretion

HepG2.2.15 cells were transfected with siNC, si*RAB27A*, and si*RAB27B* at a concentration of 40 nM for 72 h. The intracellular and secreted HBV DNA and the secreted HBsAg and HBeAg levels were detected. *P < 0.05; **P < 0.01; ***P < 0.001; and ns, not significant.

4.8.3 Knockdown of *RAB27A* and *-B* change HBV distribution

To explore the impact of *RAB27A* and *-B* knockdown on HBV distribution, we examined the subcellular localization of HBsAg. In control cells, HBsAg exhibited a homogeneous distribution throughout the cytoplasm, while *RAB27A* and *-B* silencing resulted in perinuclear accumulation (Figure 4.25, A). We further investigated the association of HBsAg with endosomes and autophagosomes. Apparently, *RAB27A* and *-B* showed different roles in HBsAg trafficking between endosomes and autophagosomes. Silencing *RAB27A* increased the number of early endosomes and autophagosomes without altering the colocalization ratio of HBsAg with RAB5A and LC3. Conversely, silencing *RAB27B* slightly decreased the colocalization ratio of HBsAg with RAB5A and LC3 but notably elevated the LC3 expression level (Figure 4.25, B-C). Next, we attempted to investigate the effects of *RAB27A* and *-B* silencing on the formation of $HBsAg^+LC3^+CD63^+$ structures. Three-color IF staining was performed in pSM2-transfected Huh7 cells. Notably, the number of $HBsAg^+LC3^+CD63^+$ structures increased (Figure 4.25, D), which was

consistent with *RAB27*'s role in amphisome regulation of release [120]. The intensity plots of the analyzed proteins within the cells confirmed a perinuclear accumulation of $HBsAg^+LC3^+CD63^+$ complexes upon *RAB27A* and -*B* silencing. Again, amphisomes are involved in HBV production and secretion. Taken together, the results highlight distinct roles for *RAB27A* and -*B* with the intracellular trafficking and release of HBV virions and SVPs. *RAB27A* appears to control HBV release near the cell membrane, while *RAB27B* is involved in HBV trafficking to organelles in the cell.

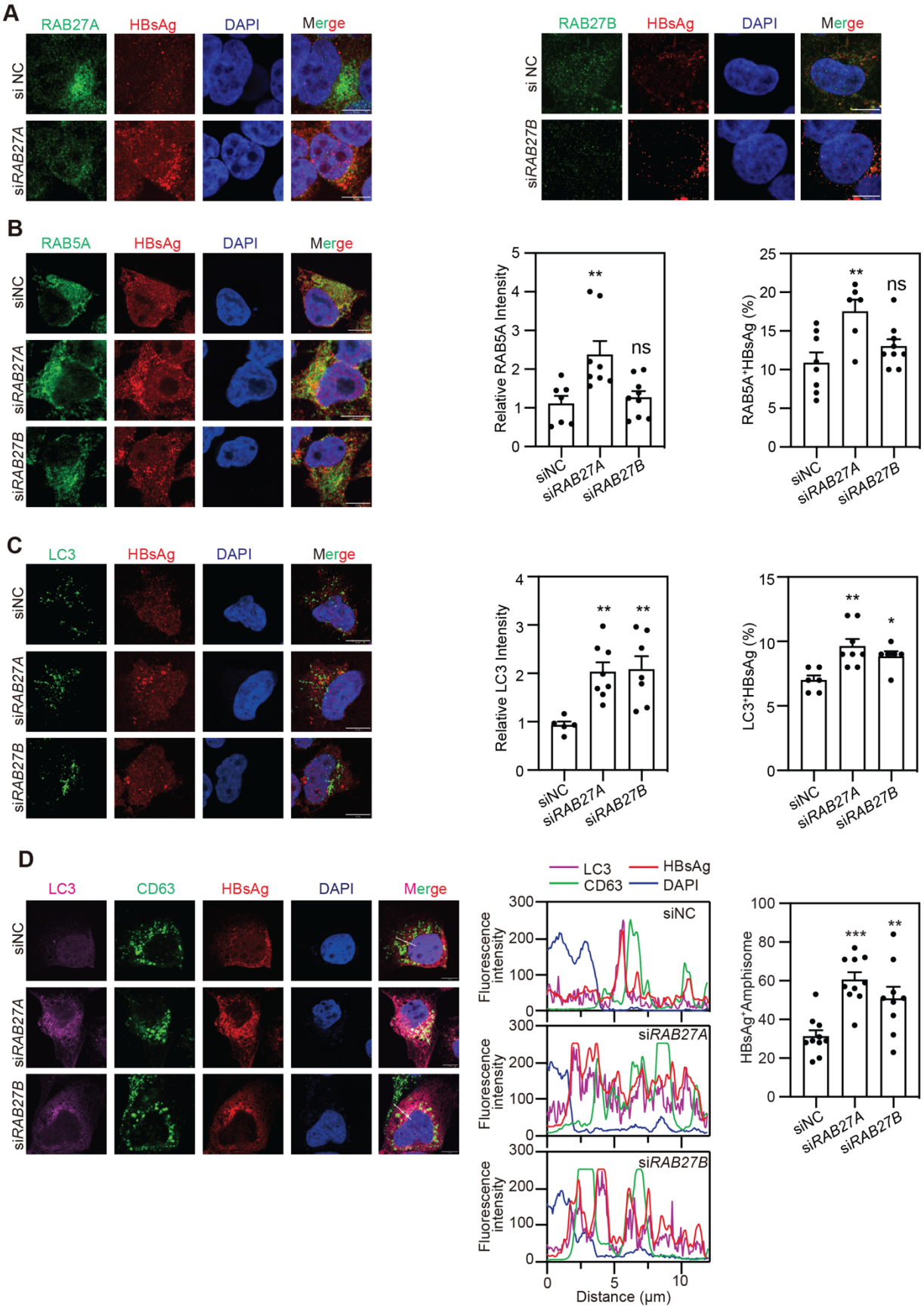
A
RAB27A
HBsAg
DAPI
Merge
si NC
siRAB27A
RAB27B
HBsAg
DAPI
Merge
si NC
siRAB27B
B
RAB5A
HBsAg
DAPI
Merge
siNC
siRAB27A
siRAB27B
Relative RAB5A Intensity
**
ns
siNC
siRAB27A
siRAB27B
RAB5A+HBsAg (%)
**
ns
siNC
siRAB27A
siRAB27B
C
LC3
HBsAg
DAPI
Merge
siNC
siRAB27A
siRAB27B
Relative LC3 Intensity
**
**
siNC
siRAB27A
siRAB27B
LC3+HBsAg (%)
**
*
siNC
siRAB27A
siRAB27B
D
LC3
CD63
HBsAg
DAPI
Merge
siNC
siRAB27A
siRAB27B
LC3
CD63
HBsAg
DAPI
siNC
siRAB27A
siRAB27B
Fluorescence intensity
Distance (μm)
HBsAg+Amphisome
***
**
siNC
siRAB27A
siRAB27B

Figure 4. 25 Knockdown of *RAB27A* and *-B* change HBV distribution

HepG2.2.15 cells were transfected with siNC, si*RAB27A,* or si*RAB27*B at the concentration of 40 nM and harvested after 72 h. (A) Cells were stained with anti-RAB27A or anti-RAB27B and anti-HBsAg, and analyzed by confocal microscopy. (B) The expressions of RAB5A and HBsAg, (C) LC3 and HBsAg, (D) LC3, CD63, and HBsAg were detected by IF staining and confocal microscopy. The colocalization of these markers was analyzed using ImageJ software. Scale bar:10 μm. *P < 0.05; **P < 0.01; ***P < 0.001.

4.9. Interferon Alpha 2a induces cellular autophagy and modulates HBV replication

Interferon alpha 2a (IFNα-2a) is commonly used for treating chronic HBV infection [121]. However, its efficacy remains relatively low. Yet, the immunological and molecular mechanisms for successful IFNα-2a treatment remain elusive. We explored whether the application of IFNα-2a may modulate cellular processes, such as autophagy, and thereby regulating HBV replication in hepatic cells.

4.9.1 IFNα-2a interferes with intracellular signal crosstalk

Previously, it has been shown that IFNα was able to interfere with multiple cellular signalings [122]. We first asked whether IFNα-2a interferes with AKT/MTOR and AMPK activities. HepG2.2.15 cells were treated with IFNα-2a at different concentrations (1000 U/ml and 6000 U/ml), and harvested after 48 h. The expression levels of total AMPK, AKT, MTOR, and their phosphorylated forms were detected by western blotting. As Figure 4.9.1 A shows, the levels of phosphorylated AKT and MTOR were decreased with the increasing IFNα-2a concentrations. Interestingly, the levels of total and phosphorylated AMPK were decreased (Figure 4.26, A-B). These data indicate that IFNα-2a attenuates AKT/MTOR signaling and AMPK signaling.

Figure 4. 26 IFNα-2a interferes with intracellular signal crosstalk

HepG2.2.15 cells were treated with the indicated concentrations of IFNα-2a and harvested after 48 h. The total and phosphorylated AKT, MTOR (A), and AMPK (B) were detected by western blotting, and their relative levels were analyzed by western blotting. The relative levels of indicated proteins were

determined by quantifying the gray scales of bands using ImageJ software and ACTB as a loading control.

4.9.2 IFNα-2a counteracts agonists-induced AKT/MTOR and AMPK activation

Previous studies have shown that insulin physiologically activates the AKT/MTOR pathway [123]. In this study, insulin was introduced into the culture medium, resulting in increased levels of phosphorylated AKT and MTOR after treatment. The simultaneous addition of 6000 U/ml IFNα-2a counteracted the increased activities of AKT and MTOR stimulated by insulin (Figure 4.27, A), confirming the suppressive effect of IFNα-2a on AKT/MTOR signaling.

To further examine the effect of IFNα-2a on the MTOR signaling pathway, HepG2.2.15 cells were treated with 6000 U/ml of IFNα-2a, either in rapamycin, an inhibitor of MTOR, or MHY1485, an MTOR agonist. The results showed that the expression level of phosphorylated MTOR decreased after rapamycin treatment, with a further reduction in cells co-treated with IFNα-2a and rapamycin. Conversely, the inhibitory effect of IFNα-2a on MTOR phosphorylation was attenuated in cells co-treated with MHY1485 (Figure 4.27, B). These results confirmed that IFNα-2a treatment inhibits the MTOR signaling pathway in hepatoma cells.

When HepG2.2.15 cells were exposed to AICAR, an AMPK agonist, for 48 h, AMPK phosphorylation markedly increased. However, cotreatment with IFNα-2a abolished the increased phosphorylation of AMPK induced by AICAR activation (Figure 4.27, C). Thus, IFNα-2a treatment also diminishes AMPK signaling in hepatoma cells.

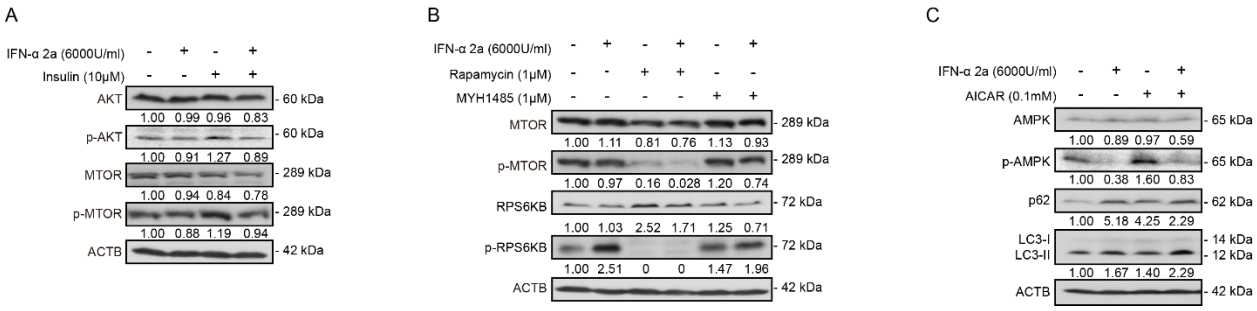

Figure 4. 27 IFNα-2a counteracts agonists-induced AKT/MTOR and AMPK activation

HepG2.2.15 cells were treated with 6000 U/ml IFNα-2a in the presence or absence of (A) 10 mM insulin, (B) 1 mM MTOR inhibitor rapamycin or activator MHY1485, (C) 0.1 mM AICAR for 48 hr. The total and phosphorylated AKT, MTOR, RPS6KB, AMPK, and the expression levels of p62 and LC3 were detected

by western blotting, and their relative levels were determined by quantifying the gray scales of bands using ImageJ software and ACTB as a loading control.

4.9.3 IFNα-2a activates AKT/MTOR and AMPK signaling pathways in PHHs

Besides the hepatoma cells, we also used PHHs in our experiment. However, uninfected PHHs had initially very low levels of phosphorylated AKT and MTOR. PHHs were incubated in a medium and treated with indicated concentrations of IFNα-2a (1000 U/ml and 6000 U/ml) for 48 hr. Differing from HepG2.2.15 cells, IFNα-2a treatment caused increased levels of phosphorylated AKT, MTOR, and AMPK in PHHs (Figure 4.28). The HBV-infected PHHs cell model is a transient and de-novo infection model and is notably different from the stable HBV-transfected cells, such as HepG2.2.15 cells.

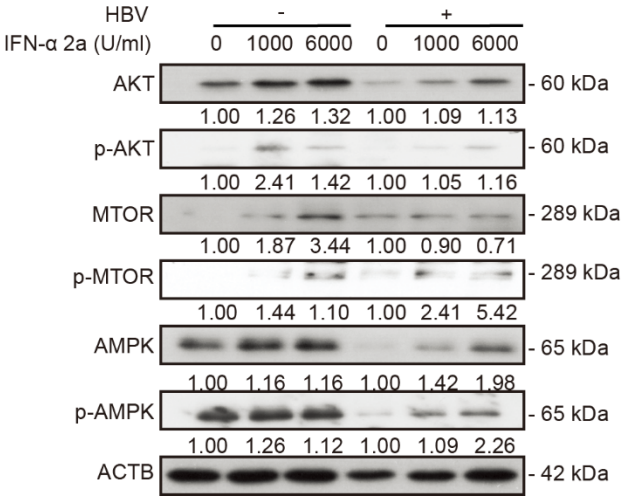

Figure 4. 28 IFNα-2a activates AKT/mTOR and AMPK signaling pathways in PHHs

PHHs were infected with HBV virions (multiplicity of infection = 30). 4 days post-infection, PHHs were treated with IFNα-2a. After 48 h, the total and phosphorylated AKT, MTOR, and AMPK were determined by quantifying the gray scales of bands using ImageJ software and ACTB as a loading control.

4.9.4 IFNα-2a induces autophagy through inhibiting AKT/MTOR signaling pathways and blocks autophagic degradation in hepatoma cells

Then we addressed the question of whether IFNα-2a treatment changes the autophagic activity in hepatoma cells. The levels of LC3 after IFNα-2a treatment were determined using IF staining and western blotting. IF staining showed that the numbers of endogenous LC3-positive autophagic puncta increased in IFNα-2a -treated cells (Figure 4.29, A). Consistently, the IFNα-2a treatment also markedly increased the levels of LC3,

as shown by western blotting analysis (Figure 4.29, B). Next, HepG2.2.15 cells were cultured in the presence of rapamycin with and without IFNα-2a, respectively. The level of LC3 was higher after rapamycin treatment and further increased by IFNα-2a co-treatment. Interestingly, the level of p62 also increased markedly after IFNα-2a treatment, similar to CQ treatment. These results indicate that IFNα-2a treatment blocked autophagic degradation and led to the accumulation of LC3 puncta. To confirm this assumption, HepG2.2.15 cells were treated with 6000 U/ml IFNα-2a for 48 h and then incubated with DQ-BSA for 30 min. Cells cultured in EBSS were used as a positive control and CQ treatment as a negative control. Confocal microscopic analysis showed that the fluorescent signal of DQ-BSA decreased upon IFNα-2a treatment, while increased upon incubation with EBSS (Figure 4.29, C), suggesting that IFNα-2a treatment blocks autophagic degradation in hepatoma cells. Taken together, these results demonstrate that IFNα-2a treatment promotes the formation of autophagosomes and blocks the autophagic degradation in lysosomes.

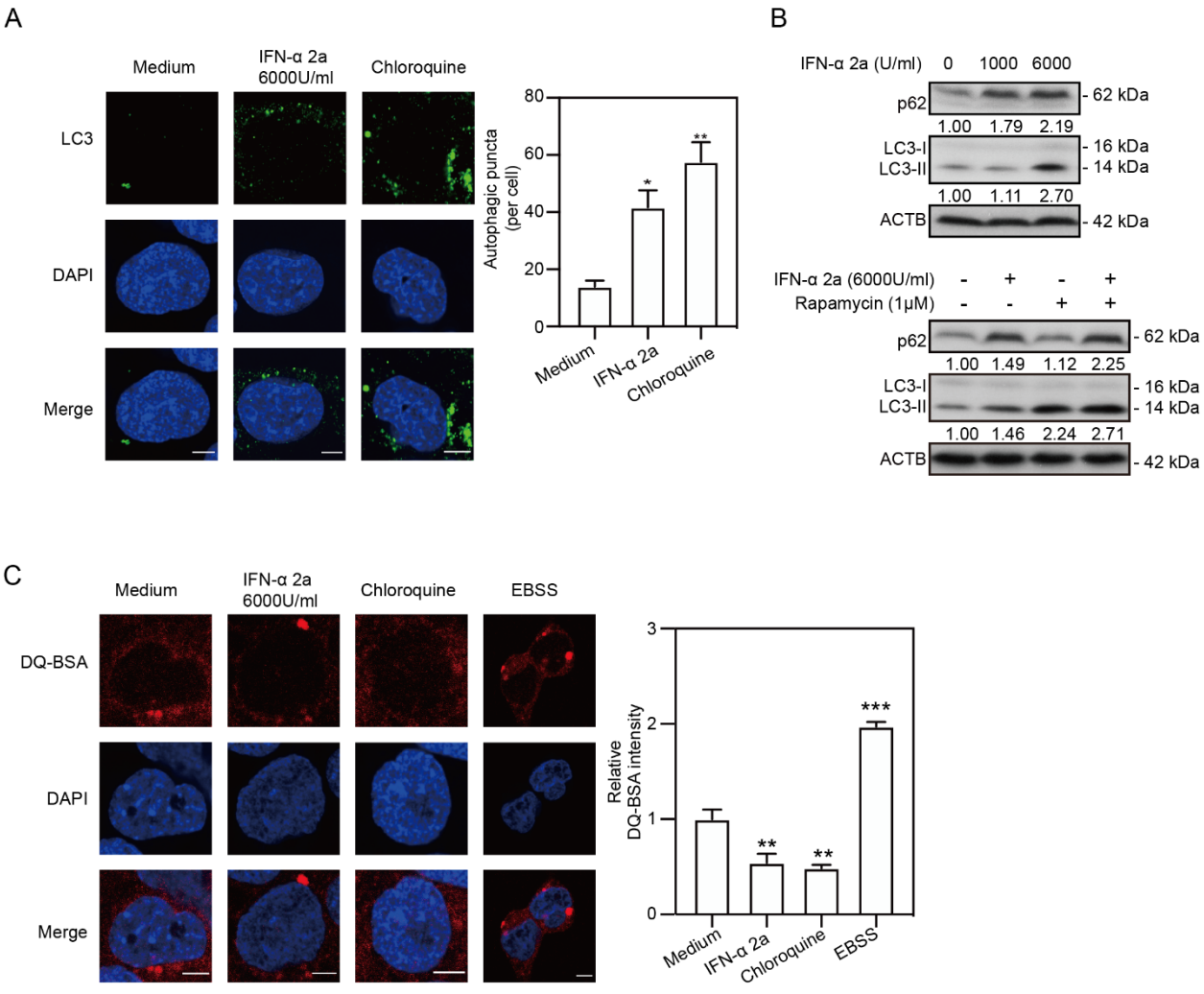

Figure 4. 29 IFNα-2a induces autophagy through Inhibiting AKT/MTOR signaling pathways and blocks autophagic degradation in hepatoma cells

HepG2.2.15 cells were treated with the indicated concentrations of IFNα-2a and harvested after 48 h. (A) Cells were stained with LC3 and analyzed by confocal microscopy. Cells treated with 10 nM CQ were used as a positive control. LC3 puncta in cells were analyzed using ImageJ software. Scale bar:10 μm. (B) p62 and LC3 were detected by western blotting and their relative levels were determined by quantifying the gray scales of bands using ImageJ software and ACTB as a loading control. (C) After the treatment of IFNα-2a, cells were incubated with 10 mg/mL DQ-BSA for 30 minutes. The fluorescent signal of DQ-BSA was detected by confocal microscopy. Cells cultured with EBSS for 2 hours were used as a positive control and CQ treatment was as a negative control. Scale bar:10 μm. *P < 0.05; **P < 0.01; ***P < 0.001.

4.9.5 IFNα-2a inhibits AKT/MTOR activation and enhances autophagy independently on glucose concentrations

Cellular energy metabolism can modulate cellular autophagy [124]. Our previous study showed that high glucose concentration reduced autophagy by activating AKT/MTOR pathway, while glucose concentration inhibited autophagy by the inhibition of AKT/MTOR and activation of AMPK [125]. Therefore, we asked whether glucose concentrations also influence IFNα-2a -mediated AKT/MTOR inhibition and enhancement of autophagy. HepG2.2.15 cells were cultured with the indicated glucose concentrations (5 mM and 25 mM, later called low glucose and high glucose conditions, respectively) and treated with 6000 U/ml IFNα-2a for 48 h. Western blotting was used to detect the levels of total AKT, MTOR, and AMPK proteins and their phosphorylated forms. IFNα-2a decreased the levels of the phosphorylated AKT, MTOR (Figure 4.30, A), and AMPK (Figure 4.30, B) both under the low and high glucose conditions. These data suggest that IFNα-2a-mediated AKT/MTOR and AMPK inhibition occurred independently of glucose concentrations. Consistently, independent of the glucose concentrations, the levels of LC3II and p62 (Figure 4.30, C) and the numbers of LC3-positive autophagic puncta (Figure 4.30, D) were increased in IFNα-2a-treated HepG2.2.15 cells. Taken together, IFNα-2a inhibits AKT/MTOR activation and enhances autophagy independently on glucose concentrations in hepatoma cells.

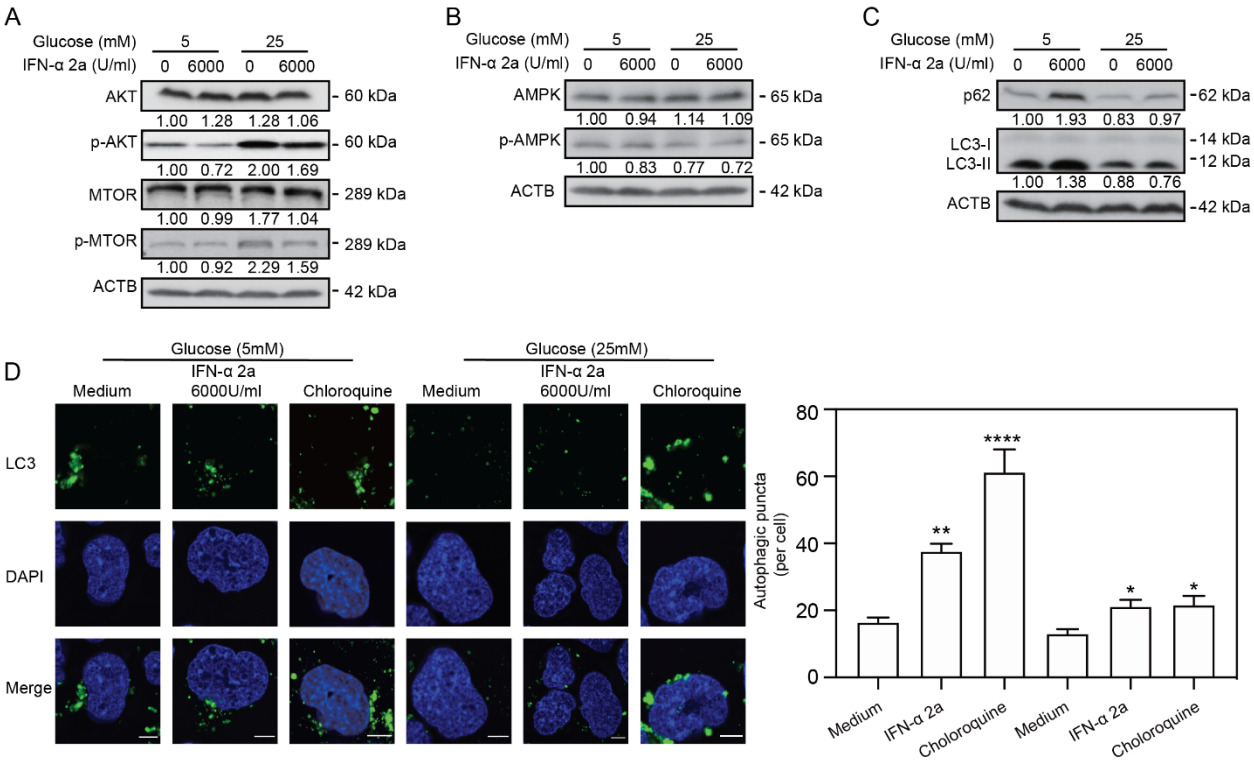

Figure 4. 30 IFNα-2a inhibits AKT/MTOR activation and enhances autophagy independently on glucose concentrations

HepG2.2.15 cells were cultured in a medium with the indicated glucose concentrations (5 and 25 mM) with or without 6000U/ml IFNα-2a and harvested after 48 h. (A) The total and phosphorylated AKT, MTOR, (B) AMPK, p-AMPK, (C) p62 and LC3 were detected by western blotting, and their relative levels were determined by quantifying the gray scales of bands using ImageJ software and ACTB as a loading control. (D) The cells were fixed and incubated with rabbit anti-LC3 antibodies, followed by staining with Alexa Fluor 488-conjugated anti-rabbit secondary antibody IgG. Finally, the distribution of LC3 was imaged by confocal microscopy. The results presented in the graphs were calculated from at least five cells. Scale bar:10 μm. *P < 0.05; **P < 0.01; ****P < 0.001.

4.9.6 IFNα-2a induces interferon-stimulated gene expression

Interferon-stimulated 15 kDa protein (ISG15) and interferon-induced transmembrane protein1 (IFITM1) are the typical antiviral proteins under the control of IFN signaling and highly expressed after IFN stimulation. IFN-a treatment activates the JAK-STAT pathway and upregulates the expression of ISGs [126, 127]. Further emerged evidence implicated that PI3K/AKT/MTOR pathway is also involved in the induction of ISGs [128, 129]. In our cell model, IFNα-2a increased levels of STAT1 and phosphorylated STAT1 (Figure 4.31, A). The expressions of ISG15 and IFITM1 were dose-dependently upregulated after

IFNα-2a treatment (Figure 4.31, B). When using an autophagy inhibitor 3-methyladenine (3-MA), ISG15 and IFITM1 were reduced (Figure 4.31, C), suggesting a positive effect of autophagy on ISG15 and IFITM1 induction.

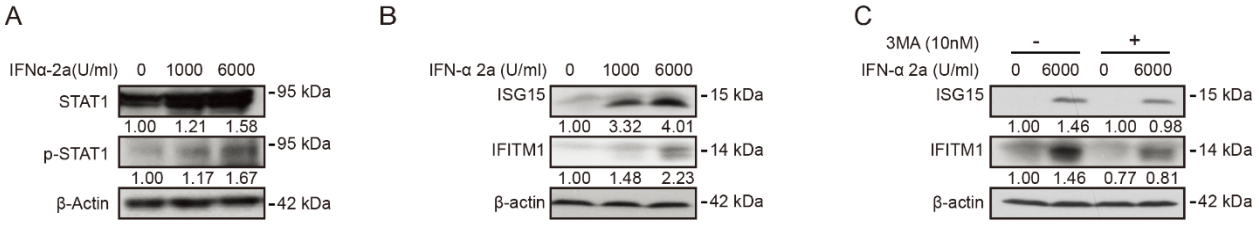

Figure 4. 31 IFNα-2a induces interferon-stimulated gene expression

(A-B) HepG2.2.15 cells were treated with the indicated concentrations of IFNα-2a and harvested after 48 h. (C) HepG2.2.15 cells were treated with 6000 U/ml IFNα-2a with or without 10 nM 3-MA and harvested after 48 h. The levels of STAT1 and phosphorylated STAT1, ISG15, and IFITM1 were detected by western blotting, and their relative levels were determined by quantifying the gray scales of bands using ImageJ software ACTB as a loading control.

4.9.7 IFNα-2a-induced interferon-stimulated gene expression is dependent on autophagy and glucose

Nest, we explored how the glucose influences ISG15 and IFITM1 expression. HepG2.2.15 cells were cultured in a medium with low and high glucose concentrations, respectively, and then treated with IFNα-2a. IFNα-2a increased levels of STAT1 and phosphorylated STAT1 both in low and high glucose conditions (Figure 4.32, A). Interestingly, IFNα-2a differently promoted ISG15 and IFITM1 expression at high glucose concentrations, if compared with their corresponding expression levels at the low glucose concentration (Figure 4.32, B). Moreover, both the expressions of IFNα-2a -induced ISG15 and IFITM1 were significantly suppressed in the presence of 3-MA (Figure 4.32, C). It can be further verified the induction of ISG15 and IFITM1 expression in different glucose conditions were also dependent on autophagy. However, the accurate mechanisms need to be investigated in the future.

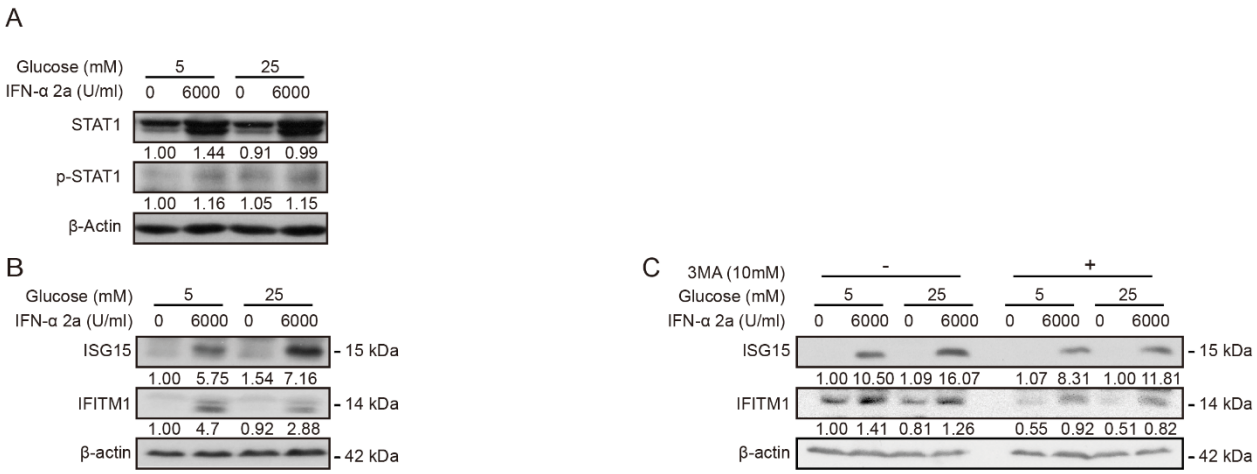

Figure 4. 32 IFNα-2a-induced interferon-stimulated gene expression is dependent on autophagy and glucose

(A-B) HepG2.2.15 cells were cultured in a medium with the indicated glucose concentrations (5 and 25 mM) with or without 6000 U/ml IFNα-2a and harvested after 48 h. (C) HepG2.2.15 cells were cultured at the indicated glucose concentrations and 6000 U/ml IFNα-2a with or without 10 nM 3-MA. The levels of STAT1 and phosphorylated STAT1, ISG15, and IFITM1 were detected by western blotting, and their relative levels were determined by quantifying the gray scales of bands using ImageJ software and ACTB as a loading control.

4.9.8 High IFNα-2a concentrations do not inhibit HBV replication and gene expression in hepatoma cells

Finally, we explored how the IFNα-2a -induced autophagy affects HBV replication. HepG2.2.15 cells were treated with the indicated concentrations of IFNα-2a and harvested after 72 hr. The levels of secreted and intracellular HBsAg and HBeAg were measured by CMIA. HBV replicative intermediates (RIs) were detected by Southern blotting. The levels of secreted and intracellular HBsAg but not HBeAg (Figure 4.33, A) as well as the amount of HBV RIs (Figure 4.33, B) were increased after IFNα-2a treatment. These data suggest that IFNα-2a has a poor antiviral response in HepG2.2.15 cells. Then, to test whether IFNα-2a-mediated enhancement of HBV replication is related to autophagy, HepG2.2.15 cells were co-treated with 3-MA and IFNα-2a. 3-MA clearly blocked the positive effect of IFNα-2a on HBsAg production and secretion (Figure 4.33, C).

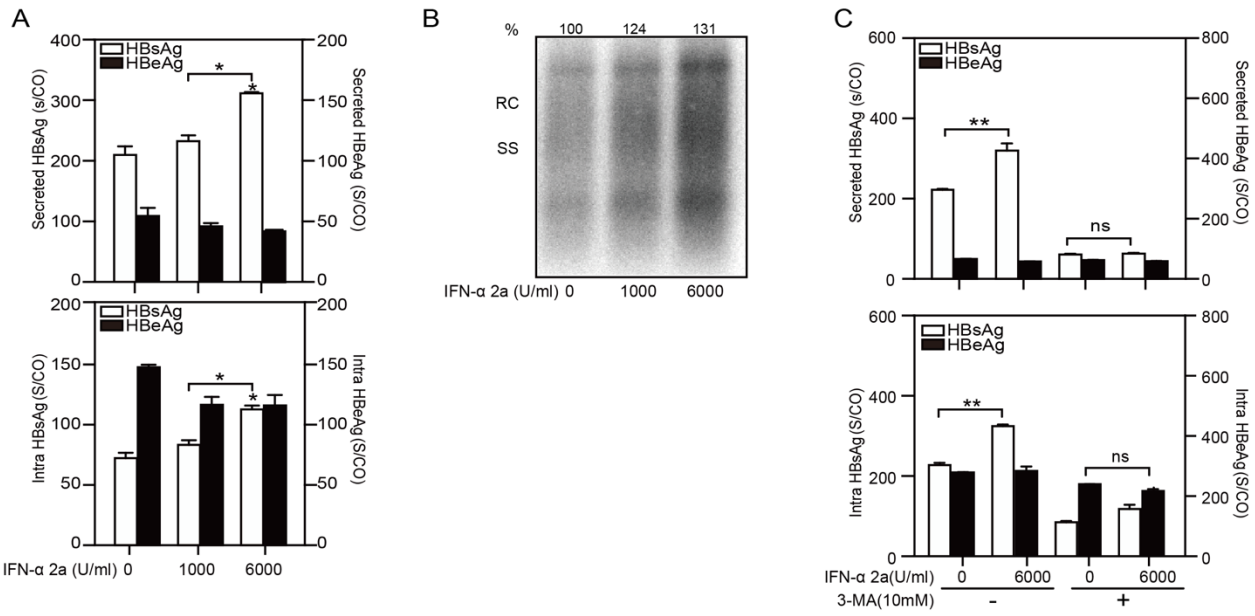

Figure 4. 33 High IFNα-2a concentrations do not inhibit HBV replication and gene expression in hepatoma cells

HepG2.2.15 cells were treated with the indicated concentrations of IFNα-2a for 72 h. (A) The levels of secreted and intracellular HBsAg and HBeAg were measured by CMIA. (B) Encapsidated HBV replicative intermediates were detected by Southern blotting. (C) HepG2.2.15 cells were treated with 6000 U/ml IFNα-2a with or without 10 nM 3-MA. The levels of secreted and intracellular HBsAg and HBeAg were measured by CMIA. *P < 0.05; **P < 0.01; and ns, not significant.

4.9.9 High IFNα-2a concentrations promote the yield of HBsAg in PHHs

PHHs were infected with HBV and treated with IFNα-2a post-infection. The levels of HBsAg and HBeAg in the culture supernatants were detected by CIMA. After the treatment at the concentration of 6000 U/ml IFNα-2a, the HBsAg levels were significantly increased (Figure 4.34). These data suggest that IFNα-2a has a poor antiviral response in HBV-infected PHHs, and has a slight but measurable virus-promoting effect at high concentrations.

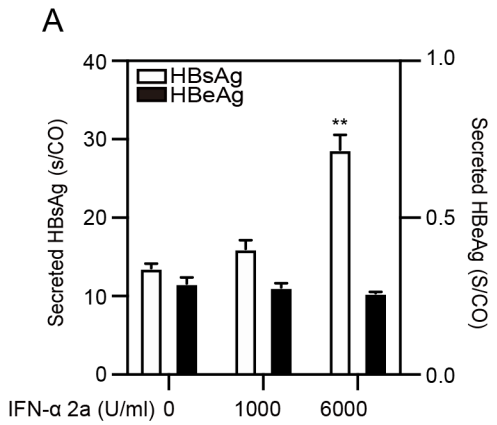

Figure 4. 34 High IFNα-2a concentrations promote the yield of HBsAg in PHHs

PHHs were infected with HBV virions (multiplicity of infection = 30). 4 days post-infection, PHHs were treated with IFNα-2a twice (1000 U/ml and 6000 U/ml). After 48 h, the levels of secreted and intracellular HBsAg and HBeAg were measured by CMIA. **P < 0.01.

4.9.10 Glucose does not change IFNα-2a-induced HBV replication and gene expression

Next, HepG2.2.15 cells were grown at the indicated glucose concentrations and treated with IFNα-2a. The results showed that the secreted and intracellular HBsAg were increased after IFNα-2a treatment both at low and high glucose conditions (Figure 4.35, A). The amount of HBV RIs decreased at the high glucose concentration, but it increased after IFNα-2a treatment independent of glucose concentrations (Figure 4.35, B). Consistently, the secreted and intracellular HBsAg decreased after co-treatment with 3-MA (Figure 4.35, C). All these results indicate that IFNα-2a enhances HBV replication at a high dose and this enhancement is dependent on autophagy.

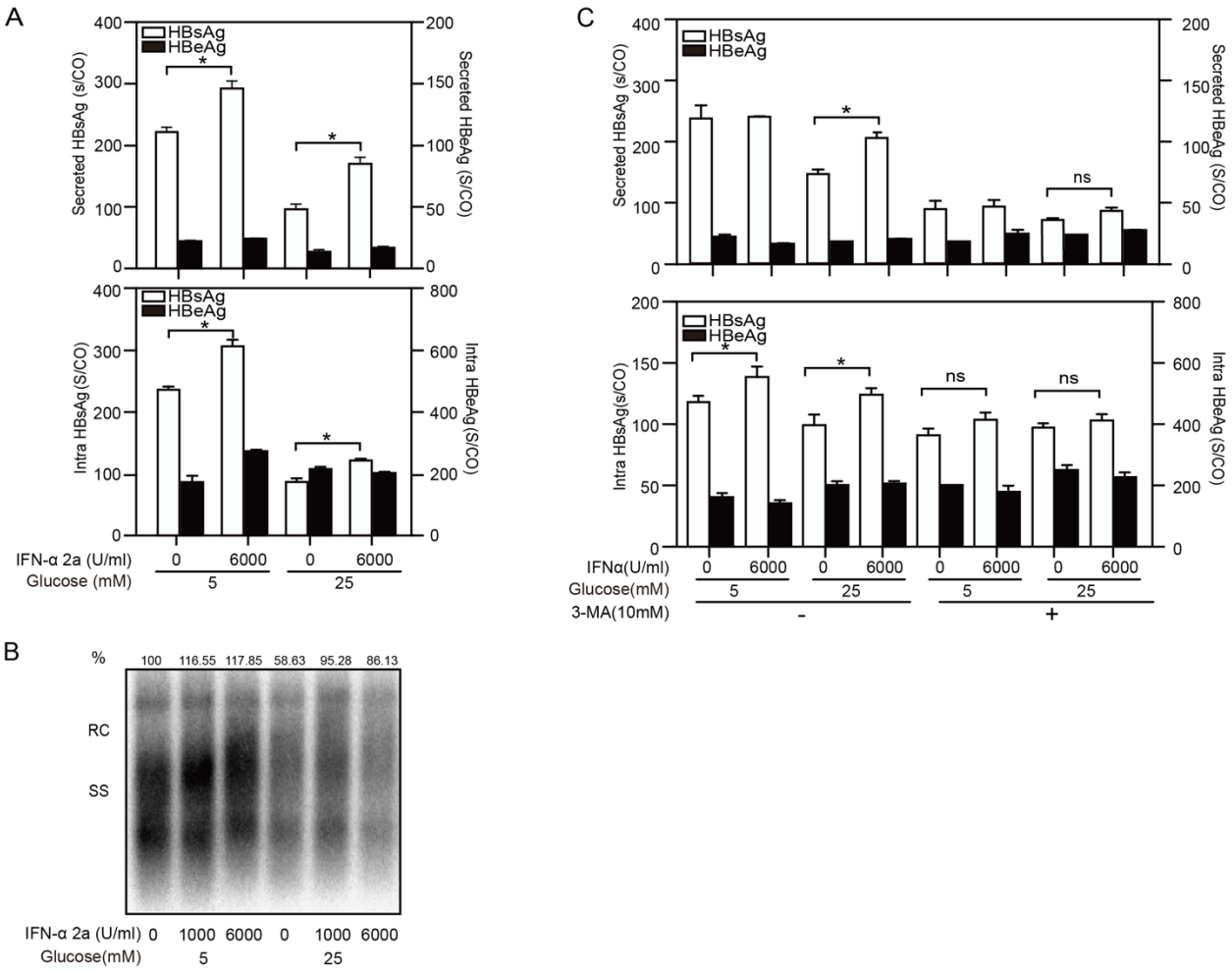

Figure 4. 35 Glucose does not change IFNα-2a-induced HBV replication and gene expression

HepG2.2.15 cells were cultured in a medium with the indicated glucose concentrations (5 and 25 mM) and treated with 6000 U/ml IFNα-2a for 72 h. (A) The levels of secreted and intracellular HBsAg and HBeAg were measured by CMIA. (B) Encapsidated HBV replicative intermediates were detected by Southern blotting. (C) HepG2.2.15 cells were cultured at the indicated glucose concentrations (5 and 25 mM) and 6000 U/ml IFNα-2a with or without 10 nM 3-MA for 72 h. The levels of secreted and intracellular HBsAg and HBeAg were measured by CMIA. *P < 0.05; and ns, not significant.

5. Discussion

5.1 GW4869 impairs HBV to enter the endosomal pathway but increases HBV secretion in the autophagic pathway

In the present study, we showed for the first time that amphisomes serve as a platform for HBV assembly and release. The disruption of ceramide-mediated inward budding of membranes by GW4869 diminished the release of HBV virions and retained HBV virions and SVPs within cells, thereby triggering cellular ER stress. GW4869 induced the inactivation of the AKT-MTOR signaling pathway, prevented autophagosome-lysosome fusion, and enhanced cellular autophagy in hepatic cells. Silencing RAB27A and -B influenced both intra- and extracellular HBV DNA levels, altering HBV distribution. Interferences with exosome secretion by GW4869, si*RAB27A*, and -*B* decreased the association of HBsAg with early endosomes but enhanced HBsAg transportation to autophagosomes, indicating that autophagy is an alternative pathway for HBV secretion. Moreover, GW4869, si*RAB27A*, -*B* treatment increased the number of intracellular $LC3^{+}CD63^{+}HBsAg^{+}$ complexes, suggesting the involvement of amphisomes in HBV production and secretion.

Numerous studies have demonstrated that GW4869 modulates HBV replication and infection by interfering with late endosomes/MVBs. For example, GW4869 impairs HBV virion secretion by inhibiting MVB or exosome formation [73]. GW4869 suppresses the production of HBV-DNA- or miR-222-containing exosomes thus reducing HBV transmission and liver fibrosis [130, 131]. However, there is no evidence showing how GW4869's interference with late endosome/MVB function affects HBV distribution and trafficking within cells. In the present study, we examined how the inhibition of exosome biogenesis changes HBV replication and distribution, and how the perturbation of the endosome pathway affects HBV trafficking between the endosomal and autophagic pathways.

Different species of incomplete viral particles, including SVPs/HBsAg, naked nucleocapsids, empty virions, and infectious HBV virions, can be released from hepatocytes utilizing diverse pathways. GW4869 blocked HBV virion secretion but also induced increased SVPs/HBsAg secretion. Thus, we hypothesize that GW4869 blocks

the late endosome/MVB pathway, triggering a feedback mechanism that leads to SVPs/HBsAg secretion from Golgi through secretory vesicles. Although GW4869 did not affect HBsAg colocalization with late endosomes/MVBs, it did prevent HBcAg from entering late endosomes/MVBs, suggesting that GW4869 might interfere with HBV assembly and reduce HBV virion secretion.

A study showed that HBV core particles localize to autophagic membranes and productively replicate HBV genomes [83]. Here, the colocalization of HBsAg and HBcAg with LC3 could be confirmed using a confocal microscope. Furthermore, an increased colocalization ratio after GW4869 treatment indicated enhanced recruitment of HBsAg and HBcAg to autophagosomes when the endosomal pathway was impaired. This was consistent with our previous finding that autophagy constitutes an alternative secretion pathway [55].

Mechanically, GW4869 inhibits nSMases, which are the enzymes responsible for the breakdown of sphingomyelin into ceramide, leading to alterations in exosome biogenesis [132, 133]. Studies have shown that the depletion of nSMase2 impairs the incorporation of endogenous LC3 into endosomes, blocking LC3-dependent-EV loading and secretion [134]. This highlights the important role of nSMase2 in endosomal and autophagic pathway coordination. To verify the role of nSMase in HBV replication and trafficking, specific siRNA was used to silence *SMPD2*, a gene encoding nSMase. *SMPD2* silencing revealed the same effect of GW4869 on HBV replication and trafficking. Overall, GW4869-mediated HBV trafficking between endosomal and autophagic pathways is dependent on neutral sphingomyelinases.

5.2 RAB27A and -B differently function in HBV trafficking

RAB27, previously implicated in exosome secretion [135], has shown involvement in the release of viruses, such as HCV [136] and HEV [137]. However, the role of RAB27A and -B in HBV release from cells remains unknown. Despite their high sequence similarity [138], RAB27A and -B exhibit functional distinctions in HBV trafficking and release. Silencing both *RAB27A* and *-B* caused HBsAg accumulation within cells, and only *RAB27A* silencing suppressed the secretion of HBV DNA and HBsAg. *RAB27B* silencing predominately impaired HBsAg trafficking to different cellular organelles, including early endosomes, late endosomes/MVBs, and autophagosomes. This finding was consistent

with Matias *et al.* 's findings [135], indicating that *RAB27A* and *-B* control distinct steps in late endosome/MVB formation and exosome release in Hela cells. *RAB27A* is required for membrane fusion, while *RAB27B* probably regulates MVBs motility. It is convincing that *RAB27B* plays a vital role in facilitating the transportation of HBV components to cellular organelles. Autophagosomes containing HBV components fuse with late endosomes/MVBs and form amphisomes. The subsequent release of cargos in amphisomes by fusion with the plasma membrane is an *RAB27A*-dependent process. *RAB27B* silencing led to a modest accumulation of HBV components, though it did not sufficiently initiate substantial ER stress. Consequently, this condition resulted in the deceleration of HBsAg transportation towards endosomes and autophagosomes but accumulated in the amphisomes.

5.3 GW4869, RAB27A, and -B block HBV secretion but retain HBV in amphisomes

Conventionally, amphisomes are intermediate organelles produced through the fusion of late endosomes with autophagosomes, which mediate the delivery of cellular cargos for lysosomal degradation. Beyond this, amphisomes have an unconventional secretory function, which has been linked to ANXA2 secretion in lung epithelial cells [139], as well as interleukin-1 β, α-synuclein and β-amyloid precursor proteins (βAPP) in neurodegenerative disorders [140-142]. In this study, we visualized the amphisomes and identified the colocalization of HBsAg with amphisomes. Treatment with GW4869 and silencing of *RAB27A* and *-B* led to the accumulation of $HBsAg^{+}LC3^{+}CD63^{+}$ structures, showing that amphisomes are involved in HBV assembly and release, and are particularly dependent on *RAB27A*. Previous work has revealed that *RAB11* silencing disturbs autophagosome-MVB fusion and reduces HBV virion release [83]. These findings have led us to explore more details on how autophagy and exosome secretion pathways cooperatively control HBV secretion. These findings may be exploited for further development in anti-viral therapy using amphisome inhibitors as potential drug targets.

In conclusion, our results demonstrated the pivotal role of the autophagy-late endosome/MVB-exosome axis in regulating HBV assembly and release. The evidence strongly supports the involvement of amphisomes as a platform for HBV release.

5.4 IFNα-2a induces cellular autophagy and modulates HBV replication

In this part, we demonstrated that IFNα-2a interferes with multiple intracellular signaling pathways, including inhibiting AKT/MTOR and AMPK signaling pathways, promoting autophagosome formation, and blocking autophagic degradation in HepG2.2.15 cells. This action of IFNα-2a resulted in enhanced HBV replication. Additionally, the induction of ISG15 and IFITM1 by IFNα-2a is dependent on AKT/MTOR signaling and autophagy, as examined in the present study.

Type I IFN (IFN-I) can modulate JAK-STAT and PI3K/AKT/MTOR pathways, which induce autophagy and drive downstream biological activities. IFN induces autophagy through IGF1–PI3K/Akt/mTOR signaling pathways and participates in controlling tumor growth, inflammatory reactions, and antiviral activities [143-146]. Leukocyte IFN failed to increase autophagosome formation after JAK1 or STAT1 knockout, which highlighted the role of the JAK/STAT pathway in IFN-α-induced autophagy in antitumor activity [147]. Therefore, IFNa triggers autophagy via both canonical and non-canonical signaling pathways and may contribute to the outcome of IFNa treatment in different diseases.

In our study, IFNα-2a treatment decreased the phosphorylation of AKT/MTOR and AMPK in hepatoma cells. However, the situation in PHHs was completely different. Since PHHs are not growing cells when cultured in the medium, thus with very low basal levels of phosphorylated MTOR and AKT. The levels of phosphorylated MTOR and AKT increased rapidly in response to stimulation of different doses of IFNα-2a, indicating that IFN activated the non-canonical pathways. Upon HBV infection, the levels of phosphorylated MTOR and AKT are increased accompanied with IFNα-2a treatment. AMPK is a sensitive indicator of the cytosolic AMP/ATP ratio [148]. Treatment with interferons mat causes a reduction in cellular ATP levels [149], thus, IFNα-2a likely induces an increased level of phosphorylated AMPK through changes in the AMP/ATP ratio in PHHs. Our previous study revealed that AMPK positively regulated autophagy and thereby increased HBV replication in PHHs, which is consistent with this finding in IFNα-2a treated PHHs [93].

Overall, naïve or transiently infected PHHs differently respond to IFNα treatment than persistently infected cells with high levels of HBV replication and gene expression.

In hepatoma cells, HBV suppression could be achieved if the cells were treated with IFNα-2a prior or early after transfection with replication-competent HBV genomes [150].

However, the suppression of established HBV replication in hepatic cells by IFNα-2a is rather ineffective [151, 152]. In our cell culture system, HBV replication was slightly enhanced when treated with 1000 or 6000 U/ml of IFNα-2a. Thus, IFNα-2a may preferentially protect uninfected hepatocytes against the establishment of HBV infection while it does not effectively clear HBV from persistently infected cells.

In the present study, it was demonstrated that the expression of ISGs, ISG15, and IFITM1, were attenuated by blocking autophagy, suggesting that induction of ISG15 and IFITM1 is dependent on the initiation of autophagy. However, IFNα-2a-induced ISG15 and IFITM1 expressions are differently regulated at low and high glucose conditions. The activation of the AKT/MTOR pathway may also allow ISG15 expression [128, 129]. Consistently, the high glucose concentration modulated higher expression levels of MTOR and AKT, which may contribute to the expression of ISG15. In conclusion, our findings demonstrated that IFNα-2a can inhibit MTOR and AKT signaling pathways, resulting in the initiation of autophagy and blockade of autophagic degradation. This non-canonical IFNα signaling may positively modulate HBV replication in hepatic cells.

6. Summary

In the present study, we investigated the influence of interferences with late endosome/MVB functionality and secretion processes on HBV replication and trafficking. While subviral particles (SVPs) are predominantly secreted via the ER-Golgi pathway, HBV virions and a part of filamentous SVPs travel through the early-late endosome/MVB pathway under normal conditions. A fraction of HBV proteins, SVPs, or virions may be directed to the autophagosome-lysosome pathway for autophagic degradation. Notably, GW4869 treatment and sphingomyelin phosphodiesterase 2 (*SMPD2*) silencing reduces cargo release from early endosomes, resulting in the accumulation of HBsAg in ER. This induces slight ER stress, leading to AKT-MTOR signaling inactivation and increasing autophagosome formation. Consequently, the association between HBsAg/SVPs and autophagosomes increased. While GW4869 treatment does not influence lysosomal enzymatic activities, it impedes autophagosome-lysosome fusion, thereby contributing to increased autophagosome levels. Furthermore, GW4869 retains HBV in amphisomes. Silencing of *RAB27A* and *-B* results in the intracellular accumulation of HBV proteins,

particularly within amphisome structures, signifying that the fusion of the autophagosome with late endosome/MVB occurs, with amphisomes serving as a platform for HBV secretion. Taken together, our results demonstrated that amphisomes may represent the way for transferring HBsAg/SVPs and HBV virions from autophagosomes to late endosomes/MBVs for subsequent release. We also found that the treatment of IFNα-2a triggers autophagosome formation, indicating that the innate immune system is also involved in autophagy. However, whether IFNα-2a affects endosomal vesicle trafficking and thereby modulates HBV replication and secretion is worth exploring.

7. Zusammenfassung

In der vorliegenden Studie haben wir den Einfluss von Interferenz der späten Endosomen/MVB-Funktionalität und Sekretionsprozesse auf die Replikation und den Transport des Hepatitis-B-Virus (HBV) untersucht. Während subvirale Partikel (SVPs) hauptsächlich über dem endoplasmatischen Retikulum (ER)-Golgi-Weg exportiert werden, nehmen HBV-Virionen und ein Teil der filamentösen SVPs unter normalen Bedingungen die früh-späten Endosomen/MVB-Route. Ein Teil der HBV-Proteine, SVPs oder Virionen kann über den Autophagolysosomen-Weg zur autophagischen Degradation zugefügt werden. Bemerkenswerterweise reduzieren die GW4869-Behandlung und das Silencing von Sphingomyelin-Phosphodiesterase 2 (SMPD2) die Freisetzung von Fracht aus den frühen Endosomen, was zu einer Anhäufung von HBsAg im ER führt. Dies führt zu leichtem ER-Stress, was in die Inaktivierung des AKT-MTOR-Signalings und einer erhöhten Autophagosomenbildung resultiert. Infolgedessen nimmt die Assoziation von HBsAg/SVPs mit Autophagosomen zu. Während die GW4869-Behandlung keinen Einfluss auf lysosomale enzymatische Aktivitäten hat, hindert sie die Fusion von Autophagosomen und Lysosomen, was ebenfalls zu einer erhöhten Menge von Autophagosomen beiträgt. Darüber hinaus führt GW4869 Behandlung zur Ansammlung von HBV in Amphisomen. Das Silencing von RAB27A und -B führt zu einer intrazellulären Anhäufung von HBV-Proteinen, insbesondere in Amphisomen, was darauf hinweist, dass die Fusion von Autophagosom mit späten Endosomen/MVB stattfindet und Amphisomen als Plattform für die HBV-Sekretion dient. Zusammenfassend zeigen unsere Ergebnisse, dass Amphisomen möglicherweise die Route darstellen, um

HBsAg/SVPs und HBV-Virionen von Autophagosomen zu späten Endosomen/MVBs für die anschließende Freisetzung zu übertragen. Wir haben auch festgestellt, dass die Behandlung mit IFNα-2a die Bildung von Autophagosomen auslöst, was darauf hinweist, dass auch das angeborene Immunsystem an der Autophagie beteiligt ist. Es ist jedoch noch zu erforschen, ob IFNα-2a den endosomalen Vesikelverkehr beeinflusst und damit die Replikation und Sekretion von HBV moduliert.

8. References

1. Alter, H.J. and B.S. Blumberg, *Further studies on a "new" human isoprecipitin system (Australia antigen).* Blood, 1966. **27**(3): p. 297-309.
2. Blumberg, B.S., et al., *A serum antigen (Australia antigen) in Down's syndrome, leukemia, and hepatitis.* Ann Intern Med, 1967. **66**(5): p. 924-31.
3. Dane, D.S., C.H. Cameron, and M. Briggs, *Virus-like particles in serum of patients with Australia-antigen-associated hepatitis.* Lancet, 1970. **1**(7649): p. 695-8.
4. Llovet, J.M., et al., *Hepatocellular carcinoma.* Nat Rev Dis Primers, 2021. **7**(1): p. 6.
5. Diseases, G.B.D. and C. Injuries, *Global burden of 369 diseases and injuries in 204 countries and territories, 1990-2019: a systematic analysis for the Global Burden of Disease Study 2019.* Lancet, 2020. **396**(10258): p. 1204-1222.
6. Hoffmann, H.H., W.M. Schneider, and C.M. Rice, *Interferons and viruses: an evolutionary arms race of molecular interactions.* Trends Immunol, 2015. **36**(3): p. 124-38.
7. Mesev, E.V., R.A. LeDesma, and A. Ploss, *Decoding type I and III interferon signalling during viral infection.* Nat Microbiol, 2019. **4**(6): p. 914-924.
8. Naggie, S. and A.S. Lok, *New Therapeutics for Hepatitis B: The Road to Cure.* Annu Rev Med, 2021. **72**: p. 93-105.
9. Xie, Q.L., et al., *The Efficacy and Safety of Entecavir and Interferon Combination Therapy for Chronic Hepatitis B Virus Infection: A Meta-Analysis.* PLoS One, 2015. **10**(7): p. e0132219.
10. Nguyen, D.H., S. Gummuluru, and J. Hu, *Deamination-independent inhibition of hepatitis B virus reverse transcription by APOBEC3G.* J Virol, 2007. **81**(9): p. 4465-

72.

11. Wang, Y.X., et al., *Interferon-inducible MX2 is a host restriction factor of hepatitis B virus replication.* J Hepatol, 2020. **72**(5): p. 865-876.
12. Liu, Y., et al., *Interferon-inducible ribonuclease ISG20 inhibits hepatitis B virus replication through directly binding to the epsilon stem-loop structure of viral RNA.* PLoS Pathog, 2017. **13**(4): p. e1006296.
13. Xia, Y., et al., *Interferon-gamma and Tumor Necrosis Factor-alpha Produced by T Cells Reduce the HBV Persistence Form, cccDNA, Without Cytolysis.* Gastroenterology, 2016. **150**(1): p. 194-205.
14. Schoggins, J.W., *Interferon-Stimulated Genes: What Do They All Do?* Annu Rev Virol, 2019. **6**(1): p. 567-584.
15. Suslov, A., et al., *Hepatitis B Virus Does Not Interfere With Innate Immune Responses in the Human Liver.* Gastroenterology, 2018. **154**(6): p. 1778-1790.
16. Ye, J. and J. Chen, *Interferon and Hepatitis B: Current and Future Perspectives.* Front Immunol, 2021. **12**: p. 733364.
17. Liang, T.J., *Hepatitis B: the virus and disease.* Hepatology, 2009. **49**(5 Suppl): p. S13-21.
18. Hu, J. and K. Liu, *Complete and Incomplete Hepatitis B Virus Particles: Formation, Function, and Application.* Viruses, 2017. **9**(3).
19. Gerlich, W.H., *Medical virology of hepatitis B: how it began and where we are now.* Virol J, 2013. **10**: p. 239.
20. Herrscher, C., P. Roingeard, and E. Blanchard, *Hepatitis B Virus Entry into Cells.* Cells, 2020. **9**(6).
21. Huovila, A.P., A.M. Eder, and S.D. Fuller, *Hepatitis B surface antigen assembles in a post-ER, pre-Golgi compartment.* J Cell Biol, 1992. **118**(6): p. 1305-20.
22. Patient, R., et al., *Hepatitis B virus subviral envelope particle morphogenesis and intracellular trafficking.* J Virol, 2007. **81**(8): p. 3842-51.
23. Bruss, V. and D. Ganem, *The role of envelope proteins in hepatitis B virus assembly.* Proc Natl Acad Sci U S A, 1991. **88**(3): p. 1059-63.
24. Patient, R., C. Hourioux, and P. Roingeard, *Morphogenesis of hepatitis B virus and its subviral envelope particles.* Cell Microbiol, 2009. **11**(11): p. 1561-70.

25. Pastor, F., et al., *Direct interaction between the hepatitis B virus core and envelope proteins analyzed in a cellular context.* Sci Rep, 2019. **9**(1): p. 16178.
26. Seitz, S., et al., *The Hepatitis B Virus Envelope Proteins: Molecular Gymnastics Throughout the Viral Life Cycle.* Annu Rev Virol, 2020. **7**(1): p. 263-288.
27. Yan, H., et al., *Sodium taurocholate cotransporting polypeptide is a functional receptor for human hepatitis B and D virus.* Elife, 2012. **1**: p. e00049.
28. Herrscher, C., et al., *Hepatitis B virus entry into HepG2-NTCP cells requires clathrin-mediated endocytosis.* Cell Microbiol, 2020. **22**(8): p. e13205.
29. Ni, Y., et al., *Hepatitis B and D viruses exploit sodium taurocholate co-transporting polypeptide for species-specific entry into hepatocytes.* Gastroenterology, 2014. **146**(4): p. 1070-83.
30. Glebe, D., et al., *Mapping of the hepatitis B virus attachment site by use of infection-inhibiting preS1 lipopeptides and tupaia hepatocytes.* Gastroenterology, 2005. **129**(1): p. 234-45.
31. Urban, S., et al., *Strategies to inhibit entry of HBV and HDV into hepatocytes.* Gastroenterology, 2014. **147**(1): p. 48-64.
32. Iwamoto, M., et al., *Epidermal growth factor receptor is a host-entry cofactor triggering hepatitis B virus internalization.* Proc Natl Acad Sci U S A, 2019. **116**(17): p. 8487-8492.
33. Hu, Q., et al., *E-cadherin Plays a Role in Hepatitis B Virus Entry Through Affecting Glycosylated Sodium-Taurocholate Cotransporting Polypeptide Distribution.* Front Cell Infect Microbiol, 2020. **10**: p. 74.
34. Verrier, E.R., et al., *A targeted functional RNA interference screen uncovers glypican 5 as an entry factor for hepatitis B and D viruses.* Hepatology, 2016. **63**(1): p. 35-48.
35. Sureau, C. and J. Salisse, *A conformational heparan sulfate binding site essential to infectivity overlaps with the conserved hepatitis B virus a-determinant.* Hepatology, 2013. **57**(3): p. 985-94.
36. Beck, J. and M. Nassal, *Hepatitis B virus replication.* World J Gastroenterol, 2007. **13**(1): p. 48-64.
37. Nassal, M., *HBV cccDNA: viral persistence reservoir and key obstacle for a cure*

of chronic hepatitis B. Gut, 2015. **64**(12): p. 1972-84.

38. Shih, C., et al., *Hepatitis B Virus.* Trends Microbiol, 2018. **26**(4): p. 386-387.
39. Bruss, V., et al., *Post-translational alterations in transmembrane topology of the hepatitis B virus large envelope protein.* EMBO J, 1994. **13**(10): p. 2273-9.
40. Bruss, V., *A short linear sequence in the pre-S domain of the large hepatitis B virus envelope protein required for virion formation.* J Virol, 1997. **71**(12): p. 9350-7.
41. Zeyen, L., T. Doring, and R. Prange, *Hepatitis B Virus Exploits ERGIC-53 in Conjunction with COPII to Exit Cells.* Cells, 2020. **9**(8).
42. Yang, S., et al., *A putative amphipathic alpha helix in hepatitis B virus small envelope protein plays a critical role in the morphogenesis of subviral particles.* J Virol, 2021. **95**(8).
43. Jiang, B., et al., *Subviral Hepatitis B Virus Filaments, like Infectious Viral Particles, Are Released via Multivesicular Bodies.* J Virol, 2015. **90**(7): p. 3330-41.
44. Ning, X., et al., *Common and Distinct Capsid and Surface Protein Requirements for Secretion of Complete and Genome-Free Hepatitis B Virions.* J Virol, 2018. **92**(14).
45. Macovei, A., et al., *Regulation of hepatitis B virus infection by Rab5, Rab7, and the endolysosomal compartment.* J Virol, 2013. **87**(11): p. 6415-27.
46. Maxfield, F.R., *Role of endosomes and lysosomes in human disease.* Cold Spring Harb Perspect Biol, 2014. **6**(5): p. a016931.
47. Huotari, J. and A. Helenius, *Endosome maturation.* EMBO J, 2011. **30**(17): p. 3481-500.
48. Rink, J., et al., *Rab conversion as a mechanism of progression from early to late endosomes.* Cell, 2005. **122**(5): p. 735-49.
49. Stenmark, H., *Rab GTPases as coordinators of vesicle traffic.* Nat Rev Mol Cell Biol, 2009. **10**(8): p. 513-25.
50. Mayor, S. and R.E. Pagano, *Pathways of clathrin-independent endocytosis.* Nat Rev Mol Cell Biol, 2007. **8**(8): p. 603-12.
51. Mayor, S., R.G. Parton, and J.G. Donaldson, *Clathrin-independent pathways of endocytosis.* Cold Spring Harb Perspect Biol, 2014. **6**(6).
52. O'Sullivan, M.J. and A.J. Lindsay, *The Endosomal Recycling Pathway-At the*

Crossroads of the Cell. Int J Mol Sci, 2020. **21**(17).

53. Liu, Z., et al., *Non-viral nanoparticles for RNA interference: Principles of design and practical guidelines.* Adv Drug Deliv Rev, 2021. **174**: p. 576-612.
54. Zhao, Z., et al., *Hepatitis B virus promotes its own replication by enhancing RAB5A-mediated dual activation of endosomal and autophagic vesicle pathways.* Emerg Microbes Infect, 2023. **12**(2): p. 2261556.
55. Wang, X., et al., *CCDC88A/GIV promotes HBV replication and progeny secretion via enhancing endosomal trafficking and blocking autophagic degradation.* Autophagy, 2022. **18**(2): p. 357-374.
56. Inoue, J., et al., *Small Interfering RNA Screening for the Small GTPase Rab Proteins Identifies Rab5B as a Major Regulator of Hepatitis B Virus Production.* J Virol, 2019. **93**(15).
57. Cooper, A. and Y. Shaul, *Clathrin-mediated endocytosis and lysosomal cleavage of hepatitis B virus capsid-like core particles.* J Biol Chem, 2006. **281**(24): p. 16563-9.
58. Schmidt, O. and D. Teis, *The ESCRT machinery.* Curr Biol, 2012. **22**(4): p. R116-20.
59. Hurley, J.H. and P.I. Hanson, *Membrane budding and scission by the ESCRT machinery: it's all in the neck.* Nat Rev Mol Cell Biol, 2010. **11**(8): p. 556-66.
60. Chou, S.F., et al., *The Dual Role of an ESCRT-0 Component HGS in HBV Transcription and Naked Capsid Secretion.* PLoS Pathog, 2015. **11**(10): p. e1005123.
61. Stieler, J.T. and R. Prange, *Involvement of ESCRT-II in hepatitis B virus morphogenesis.* PLoS One, 2014. **9**(3): p. e91279.
62. Zheng, Y., et al., *Hepatitis B virus hijacks TSG101 to facilitate egress via multiple vesicle bodies.* PLoS Pathog, 2023. **19**(5): p. e1011382.
63. Lambert, C., T. Doring, and R. Prange, *Hepatitis B virus maturation is sensitive to functional inhibition of ESCRT-III, Vps4, and gamma 2-adaptin.* J Virol, 2007. **81**(17): p. 9050-60.
64. Kian Chua, P., M.H. Lin, and C. Shih, *Potent inhibition of human Hepatitis B virus replication by a host factor Vps4.* Virology, 2006. **354**(1): p. 1-6.

65. Watanabe, T., et al., *Involvement of host cellular multivesicular body functions in hepatitis B virus budding.* Proc Natl Acad Sci U S A, 2007. **104**(24): p. 10205-10.
66. Bardens, A., et al., *Alix regulates egress of hepatitis B virus naked capsid particles in an ESCRT-independent manner.* Cell Microbiol, 2011. **13**(4): p. 602-19.
67. Rost, M., et al., *Gamma-adaptin, a novel ubiquitin-interacting adaptor, and Nedd4 ubiquitin ligase control hepatitis B virus maturation.* J Biol Chem, 2006. **281**(39): p. 29297-308.
68. Hoffmann, J., et al., *Identification of alpha-taxilin as an essential factor for the life cycle of hepatitis B virus.* J Hepatol, 2013. **59**(5): p. 934-41.
69. Vietri, M., M. Radulovic, and H. Stenmark, *The many functions of ESCRTs.* Nat Rev Mol Cell Biol, 2020. **21**(1): p. 25-42.
70. Pegtel, D.M. and S.J. Gould, *Exosomes.* Annu Rev Biochem, 2019. **88**: p. 487-514.
71. Jia, X., et al., *Label-free Proteomic Analysis of Exosomes Derived from Inducible Hepatitis B Virus-Replicating HepAD38 Cell Line.* Mol Cell Proteomics, 2017. **16**(4 suppl 1): p. S144-S160.
72. Wang, J., D. Cao, and J. Yang, *Exosomes in Hepatitis B Virus Transmission and Related Immune Response.* Tohoku J Exp Med, 2020. **252**(4): p. 309-320.
73. Wu, Q., et al., *Presence of Intact Hepatitis B Virions in Exosomes.* Cell Mol Gastroenterol Hepatol, 2023. **15**(1): p. 237-259.
74. Catalano, M. and L. O'Driscoll, *Inhibiting extracellular vesicles formation and release: a review of EV inhibitors.* J Extracell Vesicles, 2020. **9**(1): p. 1703244.
75. Kroemer, G., G. Marino, and B. Levine, *Autophagy and the integrated stress response.* Mol Cell, 2010. **40**(2): p. 280-93.
76. Yla-Anttila, P., et al., *3D tomography reveals connections between the phagophore and endoplasmic reticulum.* Autophagy, 2009. **5**(8): p. 1180-5.
77. Ge, L., et al., *The ER-Golgi intermediate compartment is a key membrane source for the LC3 lipidation step of autophagosome biogenesis.* Elife, 2013. **2**: p. e00947.
78. Puri, C., et al., *The RAB11A-Positive Compartment Is a Primary Platform for Autophagosome Assembly Mediated by WIPI2 Recognition of PI3P-RAB11A.* Dev Cell, 2018. **45**(1): p. 114-131 e8.

79. Mizushima, N., *Autophagy: process and function.* Genes Dev, 2007. **21**(22): p. 2861-73.
80. Glick, D., S. Barth, and K.F. Macleod, *Autophagy: cellular and molecular mechanisms.* J Pathol, 2010. **221**(1): p. 3-12.
81. Lin, Y., et al., *Interplay between Cellular Autophagy and Hepatitis B Virus Replication: A Systematic Review.* Cells, 2020. **9**(9).
82. Liu, S., et al., *Autophagy: Regulator of cell death.* Cell Death Dis, 2023. **14**(10): p. 648.
83. Chu, J.Y.K., et al., *Autophagic membranes participate in hepatitis B virus nucleocapsid assembly, precore and core protein trafficking, and viral release.* Proc Natl Acad Sci U S A, 2022. **119**(30): p. e2201927119.
84. Tian, Y., et al., *Autophagy required for hepatitis B virus replication in transgenic mice.* J Virol, 2011. **85**(24): p. 13453-6.
85. Bagga, S., et al., *Hepatitis B virus (HBV) X protein-mediated regulation of hepatocyte metabolic pathways affects viral replication.* Virology, 2016. **498**: p. 9-22.
86. Sir, D., et al., *The early autophagic pathway is activated by hepatitis B virus and required for viral DNA replication.* Proc Natl Acad Sci U S A, 2010. **107**(9): p. 4383-8.
87. Li, J., et al., *Subversion of cellular autophagy machinery by hepatitis B virus for viral envelopment.* J Virol, 2011. **85**(13): p. 6319-33.
88. Huang, W., et al., *Rapamycin enhances HBV production by inducing cellular autophagy.* Hepat Mon, 2014. **14**(10): p. e20719.
89. He, Q., et al., *Dexamethasone Stimulates Hepatitis B Virus (HBV) Replication Through Autophagy.* Med Sci Monit, 2018. **24**: p. 4617-4624.
90. Chen, X., et al., *Cisplatin induces autophagy to enhance hepatitis B virus replication via activation of ROS/JNK and inhibition of the Akt/mTOR pathway.* Free Radic Biol Med, 2019. **131**: p. 225-236.
91. Doring, T., et al., *Hepatitis B Virus Subverts the Autophagy Elongation Complex Atg5-12/16L1 and Does Not Require Atg8/LC3 Lipidation for Viral Maturation.* J Virol, 2018. **92**(7).

92. Lin, Y., et al., *Glucosamine promotes hepatitis B virus replication through its dual effects in suppressing autophagic degradation and inhibiting MTORC1 signaling.* Autophagy, 2020. **16**(3): p. 548-561.
93. Wang, X., et al., *AMPK and Akt/mTOR signalling pathways participate in glucose-mediated regulation of hepatitis B virus replication and cellular autophagy.* Cell Microbiol, 2020. **22**(2): p. e13131.
94. Wang, X., et al., *O-GlcNAcylation modulates HBV replication through regulating cellular autophagy at multiple levels.* FASEB J, 2020. **34**(11): p. 14473-14489.
95. Li, J., et al., *Interferon Alpha Induces Cellular Autophagy and Modulates Hepatitis B Virus Replication.* Front Cell Infect Microbiol, 2022. **12**: p. 804011.
96. Lin, Y., et al., *The microRNA-99 family modulates hepatitis B virus replication by promoting IGF-1R/PI3K/Akt/mTOR/ULK1 signaling-induced autophagy.* Cell Microbiol, 2017. **19**(5).
97. Li, F., et al., *Human hepatocyte-enriched miRNA-192-3p promotes HBV replication through inhibiting Akt/mTOR signalling by targeting ZNF143 in hepatic cell lines.* Emerg Microbes Infect, 2022. **11**(1): p. 616-628.
98. Liu, B., et al., *Hepatitis B virus X protein inhibits autophagic degradation by impairing lysosomal maturation.* Autophagy, 2014. **10**(3): p. 416-30.
99. Lin, Y., et al., *Hepatitis B virus is degraded by autophagosome-lysosome fusion mediated by Rab7 and related components.* Protein Cell, 2019. **10**(1): p. 60-66.
100. Lin, Y., et al., *Synaptosomal-associated protein 29 is required for the autophagic degradation of hepatitis B virus.* FASEB J, 2019. **33**(5): p. 6023-6034.
101. Zheng, J., et al., *Lipid phosphatase SAC1 suppresses hepatitis B virus replication through promoting autophagic degradation of virions.* Antiviral Res, 2023. **213**: p. 105601.
102. Zhong, L., et al., *Epigallocatechin-3-gallate opposes HBV-induced incomplete autophagy by enhancing lysosomal acidification, which is unfavorable for HBV replication.* Cell Death Dis, 2015. **6**(5): p. e1770.
103. Xie, N., et al., *PRKAA/AMPK restricts HBV replication through promotion of autophagic degradation.* Autophagy, 2016. **12**(9): p. 1507-20.
104. Yu, J., et al., *Inhibition of HBV replication by EVA1A via enhancing cellular*

degradation of HBV components and its potential therapeutic application. Antiviral Res, 2023. **216**: p. 105643.

105. Hurley, J.H., *ESCRTs are everywhere.* EMBO J, 2015. **34**(19): p. 2398-407.
106. Rusten, T.E. and H. Stenmark, *How do ESCRT proteins control autophagy?* J Cell Sci, 2009. **122**(Pt 13): p. 2179-83.
107. Murrow, L., R. Malhotra, and J. Debnath, *ATG12-ATG3 interacts with Alix to promote basal autophagic flux and late endosome function.* Nat Cell Biol, 2015. **17**(3): p. 300-10.
108. Takahashi, Y., et al., *An autophagy assay reveals the ESCRT-III component CHMP2A as a regulator of phagophore closure.* Nat Commun, 2018. **9**(1): p. 2855.
109. Wang, X., et al., *Endoplasmic reticulum stress promotes HBV production by enhancing use of the autophagosome/multivesicular body axis.* Hepatology, 2022. **75**(2): p. 438-454.
110. Zhao, Y.G. and H. Zhang, *Autophagosome maturation: An epic journey from the ER to lysosomes.* J Cell Biol, 2019. **218**(3): p. 757-770.
111. Li, J., et al., *Interconnection of cellular autophagy and endosomal vesicle trafficking and its role in hepatitis B virus replication and release.* Virol Sin, 2024.
112. Stanssens, P., et al., *Efficient oligonucleotide-directed construction of mutations in expression vectors by the gapped duplex DNA method using alternating selectable markers.* Nucleic Acids Research, 1989. **17**(12): p. 4441-4454.
113. Lin, Y., et al., *Synaptosomal-associated protein 29 is required for the autophagic degradation of hepatitis B virus.* FASEB J, 2019: p. fj201801995RR.
114. Berg, T.O., et al., *Isolation and characterization of rat liver amphisomes. Evidence for fusion of autophagosomes with both early and late endosomes.* J Biol Chem, 1998. **273**(34): p. 21883-92.
115. Fader, C.M. and M.I. Colombo, *Autophagy and multivesicular bodies: two closely related partners.* Cell Death Differ, 2009. **16**(1): p. 70-8.
116. Ganesan, D. and Q. Cai, *Understanding amphisomes.* Biochem J, 2021. **478**(10): p. 1959-1976.
117. Ludwig, A.K., et al., *Precipitation with polyethylene glycol followed by washing and pelleting by ultracentrifugation enriches extracellular vesicles from tissue culture*

supernatants in small and large scales. J Extracell Vesicles, 2018. **7**(1): p. 1528109.

118. Solvik, T.A., et al., *Secretory autophagy maintains proteostasis upon lysosome inhibition.* J Cell Biol, 2022. **221**(6).
119. Xu, J., et al., *Chloroquine treatment induces secretion of autophagy-related proteins and inclusion of Atg8-family proteins in distinct extracellular vesicle populations.* Autophagy, 2022. **18**(11): p. 2547-2560.
120. Hassanpour, M., et al., *Exosomal cargos modulate autophagy in recipient cells via different signaling pathways.* Cell Biosci, 2020. **10**: p. 92.
121. Ferir, G., et al., *Antiviral treatment of chronic hepatitis B virus infections: the past, the present and the future.* Rev Med Virol, 2008. **18**(1): p. 19-34.
122. Caraglia, M., et al., *Alpha-interferon and its effects on signal transduction pathways.* J Cell Physiol, 2005. **202**(2): p. 323-35.
123. Molinaro, A., et al., *Insulin-Driven PI3K-AKT Signaling in the Hepatocyte Is Mediated by Redundant PI3Kalpha and PI3Kbeta Activities and Is Promoted by RAS.* Cell Metab, 2019. **29**(6): p. 1400-1409 e5.
124. Meijer, A.J. and P. Codogno, *Autophagy: regulation by energy sensing.* Curr Biol, 2011. **21**(6): p. R227-9.
125. Wang, X.Y., et al., *AMPK and Akt/mTOR signalling pathways participate in glucose-mediated regulation of hepatitis B virus replication and cellular autophagy.* Cellular Microbiology, 2020. **22**(2).
126. Darnell, J.E., Jr., I.M. Kerr, and G.R. Stark, *Jak-STAT pathways and transcriptional activation in response to IFNs and other extracellular signaling proteins.* Science, 1994. **264**(5164): p. 1415-21.
127. van Boxel-Dezaire, A.H., M.R. Rani, and G.R. Stark, *Complex modulation of cell type-specific signaling in response to type I interferons.* Immunity, 2006. **25**(3): p. 361-72.
128. Kaur, S., et al., *Role of the Akt pathway in mRNA translation of interferon-stimulated genes.* Proc Natl Acad Sci U S A, 2008. **105**(12): p. 4808-13.
129. Kaur, S., et al., *Regulatory effects of mTORC2 complexes in type I IFN signaling and in the generation of IFN responses.* Proc Natl Acad Sci U S A, 2012. **109**(20):

p. 7723-8.

130. Sanada, T., et al., *Transmission of HBV DNA Mediated by Ceramide-Triggered Extracellular Vesicles.* Cell Mol Gastroenterol Hepatol, 2017. **3**(2): p. 272-283.
131. Zhang, Q., et al., *Exosomes derived from hepatitis B virus-infected hepatocytes promote liver fibrosis via miR-222/TFRC axis.* Cell Biol Toxicol, 2023. **39**(2): p. 467-481.
132. Guo, B.B., S.A. Bellingham, and A.F. Hill, *The neutral sphingomyelinase pathway regulates packaging of the prion protein into exosomes.* J Biol Chem, 2015. **290**(6): p. 3455-67.
133. Trajkovic, K., et al., *Ceramide triggers budding of exosome vesicles into multivesicular endosomes.* Science, 2008. **319**(5867): p. 1244-7.
134. Leidal, A.M., et al., *The LC3-conjugation machinery specifies the loading of RNA-binding proteins into extracellular vesicles.* Nat Cell Biol, 2020. **22**(2): p. 187-199.
135. Ostrowski, M., et al., *Rab27a and Rab27b control different steps of the exosome secretion pathway.* Nat Cell Biol, 2010. **12**(1): p. 19-30; sup pp 1-13.
136. Chen, T.C., C.H. Hsieh, and P. Sarnow, *Supporting Role for GTPase Rab27a in Hepatitis C Virus RNA Replication through a Novel miR-122-Mediated Effect.* PLoS Pathog, 2015. **11**(8): p. e1005116.
137. Nagashima, S., et al., *Hepatitis E virus egress depends on the exosomal pathway, with secretory exosomes derived from multivesicular bodies.* J Gen Virol, 2014. **95**(Pt 10): p. 2166-2175.
138. Izumi, T., *In vivo Roles of Rab27 and Its Effectors in Exocytosis.* Cell Struct Funct, 2021. **46**(2): p. 79-94.
139. Chen, Y.D., et al., *Exophagy of annexin A2 via RAB11, RAB8A and RAB27A in IFN-gamma-stimulated lung epithelial cells.* Sci Rep, 2017. **7**(1): p. 5676.
140. Duran, J.M., et al., *Unconventional secretion of Acb1 is mediated by autophagosomes.* J Cell Biol, 2010. **188**(4): p. 527-36.
141. Minakaki, G., et al., *Autophagy inhibition promotes SNCA/alpha-synuclein release and transfer via extracellular vesicles with a hybrid autophagosome-exosome-like phenotype.* Autophagy, 2018. **14**(1): p. 98-119.
142. Zhang, M., et al., *Translocation of interleukin-1beta into a vesicle intermediate in*

autophagy-mediated secretion. Elife, 2015. **4**.

143. Ma, R.J., Y.Q. Tan, and G. Zhou, *Aberrant IGF1-PI3K/AKT/MTOR signaling pathway regulates the local immunity of oral lichen planus.* Immunobiology, 2019. **224**(3): p. 455-461.
144. Degtyarev, M., et al., *Akt inhibition promotes autophagy and sensitizes PTEN-null tumors to lysosomotropic agents.* J Cell Biol, 2008. **183**(1): p. 101-16.
145. Perot, B.P., et al., *Autophagy diminishes the early interferon-beta response to influenza A virus resulting in differential expression of interferon-stimulated genes.* Cell Death Dis, 2018. **9**(5): p. 539.
146. Gu, W., et al., *Simvastatin alleviates airway inflammation and remodelling through up-regulation of autophagy in mouse models of asthma.* Respirology, 2017. **22**(3): p. 533-541.
147. Zhu, S., et al., *Inhibiting autophagy potentiates the anticancer activity of IFN1@/IFNalpha in chronic myeloid leukemia cells.* Autophagy, 2013. **9**(3): p. 317-27.
148. Towler, M.C. and D.G. Hardie, *AMP-activated protein kinase in metabolic control and insulin signaling.* Circ Res, 2007. **100**(3): p. 328-41.
149. Lewis, J.A., A. Huq, and P. Najarro, *Inhibition of mitochondrial function by interferon.* J Biol Chem, 1996. **271**(22): p. 13184-90.
150. Rang, A., S. Gunther, and H. Will, *Effect of interferon alpha on hepatitis B virus replication and gene expression in transiently transfected human hepatoma cells.* J Hepatol, 1999. **31**(5): p. 791-9.
151. Caselmann, W.H., et al., *Type I interferons inhibit hepatitis B virus replication and induce hepatocellular gene expression in cultured liver cells.* J Infect Dis, 1992. **166**(5): p. 966-71.
152. Hayashi, Y. and K. Koike, *Interferon inhibits hepatitis B virus replication in a stable expression system of transfected viral DNA.* J Virol, 1989. **63**(7): p. 2936-40.

9. Abbreviations

Abbreviation	Full name
AO	acridine orange

ATF6	activating transcription factor 6
AMPK	AMP-activated protein kinase
Alix	apoptosis-linked gene 2-interacting protein X
Bip	immunoglobulin binding protein
CTD	C Terminal Domain
CQ	chloroquine
cccDNA	converted into covalently closed circular DNA
CHB	chronic hepatitis B
CMIA	chemiluminescence immunoassay
DNA	deoxyribonucleic acid
EcDNA	encapsidated HBV DNA
ER	endoplasmic reticulum
ESCRT	endosomal sorting complexes required for transport
EGFR	epidermal growth factor receptor
EGCG	epigallocatechin-3-gallate
eIF2α	eukaryotic initiation factor-2α
ERGIC	ER-Golgi intermediate compartment
EVA1A	Eva-1 homolog A
EV	extracellular vesicles
GRP78	78-kDa glucose-regulated protein
HBcAg	hepatitis B core protein
HBsAg	hepatitis surface core protein
HBeAg	hepatitis e core protein
HBx	hepatitis x core protein
HCC	hepatocellular carcinoma
HBV	hepatitis B virus
HCV	hepatitis C virus
HCC	hepatocellular carcinoma
HSPGs	heparan sulfate proteoglycans
IF	Immunofluorescence
IFITM	interferon-induced transmembrane proteins

IGF1R	insulin-like growth factor 1 receptor
ISG	IFN Stimulated Gene
ISG15	Interferon Stimulated Gene 15
IVL	intraluminal vesicles
l	litter
kb	kilo base pair
LAMP1	lysosomal-associated membrane protein 1
LC3	MAP1LC3, microtubule-associated protein 1 light chain 3 beta
m	mili
min	minute
MVB	multivesicular body
mTOR	mammalian target of rapamycin
NTD	N-terminal domain
NTCP	Na^+-taurocholate co-transporting polypeptide
nSMase	neutral sphingomyelinase
NC	nucleocapsid
ORF	open reading frame
PCR	polymerase chain reaction
PI4P	phosphatidylinositol-4-phosphate
PtdIns3K-C1	phosphoinositide 3-kinase complex I
pgRNA	pregenomic RNA
PHH	primary human hepatocytes
PDIA2	protein disulfide isomerase Family A Member 2
pSM2	a HBV replication-competent plasmid
p62	SQSTM1, sequestosome 1
RC-DNA	relaxed circular viral DNA
SAC1	SAC1-like phosphatidylinositol phosphatase
SNARE	soluble N-ethylmaleimide-sensitive factor attachment protein receptor
siNC	control small interfering RNA
siRNA	small interfering RNA

SVP	subviral particles
SNAP29	synaptosomal-associated protein 29
STX17	syntaxin 17
UPR	unfolded protein response
VAMP8	vesicle-associated membrane protein 8
VPS4A	vacuolar protein sorting 4 ATPase
WHO	world health organization

10. List of figures

11. Acknowledgements

I started my PhD just before the onset of the COVID-19 pandemic, a period that presented numerous challenges and uncertainties. Nonetheless, I made it to the finish line! I would like to express my deepest gratitude to the exceptional individuals who supported and guided me throughout this journey, enabling me to successfully obtain my doctorate.

First and foremost, I would extend my sincere gratitude to my supervisor, Prof. Dr. Mengji Lu, for his constant support, guidance, and encouragement throughout my scientific research. Prof. Lu always encourages me to participate in various academic conferences, providing me with the opportunity to learn from others' outstanding achievements and showcase my own work. He always thoroughly and earnestly discusses every experiment data with me and meticulously examined my research papers. I am truly grateful for the mentorship that has shaped my ability to independently conduct research and write effectively.

I also would like to thank our technician Mrs. Thekla Kemper. Her technical assistance and help were very important for my PhD project. Many thanks to Dr. Anthony Squire from Imaging Center Essen. With his excellent technical support, I have more beautiful and higher-quality IF images. I also would like to appreciate our collaborator Dr. Yong Lin and my colleagues Dr. Xueyu Wang and all the other lab mates. Their grateful help and care made my life much more enjoyable in Germany. Moreover, I want to appreciate the support and help from Ms. Ursula Schrammel in my work and daily life during my stay in Germany.

I appreciate the support and help from the Research Training Group 1949. I want to convey my thanks to the financial support provided by Deutsche Forschungsgemeinschaft (RTG1949/2).

Lastly, I want to express my deepest gratitude to my family whose belief in my abilities and support. Your encouragement played an integral role in my accomplishments. To my mom, dad, and husband: Thank you for everything.

Curriculum vitae

The CV is not included in the online version for reasons of data protection.

The CV is not included in the online version for reasons of data protection.

The CV is not included in the online version for reasons of data protection.

Declaration

Declaration:

In accordance with § 6 (para. 2, clause g) of the Regulations Governing the Doctoral Proceedings of the Faculty of Biology for awarding the doctoral degree Dr. rer. nat., I hereby declare that I represent the field to which the topic "I*nterconnection of cellular autophagy and endosomal vesicle trafficking and its role in hepatitis B virus replication and release"* is assigned in research and teaching and that I support the application of *Jia Li*.

Essen, date:_____

Name of the scientific supervisor/member of the Essen University of Duisburg-Essen	Signature of the supervisor/ member of the University of Duisburg-Essen

Declaration:

In accordance with § 7 (para. 2, clause d and f) of the Regulations Governing the Doctoral Proceedings of the Faculty of Biology for awarding the doctoral degree Dr. rer. nat., I hereby declare that I have written the herewith submitted dissertation independently using only the materials listed, and have cited all sources taken over verbatim or in content as such.

Essen, date _____

Signature of the doctoral candidate

Declaration:

In accordance with § 7 (para. 2, clause e and g) of the Regulations Governing the Doctoral Proceedings of the Faculty of Biology for awarding the doctoral degree Dr. rer. nat., I hereby declare that I have undertaken no previous attempts to attain a doctoral degree, that the current work has not been rejected by any other faculty, and that I am submitting the dissertation only in this procedure.

Essen, date _____

Signature of the doctoral candidate